

# Thermodynamics and dynamical properties of the $\text{KH}_2\text{PO}_4$ type ferroelectric compounds. A unified model

R.R.Levitskii<sup>1</sup>, I.R.Zachek<sup>2</sup>, A.S.Vdovych<sup>1</sup>, S.I.Sorokov<sup>1</sup>

<sup>1</sup> Institute for Condensed Matter Physics of the National Academy of Sciences of Ukraine,  
1 Svientsitskii Str., 79011 Lviv, Ukraine

<sup>2</sup> Lviv Polytechnic National University, 12 Bandera Str., 79013 Lviv, Ukraine

Received November 21, 2008, in final form January 15, 2009

Within the framework of the proposed unified proton ordering model for the ferroelectric compounds of the  $\text{KH}_2\text{PO}_4$  family, in the four-particle cluster approximation for the short-range interactions and mean field approximation for the long-range interactions, we calculate thermodynamic and longitudinal dynamic characteristics of the  $\text{KD}_2\text{PO}_4$  type ferroelectrics and  $\text{ND}_4\text{D}_2\text{PO}_4$  type antiferroelectrics. Calculations for partially deuterated  $\text{K}(\text{H}_{1-x}\text{D}_x)_2\text{PO}_4$  type ferroelectrics and  $\text{N}(\text{H}_{1-x}\text{D}_x)_4(\text{H}_{1-x}\text{D}_x)_2\text{PO}_4$  type antiferroelectrics are performed within the mean crystal approximation. It is shown that at the proper choice of the theory parameters, a good quantitative description of experimental data for the  $\text{KH}_2\text{PO}_4$  family crystals is obtained.

**Key words:** *ferroelectrics, cluster approximation*

**PACS:** *77.22.Ch, 77.22.Gm, 77.84.Fa*

## 1. Introduction

Investigations of the physical properties of ferroelectric materials occupy a central position in the condensed matter physics due to their practical importance. The existence of numerous classes of ferroelectric compounds with different crystal structure and chemical composition requires universal methods of investigation of phase transition mechanisms and general microscopic approaches that would allow us to explain the anomalies of their physical characteristics accompanying the transitions. Therefore, the development of microscopic theories for each particular type of ferroelectric compounds is a very important problem. Hydrogen bonded ferroelectrics of the orthophosphate type have a general formula  $\text{MH}_2\text{XO}_4$  ( $\text{MD}_2\text{XO}_4$ ) ( $\text{M} = \text{K, Rb, Cs, NH}_4$  ( $\text{ND}_4$ );  $\text{X} = \text{P, As}$ ). Wide possibilities for isomorphic replacement of atoms and for easy growing of high quality crystals, along with a number of interesting physical properties and relatively simple crystal structure, made the  $\text{KH}_2\text{PO}_4$  family crystals very popular objects for theoretical and experimental studies.

Ferroelectric properties of  $\text{KH}_2\text{PO}_4$  family crystals have been discovered more than seventy years ago. A huge number of theoretical and experimental papers, many books and reviews (see e. g. [1–26]) have been devoted to the investigation of phase transitions and the physical characteristics of this type of ferroelectrics. The most prominent peculiarity of these investigations is a strong connection between theory and experiment, which is believed to be an important source of the obtained progress in a microscopic understanding of the properties of the crystals. However, a consistent microscopic theory of these hydrogen bonded ferroelectrics, which would provide a quantitative description of numerous available experimental data within a single approach, has not been developed yet.

Peculiar to the crystal structure of these compounds is the existence of short  $\text{O}-\text{H}\cdots\text{O}$  hydrogen bonds, connecting  $\text{PO}_4$  groups (see [4–12]). These bonds are quite strong and do not perceptibly change with temperature. It is believed that the phase transitions in the  $\text{KH}_2\text{PO}_4$  family crystals are closely related to the proton ordering on the  $\text{O}-\text{H}\cdots\text{O}$  bonds, whose effective potential has

two minima. Above the phase transition temperature both minima are populated by protons statistically equivalently, while in the low-temperature phase a spontaneous asymmetry of population is observed. In the  $\text{NH}_4\text{H}_2\text{PO}_4$  type antiferroelectrics there are also  $\text{N-H}\cdots\text{O}$  bonds, which are longer and weaker than the  $\text{O-H}\cdots\text{O}$  bonds and notably temperature dependent. Even though these bonds are not taken into account within the known proton ordering models, they are directly related to the proton ordering. Their role was established in [27], where it was shown that they can give rise to an effective antiferroelectric coupling between protons on the  $\text{O-H}\cdots\text{O}$  bonds. This coupling can be ferroelectric as well, but should be lower than a certain limiting value.

The structure of the  $\text{KH}_2\text{PO}_4$  family crystals was determined by the X-ray and neutron scattering studies [28–31]. In the paraelectric phase these compounds crystallize in the  $\bar{4}m$  class with four molecules in the body-centered unit cell (space group  $\bar{I}4_2d$  with non-centrosymmetric point group  $D_{2d}^{12}$ ) [28–31]. In the polar phase the space group is  $Fdd$  (point group  $C_{2v}^{19}$ ) of the rhombic syngony with the axes rotated by  $45^\circ$  with respect to the crystallographic axes of the paraelectric phase. The unit cell contains eight formula units. The phase transition to the rhombic phase is due to the ordering of protons on the  $\text{O-H}\cdots\text{O}$  bonds, leading to a small rhombic distortion of the initial cell. The major structural changes in the  $\text{KH}_2\text{PO}_4$  family ferroelectrics at the phase transition [28,29] are related to the rotation of the  $\text{PO}_4$  tetrahedra and the shifts of the K and P atoms along the  $c$ -axis in the opposite directions. The  $\text{PO}_4$  groups do not deform, and the hydrogen bond length practically does not change.

The space group of the  $\text{NH}_4\text{H}_2\text{PO}_4$  type antiferroelectrics below the phase transition temperature is  $P2_12_12_1$  [30]. The transition is also accompanied by a slight rhombic distortion of the tetragonal cell. However, the new  $a$ ,  $b$  axes coincide with the old ones. The number of molecules in the unit cell does not change. Principally important for understanding of the microscopic mechanism of the phase transition in the  $\text{NH}_4\text{H}_2\text{PO}_4$  type antiferroelectrics were the neutron scattering experiments by Hewat [32], where the character of the proton ordering in the crystals of this type was established. It should be noted that the proton ordering here is accompanied by essential displacements of nitrogen and phosphorus atoms in the opposite directions perpendicular to the  $c$ -axis. The  $\text{NH}_4$  and  $\text{PO}_4$  groups become essentially deformed, and the neighboring  $\text{NH}_4$  and  $\text{PO}_4$  groups polarize in the opposite directions [32]. The  $\text{NH}_4\text{H}_2\text{PO}_4$  type antiferroelectrics undergo a clear first order phase transition, accompanied by jumps of the components of the dielectric susceptibility tensor and specific heat [8,12]. Optical measurements have shown that a superstructure arises in these crystals below the transition point [33]. The center of the body-centered tetragonal unit cell, which is equivalent to its vertices above the transition temperature, becomes non-equivalent to them below this temperature.

Isomorphic replacements essentially change the properties of the  $\text{KH}_2\text{PO}_4$  type crystals. This effect is the strongest at replacing K with  $\text{NH}_4$  or Cs. In the first case, the phase transition becomes antiferroelectric; in the second case the crystal symmetry and structure of the hydrogen bond system change. In the  $\text{CsH}_2\text{PO}_4$  type ferroelectrics, the proton ordering on hydrogen bonds is quasi-one-dimensional (see [34–40]). The same holds for  $\text{PbHPO}_4$  ferroelectrics (see [41–44]). In the  $\text{RbD}_2\text{PO}_4$  ferroelectrics the system of hydrogen bonds changes even more, and two phase transitions take place [45].

The most fundamental results were obtained from the studies of the partially deuterated crystals of the  $\text{KH}_2\text{PO}_4$  family. It has been established [4–16,26,46–48] that replacement of protons with deuterons significantly changes the transition temperatures, domain wall mobilities, thermal and dielectric properties of the crystals. These results indicate an importance of hydrogen bonds in the phase transitions in these types of crystals.

Depending on the arrangement of protons within the double potential wells on the hydrogen bonds, different configurations of  $\text{H}_n\text{PO}_4$  groups ( $n = 0, 1, \dots, 4$ ) are possible. We shall call them polarization groups, according to [1]. There exist  $2^4 = 16$  possible configurations of four protons surrounding each  $\text{PO}_4$  group. Amongst them the most likely are six configurations with two protons next to a  $\text{PO}_4$  group (see [1–5]). In the case of  $\text{KH}_2\text{PO}_4$ , two of these with protons next to the “lower” or “upper” (with respect to the  $c$ -axis) oxygen atoms have the lowest energy. These two complexes have dipole moments along the  $c$ -axis of the crystal. The other four  $\text{H}_2\text{PO}_4$  configurations

(lateral configurations), where one of the protons is associated with the upper oxygen atom, and the other proton is associated with the lower oxygen, have the energy  $\varepsilon$ . Eight configurations  $\text{H}_3\text{PO}_4$  and  $\text{HPO}_4$  have a yet higher energy  $w$ . The states without protons or with four protons near a  $\text{PO}_4$  group have the highest energy  $w_1$ .

The first microscopic model of the phase transition in the  $\text{KH}_2\text{PO}_4$  type ferroelectrics has been proposed by Slater [49]. This model is based on the following assumptions: there is a single proton per each hydrogen bond; there are only two protons near each  $\text{PO}_4$  group (the so-called ice rule); energy of  $\text{H}_2\text{PO}_4$  groups with protons on two upper or lower bonds is lower than the energy of  $\text{H}_2\text{PO}_4$  groups with other proton configurations by  $\varepsilon$ . Slater obtained an expression for the free energy and calculated dielectric susceptibility, phase transition temperature  $T_c$  and transition entropy. One of the biggest achievements of the Slater model is that it provides a value of the transition entropy close to the experiment. The drawbacks of the model are as follows: the free energy of the system in the ferroelectric phase is a polarization independent constant, and the temperature curve of spontaneous polarization is not correct.

Later, the Slater model was improved: polarization Takagi groups [50]  $\text{HPO}_4$  and  $\text{H}_3\text{PO}_4$ , as well as  $\text{H}_4\text{PO}_4$  and  $\text{PO}_4$  groups [1,2] were taken into account; dipole-dipole interactions were effectively introduced into the theory [51]. A detailed analysis of the above models is given in [1,2]. It has been shown that the improved Slater model can describe several experimental data for  $\text{KH}_2\text{PO}_4$  crystals. In [52] by taking into account the splitting of the “upper” and “lower” proton configuration energy by the strain  $u_6$ , the Slater model was extended to the studies of piezoelectric characteristics of the  $\text{KH}_2\text{PO}_4$  ferroelectrics. Static dielectric susceptibilities, piezomodules, and elastic constant were calculated.

The Slater model was also modified in order to describe the antiferroelectric transition in  $\text{NH}_4\text{H}_2\text{PO}_4$ . Initially, this transition was associated with the rotation of ammonium groups and was believed to be principally different from the transition in  $\text{KH}_2\text{PO}_4$ . Associating the transition in  $\text{NH}_4\text{H}_2\text{PO}_4$  with proton ordering, Nagamiya [53] used the Slater model to describe the physical characteristics of this crystal. Here, the lateral proton configurations were considered to be more energy favorable. Nagamiya also proposed a scheme of proton ordering in this crystal below the transition temperature, which leads to the antiferroelectric ordering along the  $a(b)$  axis. Later this character of the ordered structure of  $\text{NH}_4\text{H}_2\text{PO}_4$  was experimentally confirmed [32]. However, the assumption made by Nagamiya alone is not capable of precisely describing the type of the phase transition in  $\text{NH}_4\text{H}_2\text{PO}_4$ , since at negative Slater energy  $\varepsilon$ , both antiferroelectric and ferroelectric dipole ordering in the  $(ab)$  plane is possible [54]. In order to stabilize the type of dipole ordering observed in  $\text{NH}_4\text{H}_2\text{PO}_4$  [32,53] it suffices to take into account the long-range interactions within the mean field approximation [54]. A need to revisit the developed theory of the phase transitions in antiferroelectric orthophosphates was indicated by the results of EPR studies.[55]. They showed that in the disordered phase in  $\text{NH}_4\text{H}_2\text{AsO}_4$  there exist more upper/lower configurations of  $\text{H}_2\text{AsO}_4$  groups than lateral ones. This indicates that the  $\varepsilon$  energy in this crystal can be positive, that is, the condition  $\varepsilon < 0$  is not a necessary condition for the existence of antiferroelectricity. Later this conclusion was confirmed in [56], where it was shown that strong electrostatic dipole-dipole interactions along the  $a$  or  $b$  axis can provide an antiferroelectric phase transition with the predicted by Nagamiya ordering being established, under condition that the positive Slater energy  $\varepsilon$  is smaller than a certain critical value.

It should be noted that the Slater theory and its sophisticated versions concentrate their attention on short-range interactions of protons. Some of these versions also take into account the long-range interactions, but all of them neglect quantum effects due to overlapping proton wave functions of the two equilibrium positions of a proton on a bond.

An essential contribution to the development of the statistical theory of  $\text{KH}_2\text{PO}_4$  type ferroelectrics was made by R. Blinc [57]. He proposed a model, based on the assumption that protons on the  $\text{O-H}\cdots\text{O}$  bonds in  $\text{KH}_2\text{PO}_4$  type crystals move in double-well potentials. Jumps between the minima are performed via tunneling. Using the Blinc idea, de Gennes [58] proposed a pseudospin model of hydrogen bonded ferroelectrics. Theories, based on this model, explain the isotope effect for the transition temperature, Curie-Weiss constant, and spontaneous polarization by changes in

the tunneling parameter due to the difference in masses of a proton and a deuteron.

The simple pseudospin model of hydrogen bonded ferroelectrics proposed by de Gennes was further developed in many papers. The coupling of interactions and tunneling [3,59,60], the real structure of the  $\text{KH}_2\text{PO}_4$  type crystals, as well as short-range configurational interactions of protons [3–6,59,61,62] were taken into account.

The appearance of spontaneous polarization in the  $\text{KH}_2\text{PO}_4$  type ferroelectrics due to ionic displacements and unit cell deformation should be related to instabilities of the crystal lattice against certain optical (ferroelectric) and acoustic vibrations. These instabilities are due to the coupling of heavy ions (K and  $\text{PO}_4$  groups) with proton motion. Proton ordering triggers the corresponding ionic displacements and leads to the phase transition. For the first time, the proton-lattice interactions in the  $\text{KH}_2\text{PO}_4$  type ferroelectrics were studied in [63]. The behavior of a single proton surrounded by vibrating ions was explored. In a general form the problem of the proton-lattice coupling in the  $\text{KH}_2\text{PO}_4$  family crystals was considered in [64]. In [59] an importance of ionic displacements along the  $c$ -axis was noted for the first time, and a new model of an order-disorder type phase transition was discussed, assuming that two configurations of a  $(\text{K-PO}_4)$  complex are possible. Using this idea, Kobayashi [65] proposed a simplified model of  $\text{KH}_2\text{PO}_4$  that takes into account proton interactions with a single optical vibration of the  $(\text{K-PO}_4)$  complex. Later this model was discussed in [66]. The most complete investigation of proton interactions with acoustic and optic vibrations in the  $\text{KH}_2\text{PO}_4$  type crystals is given in [67–69]. In [69] the role of the long-range dipole-dipole interactions in the phase transitions in these crystals and their effect on the spontaneous strain and polarization were explored. The fourth-order phonon anharmonicities were added to the pseudospin-phonon model of hydrogen bonded ferroelectrics (see e. g. [70–73]), but their role in the  $\text{KH}_2\text{PO}_4$  type crystals has not been completely clarified, because of the essential short-range correlations neglected in these models.

Dynamic theories of the  $\text{NH}_4\text{H}_2\text{PO}_4$  type antiferroelectrics were developed too. In [74] a two-sublattice model of this type of antiferroelectrics was proposed, consisting of two oppositely polarized sublattices of protons, tunneling on the  $\text{O-H} \cdots \text{O}$  bonds. Later [75] the proton-lattice interactions were taken into account. The real structure of the  $\text{NH}_4\text{H}_2\text{PO}_4$  type crystals and the proton-lattice interactions were taken into account in [76–79].

Hence, the effective pseudospin-phonon Hamiltonian for the  $\text{KH}_2\text{PO}_4$  family crystals was obtained, using the idea of the decisive role of the proton subsystem in the phase transitions in these crystals and taking into account the interactions of protons with vibrations of heavy ions. The configurational correlations and long-range interactions between protons and tunneling were also taken into account. This was crucial for a further development of a microscopic theory for the hydrogen-bonded ferroelectrics. Here we should mention that for the last forty years the investigations of the order-disorder type compounds (also with hydrogen bonds) have been performed in two sectors.

In the papers of the first sector, the models of ferroelectric hydrogen bonded compounds (also of the orthophosphates), were explored using the Green's functions method with different methods of decoupling of the equation chain for them [60–68,71–75,77–86] and diagram method for the Matsubara Green's functions (see [62,87–93]) used. In [94] within the functional integration method (see [95]), free energy and Green's functions of a simple proton-ionic model of hydrogen bonded ferroelectrics were calculated. It was shown that within the self-consistent approach to the calculation of thermodynamic and dynamic characteristics of the models, the equation for the order parameter should be obtained from the condition of the free energy minimum. This condition is satisfied by equations for the order parameter obtained in [88–92] using the diagram method. Equations for the order parameter obtained within the two-time temperature Green's functions method should be considered as interpolation ones.

In the works based on the de Gennes model and its modifications, the major attention was concentrated on the dynamics problems of the hydrogen bonded ferroelectrics theory. Elementary excitation spectrum and its damping as well as some thermodynamic characteristics of these compounds were explored. It was thought to be established that the proton tunneling being taken into account made it possible to explain the observed isotopic effect in the phase transition temperature

and some thermodynamic characteristics of the  $\text{KH}_2\text{PO}_4$  type ferroelectrics and  $\text{NH}_4\text{H}_2\text{PO}_4$  type antiferroelectrics. It was also shown that there is a soft mode in the collective excitation spectrum of the  $\text{KH}_2\text{PO}_4$  family ferroelectrics, approaching zero at the transition point at  $\vec{k} \rightarrow \vec{\kappa}$  (the vectors  $\vec{\kappa}$  in the  $\text{KH}_2\text{PO}_4$  type crystals form a star that determines a direction of spontaneous polarization and crystal strain at a transition to the low temperature phase). According to [69] the star  $\{\kappa\}$  in the case of  $\text{KH}_2\text{PO}_4$  consists of four vectors starting from the center of the Brillouin zone and directed along the  $a$  and  $b$  axes (directions of these axes coincide with the directions of hydrogen bonds). In the case of the  $\text{NH}_4\text{H}_2\text{PO}_4$  type antiferroelectrics,  $\vec{\kappa}^i = \vec{k}_z = \frac{1}{2}(\vec{b}_1 + \vec{b}_2 + \vec{b}_3)$  ( $\vec{b}_1, \vec{b}_2, \vec{b}_3$  are the vectors of the reciprocal lattice). The soft antiferroelectric mode in  $\text{NH}_4\text{H}_2\text{PO}_4$  obtained in [75] was observed in neutron scattering experiments [96].

Attempts to describe experimental data for thermodynamic and dynamic characteristics of the  $\text{KH}_2\text{PO}_4$  type ferroelectrics and  $\text{NH}_4\text{H}_2\text{PO}_4$  type antiferroelectrics have been made (see e. g. [4–16,97–111]). However, due to the neglected piezoelectric and short-range interactions, important in these compounds, the obtained there results (see [112–114]) cannot provide a proper qualitative, let alone quantitative, description of the experiment.

In the papers of the second sector (see [4–6,17–19,26,59,61,76–79]) the major attention was concentrated on a statistical theory of the  $\text{KH}_2\text{PO}_4$  type ferroelectrics and  $\text{NH}_4\text{H}_2\text{PO}_4$  type antiferroelectrics. It should be noted that peculiar to the phase transition in the orthophosphate type ferroelectrics is a narrowness of the temperature range where their dynamic and thermodynamic characteristics change and have certain peculiarities. Therefore, the most successful description of thermodynamic and dynamic characteristics of these compounds can be obtained within the cluster expansion method, which due to the short-range correlations between protons being more consistently taken into account provides more accurate results than, for instance, the mean field approximation (MFA).

A considerable progress in the development of microscopic theory of the  $\text{KH}_2\text{PO}_4$  family ferroelectrics was made in [59,61]. In these works, using rather general principles, the main pseudospin Hamiltonian of a proton ordering model for the  $\text{KH}_2\text{PO}_4$  type ferroelectrics was obtained; in a simplified form it reduces to the Hamiltonian of [58]. The results of [59] obtained within the four-particle cluster approximation (FPCA) agree with the results of model theories [1,2]. In [61] the free energy and thermodynamic characteristics of the  $\text{KH}_2\text{PO}_4$  type ferroelectrics were calculated within the four-particle cluster approximation for short-range correlations and mean field approximation for long-range interactions. In the classic limit their results agree with the results of [59] and of the model theories [1,2].

Thorough experimental studies of the physical characteristics of the  $\text{KH}_2\text{PO}_4$  family ferroelectrics shed light on the details of a microscopic mechanism of the phase transitions in these crystals. Thus, the isomorphic structure of the orthophosphates in the paraelectric phase and a qualitative similarity of the behavior of most of the physical characteristics of the  $\text{KH}_2\text{PO}_4$  type ferroelectrics and  $\text{NH}_4\text{H}_2\text{PO}_4$  type antiferroelectrics indicated a need to search for a unified approach to the microscopic theory for both types of the crystals.

In [76], using the idea about the crucial role of the proton subsystem in the behavior of the  $\text{KH}_2\text{PO}_4$  family compounds, an effective Hamiltonian of the proton model for these compounds was consistently obtained. A statistical theory of the orthophosphate type ferroelectrics was proposed. Within this theory, in the FPCA with taking into account the short-range and long-range interactions, the free energy of the proton subsystem was calculated and explored. Possible types of proton ordering in the orthophosphate types were determined. It turned out that two of them are observed in the  $\text{KH}_2\text{PO}_4$  type ferroelectrics and  $\text{NH}_4\text{H}_2\text{PO}_4$  type antiferroelectrics. It was shown that the phase transition in antiferroelectric orthophosphates is possible only when the long-range interactions are taken into account. As we have already mentioned, the same conclusion was made in [54] within the framework of a simpler model. Later [115,116] the deuteron distribution functions and components of the static dielectric permittivity tensor of the  $\text{KD}_2\text{PO}_4$  type ferroelectrics and  $\text{ND}_4\text{D}_2\text{PO}_4$  type antiferroelectrics were calculated within the FPCA.

The above short analysis of the available works of the second sector indicates that the most consistent results for the thermodynamic characteristics of these compounds are obtained within the

four-particle cluster approximation. To verify the validity of the developed model it was necessary to perform a detailed numerical analysis of the obtained results and determine the values of the model parameters. However, the fitting procedures have not always been consistent. Mostly, the experimental data were discussed only for a limited number of physical characteristics, whereas all the theory parameters, entering the expressions for these characteristics were determined. Other characteristics were not always calculated with the obtained values of the theory parameters. As a result, quite frequently the determined values of the theory parameters using a limited number of physical characteristics were not optimal. It should be mentioned that the problem of determination of the optimal values of the theory parameters for the orthophosphates was approached by different methods. Of course, the most favorable is the situation when the number of the calculated physical characteristics exceeds the number of the model parameters to be determined.

It should be noted that the theory proposed in [61] required a huge amount of numerical calculations, that were not possible to be carried out at the time. Therefore, the authors only explored the possible effect of the changes in the theory parameters on the calculated physical characteristics. In order to use the theory [61] in describing the experimental data for the  $\text{KH}_2\text{PO}_4$  type ferroelectrics and to avoid cumbersome calculations, in [117] the tunneling contributions were taken into account via some approximations. Free energy was calculated within the first order of the expansion of the four-particle Hamiltonian eigenvalues over a small parameter. In order to solve transcendent equations for the variational parameters of the theory some approximations were made too. Overall, these approximations led to a perceptible error in the evaluated physical characteristics of the explored  $\text{KH}_2\text{PO}_4$  type ferroelectrics. According to [118] the error in calculations of the physical characteristics made in [117] exceeds 10% even near the phase transition temperature. An important point of [117] is a discussion of the reasons for a non-physical behavior of thermodynamic characteristics of the proton ordering model with tunneling yielded by FPCA. This was attributed to the replacement of interactions within the four-particle cluster by classical fields, which is not allowed in the presence of non-commuting operators in the Hamiltonian. Such a replacement is equivalent to the presence of two self-consistency conditions. The authors also stated that if there is no transverse self-consistency condition, then there is no low-temperature non-physical behavior either. However, in describing the phase transition when thermal fluctuations are more significant than the quantum ones, the absence of the transverse self-consistency condition essentially worsens the precision with which the free energy is calculated, which follows from the variational reasons.

We should particularly note the paper [118], where the first systematic investigation of the variation of the temperature curve of the proton ordering parameter, phase transition temperature, Curie-Weiss temperature and constant ( $T_0, C_{CW}$ ), transition entropy  $S_c(T_c + 0)$ , as well as specific heat with the theory parameters was performed within the cluster approximation for the proton ordering model of the  $\text{KH}_2\text{PO}_4$  family ferroelectric with tunneling. In this paper the theory parameters were determined for all ferroelectrics of the  $\text{KH}_2\text{PO}_4$  type. The major criterion for the choice of these parameters was to fit the theory to experimental data for the temperature dependence of the quantity  $\sqrt{\Delta S/S_c}$  ( $\Delta S = S_c - S$ ) in the phase transition region ( $T_c - T/T_c \leq 0.005$ ), whose width is less than 1.5 K. The main drawback of this criterion is that a very narrow temperature range should be considered. This is due to the following two factors. First, the proportionality between the proton ordering parameter and the quantity  $\sqrt{\Delta S/S_c}$  is mostly precisely obeyed in the vicinity of the phase transition. Second, the error in the quantity  $\sqrt{\Delta S/S_c}$  calculated from the experimental data for the specific heat is also the smallest in close vicinity of  $T_c$ .

Even though [118] became a certain conclusion of the persistent studies of the proton tunneling model initiated in [61], this paper does not give a complete picture of real capabilities of this model in describing the experimental data for the  $\text{KH}_2\text{PO}_4$  family ferroelectrics. In fact, an algorithm for determination of the optimal values of the theory parameters has not been proposed. Other characteristics of the crystals, not used in the fitting procedure, were not calculated with the obtained values of the parameters. These remarks also apply to the results of [119], where the values of the theory parameters found in [118] were corrected in order to improve and agreement with experiment for spontaneous polarization. An important result obtained in [118] is the proof that the cluster energies of deuterated crystals are much higher than those of undeuterated crystals.

Along with tunneling, the mentioned fact is very important in describing the isotopic effect in thermodynamic and dynamic properties of the  $\text{KH}_2\text{PO}_4$  family ferroelectrics.

A thorough investigation of the proton ordering model for the  $\text{KH}_2\text{PO}_4$  type ferroelectrics with short-range and long-range interactions and tunneling was made in [120,121]. A method for analytic calculations of the static dielectric susceptibility tensor components was proposed. Thermodynamic and dielectric characteristics of the model were calculated and analyzed numerically; peculiarities of the phase transition in the  $\text{KH}_2\text{PO}_4$  type ferroelectrics were explored. General dependences of the physical characteristics of these crystals on the values of the model parameters were established. Using these dependences an approach was proposed to determine optimal values of the model parameters for different  $\text{KH}_2\text{PO}_4$  type ferroelectrics, which provided an optimal quantitative agreement of the calculated characteristics with experimental data. The optimal sets of the model parameters for all undeuterated ferroelectrics of the  $\text{KH}_2\text{PO}_4$  family were determined within the proposed approach. It was established that tunneling, Slater-Takagi energies, and the long-range interaction parameter are essentially determined only by a whole set of characteristics, namely, the Curie-Weiss temperature and temperature curves of spontaneous polarization and proton specific heat. A range of the theory applicability was determined due to the presence of non-physical behavior in the temperature curves of the calculated characteristics at low temperatures.

Similar investigations of the proton ordering model for the  $\text{NH}_4\text{H}_2\text{PO}_4$  type antiferroelectrics with short-range and long-range interactions and tunneling were performed in [122]. The temperature behavior of sublattice spontaneous polarization, proton specific heat, and dielectric permittivities of undeuterated antiferroelectrics of the  $\text{NH}_4\text{H}_2\text{PO}_4$  are described; at the proper choice of the theory parameters the theoretical results well agree with experimental data. Due to the non-physical temperature behavior of the system characteristics at low temperatures, the range of the theory applicability is indicated.

In [123–126] within the framework of proton ordering model with tunneling being taken into account and within four-particle cluster approximation, using the results of [120,121], the thermodynamic and dielectric characteristics of the partially deuterated  $\text{Rb}(\text{H}_{1-x}\text{D}_x)_2\text{PO}_4$  and  $\text{K}(\text{H}_{1-x}\text{D}_x)_2\text{PO}_4$  ferroelectrics were calculated in the mean crystal approximation. A good agreement of the obtained results with the corresponding experimental data was obtained.

At the end of 1960-ies most theoretical and experimental studies of ferroelectrics were concentrated on the dynamic phenomena [127]. At low frequencies, the dispersion of the dielectric permittivity of ferroelectrics was explored, providing an important information on the mechanisms of phase transitions. The obtained experimental results for the dielectric permittivity dispersion in the order-disorder type ferroelectrics, including those of the  $\text{KH}_2\text{PO}_4$  family, were interpreted mostly within phenomenological models (see [127–130]). In many cases, contradictions between the phenomenological theory and experiment were revealed, especially for materials exhibiting nonlinearities in the temperature dependences of their dynamic characteristics.

It should be noted that phenomenological theories do not allow us to establish a microscopic nature of the dispersion of dielectric permittivity and to adequately describe the effect of various factors on the character of its temperature and frequency dependences. Therefore, of great importance were the studies of dynamic characteristics of ferroelectrics within the Bloch equations method [5]. In [131–134] using this method, the dynamic properties of an order-disorder type ferroelectrics (also of the  $\text{KH}_2\text{PO}_4$  type) were explored with the help of simple models of these crystals. A satisfactory description of the dynamic characteristics of  $\text{KH}_2\text{PO}_4$  in the paraelectric phase was obtained. Later, in [135,136] a real structure of the  $\text{KH}_2\text{PO}_4$  family ferroelectrics and the proton-lattice interactions were taken into account; the relaxation times, longitudinal and transverse components of the dynamic permittivity tensor of the  $\text{KH}_2\text{PO}_4$  and  $\text{NH}_4\text{H}_2\text{PO}_4$  type antiferroelectrics were calculated within the Bloch equation method. It should be noted that the Bloch method allows one to take tunneling into account, but it is based on the mean field approximation, which is not appropriate for these crystals, in principle. In [77–79], using the original approach proposed by the authors, the dynamics of the  $\text{KH}_2\text{PO}_4$  family ferroelectrics was considered within the cluster approximation with tunneling taken into account. It was shown that within the reference approach, with the short-range correlations taken into account in the cluster approx-

imation and with the long-range interactions considered in the chaotic phase approximation, the dynamic characteristics of the  $\text{KH}_2\text{PO}_4$  family crystals are essentially determined by an effective tunneling parameter, which is much smaller than the corresponding parameter entering the model Hamiltonian. In fact, an essential suppression of proton tunneling by short-range interactions takes place. Unfortunately, the expressions for dynamic (at  $\mathbf{q} = 0$  and  $\omega = 0$ ) and static characteristics obtained in [77–79] do not agree. This is related to the fact that the dynamics of the compounds studied therein was treated within the two-time temperature Green's functions method, equations for which were decoupled with respect to the long-range interactions in the spirit of Tyablikov approximation [137]. The intracluster correlation functions of the reference system are connected only via the long-range interactions, whereas the short-range intercluster correlations were not taken into account within the proposed in [77] approach.

Later [26,138–140] a self-consistent approach to the calculation of thermodynamic and dynamic characteristics of pseudospin systems with essential short-range and long-range interactions was proposed, based on calculations of the free energy functional with the reference taking into account the short-range correlations. A general method for obtaining consistent approximations for thermodynamic and dynamic characteristics was formulated. It should be noted that the obtained expressions for thermodynamic and dynamic characteristics of the pseudospin systems [26,138–140] contain thermodynamic and correlation functions of the reference system, which includes the short-range correlations and the long-range interactions considered within the mean field approximation. For quantum reference pseudospin systems, a consistent formulation of the cluster expansion method was proposed for the first time. A method was suggested that permits within the cluster approximation to obtain the Ornstein-Zernike type equations for reference temperature cumulant Green's functions of an arbitrary order [26,116,141,142].

In [138,140,141] the thermodynamic and dynamic characteristics of quasi-one-dimensional Ising model in transverse field were calculated within the reference approach. The obtained results were used in describing the experimental data for a quasi-one-dimensional ferroelectric  $\text{CsH}_2\text{PO}_4$  in the paraelectric phase. Special attention was paid to the studies of the spectrum of elementary excitations of this model obtained within the cluster chaotic phase approximation. It was established that an essential suppression of the soft vibration mode by short-range correlations takes place in a wide temperature range. This fact is directly related to the dispersion observed in  $\text{CsH}_2\text{PO}_4$  Debye type of longitudinal dielectric permittivity. It seems that similar studies [142] for  $\text{KH}_2\text{PO}_4$  would be of principal importance. They would make it possible to explore the effect of suppression of the soft mode in the  $\text{KH}_2\text{PO}_4$  type ferroelectrics more consistently than in [77] and thereby to explain the Debye character of the dielectric permittivity dispersion in these crystals.

A vast majority of studies on the theory of relaxation phenomena in the  $\text{KH}_2\text{PO}_4$  family ferroelectrics is based on the stochastic Glauber model [143]. For the first time the relaxation dynamics of the  $\text{KD}_2\text{PO}_4$  type ferroelectrics was studied using this method in [128]. Within the FPCA for short-range correlations between deuterons the relaxation times and longitudinal dynamic dielectric permittivity of these compounds were calculated for the case of paraelectric phase. However, the long-range interactions were not taken into account; the corresponding experimental data for the  $\text{KD}_2\text{PO}_4$  type ferroelectrics were not discussed. Later [129,144–151] a unified approach to a description of experimentally observed thermodynamic and dynamic characteristics of the ferroelectric orthophosphates was suggested. A more consistent dynamic model of deuterated ferroelectric compounds of the  $\text{KH}_2\text{PO}_4$  family based on the stochastic Glauber model was proposed. Within the framework of this model, using the four-particle cluster approximation, taking into account the short-range configurational interactions between deuterons near the  $\text{PO}_4$  groups and effective long-range interactions, the relaxation times, longitudinal and transverse static and complex dielectric permittivities, free energy, specific heat, equations for the phase transition temperatures, and equations for the order parameters of these compounds were calculated. In [46–48,151–159] a detailed numerical analysis of the obtained results was performed. It was shown that at the proper choice of theory parameters a satisfactory description of experimental data for the  $\text{K}(\text{H}_{1-x}\text{D}_x)_2\text{PO}_4$  type ferroelectrics [46–48] and  $\text{N}(\text{H}_{1-x}\text{D}_x)_4(\text{H}_{1-x}\text{D}_x)_2\text{PO}_4$  type antiferroelectrics [151,157–159] could be obtained even without tunneling taken into account.



In the 1980-ies much attention was paid to the investigation of higher-frequency modes in the  $\text{KH}_2\text{PO}_4$  type crystals, related to internal vibrations of ionic groups (see [16,20,160–163]). A series of anomalies and additional lines were revealed in Raman spectra of the crystals on these modes. So far there is no unequivocal interpretation of these results. In [164] an approach was suggested to describing a single-phonon Raman scattering by internal vibrations of ionic groups. It was shown that an appropriate description of the data obtained in [160–162] for  $\text{KH}_2\text{PO}_4$  can be obtained within the proton ordering model. Since in this model the lateral configurations are present, in [164] there was a particular stress on the need for a thorough experimental investigation of the cases when only these configurations are revealed in scattering experiments. The importance of solving this problem is supported by the fact that in [20,161–163] the other model of the phase transition in the  $\text{KH}_2\text{PO}_4$  type ferroelectrics was discussed: the transition was associated with the ordering of the  $\text{H}_2\text{PO}_4$  groups being in configurations with protons near the “upper” or “lower” oxygen ions. Practical realization of this model faces some difficulties due to breaking of the “ice rule” in the ordered state (see [164]). It should be noted that the data of [165] do not confirm the validity of this model but rather support the proton ordering model.

Validity of the proton ordering model for the  $\text{KH}_2\text{PO}_4$  family ferroelectric crystals has not been proved yet. The results obtained in the works of the second sector of investigations have significantly strengthened the positions of the proton ordering model. The investigations (also theoretical [166–180]) of the field effects in these crystals turned out to be of particular importance here. The major microscopic mechanisms of the effect of external pressures of different symmetries on the short-range and long-range interactions in the  $\text{KD}_2\text{PO}_4$  family ferroelectrics were analyzed. It was established that stresses of different symmetries can lead to qualitatively different changes in the character of phase transitions in these crystals. It was shown that the proton ordering model provides a satisfactory description of the available experimental data for pressure and field dependences of physical characteristics of the  $\text{KH}_2\text{PO}_4$  family ferroelectrics. Validity of the proton ordering model for the  $\text{KH}_2\text{PO}_4$  family crystals was also indicated in [181–184].

Since 1980-ies, much attention has been paid [185–195] to the studies of the  $\text{Rb}_{1-x}(\text{NH}_4)_x\text{H}_2\text{PO}_4$  type materials that can undergo a transition to the proton glass phase at low temperatures. Their thermodynamic and dynamic characteristics were calculated using simple models of the  $\text{KH}_2\text{PO}_4$  family ferroelectrics (see [196]). Only in [193–195] the cluster approach was used in describing the experimentally observed phase diagrams of the  $\text{Rb}_{1-x}(\text{NH}_4)_x\text{H}_2\text{PO}_4$  type systems. Other characteristics in this approach were not calculated.

Hence, a theoretical description of thermodynamic and dielectric properties of the  $\text{Rb}_{1-x}(\text{NH}_4)_x\text{H}_2\text{PO}_4$  type compounds, which can undergo a transition to the proton glass state, with taking into account their structural peculiarities and different types of interactions, is still a complicated unresolved problem in statistical physics. Of special importance is to formulate the model and to develop a microscopic theory for this type of materials, as well to calculate the thermodynamic and dynamic characteristics of the system within this theory. A unified model is needed capable of describing the proton ordering in ferroelectric and antiferroelectric crystals of the  $\text{KH}_2\text{PO}_4$  family crystals.

In the present paper we propose a unified model of ferroelectric compounds of the  $\text{KH}_2\text{PO}_4$  family. Within this model in the framework of the four-particle cluster approximation we calculate thermodynamic and longitudinal dynamic characteristics of the  $\text{KD}_2\text{PO}_4$  type ferroelectrics and  $\text{ND}_4\text{D}_2\text{PO}_4$  type antiferroelectrics. A thorough analysis of the available experimental data for the  $\text{K}(\text{H}_{1-x}\text{D}_x)_2\text{PO}_4$  type ferroelectrics and  $\text{N}(\text{H}_{1-x}\text{D}_x)_4(\text{H}_{1-x}\text{D}_x)_2\text{PO}_4$  type antiferroelectrics is performed. The obtained results are analyzed numerically and compared with the corresponding experimental data for these compounds.

## 2. Problem formulation. Static dielectric and thermal characteristics of the $\text{MD}_2\text{XO}_4$ type ferroelectrics and $\text{ND}_4\text{D}_2\text{XO}_4$ type antiferroelectrics

We shall consider a system of deuterons moving on the O-D...O bonds in deuterated ferroelectric  $\text{MD}_2\text{XO}_4$  and antiferroelectric  $\text{ND}_4\text{D}_2\text{XO}_4$  orthophosphates (M=K, Rb, X=P, As). The

primitive cell of the Bravais lattice of these crystals consists of two neighboring tetrahedra  $\text{PO}_4$  along with four hydrogen bonds attached to one of them (the ‘‘A’’ type tetrahedron). The hydrogen bonds attached to the other tetrahedron (‘‘B’’ type) belong to the four structural elements surrounding it (figure 1).

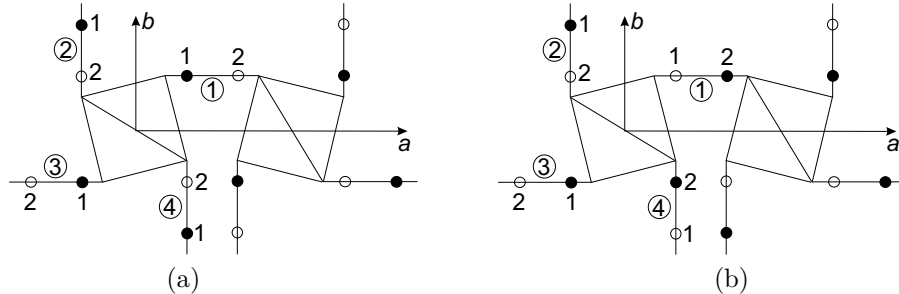


**Figure 1.** A primitive cell of  $\text{MD}_2\text{XO}_4$  (a) and  $\text{ND}_4\text{D}_2\text{XO}_4$  (b) crystals. The numbers in circles denote the hydrogen bonds; 1, 2 are deuteron equilibrium positions on bonds.

The Hamiltonian of the deuteron subsystem of  $\text{MD}_2\text{XO}_4$  and  $\text{ND}_4\text{D}_2\text{XO}_4$  with taking into account short-range and long-range interactions in the presence of external electric fields  $E_\gamma$  ( $\gamma = 1, 2, 3$ ) applied along the crystallographic axes ( $a, b, c$ ), reads [76]

$$\begin{aligned} \hat{H}_\gamma = & -\frac{\bar{v}}{2} N \chi_{\gamma\gamma}^0 E_\gamma^2 - \frac{1}{2} \sum_{qf q' f'} J_{ff'}(qq') \frac{\sigma_{qf}}{2} \frac{\sigma_{q' f'}}{2} \\ & + \sum_{q_1 q_2 q_3 q_4} \left\{ \frac{1}{2} \sum_{ff'} V_{ff'}(q_f q_{f'}) \frac{\sigma_{q_f f}}{2} \frac{\sigma_{q_{f'} f'}}{2} + \Phi \frac{\sigma_{q_1 1}}{2} \frac{\sigma_{q_2 2}}{2} \frac{\sigma_{q_3 3}}{2} \frac{\sigma_{q_4 4}}{2} \right\} \\ & \times \left( \delta_{\mathbf{R}_{q_1} \mathbf{R}_{q_2}} \delta_{\mathbf{R}_{q_1} \mathbf{R}_{q_3}} \delta_{\mathbf{R}_{q_1} \mathbf{R}_{q_4}} + \delta_{\mathbf{R}_{q_1+\mathbf{r}_2} \mathbf{R}_{q_2}} \delta_{\mathbf{R}_{q_1+\mathbf{r}_3} \mathbf{R}_{q_3}} \delta_{\mathbf{R}_{q_1+\mathbf{r}_4} \mathbf{R}_{q_4}} \right) - \sum_{qf} \mu_{f\gamma} E_\gamma \frac{\sigma_{qf}}{2}. \quad (2.1) \end{aligned}$$

The first term in (2.1) is the energy that is related to polarization induced by external electric field and is independent of the hydrogen bonds configurations ( $\chi_{\gamma\gamma}^0$  is the ‘‘seed’’ dielectric susceptibility;  $\bar{v} = \frac{v}{k_B}$ ,  $v$  is the primitive cell volume,  $k_B$  is the Boltzmann constant). The second term describes effective long-range interactions between deuterons including indirect lattice mediated interactions [67]. The third term is the short-range deuteron interactions near the ‘‘A’’ type (the first product of the Kronecker symbols) and ‘‘B’’ type (the second product of the Kronecker symbols) tetrahedra.  $\sigma_{qf}$  is the  $z$ -th component of the pseudospin operator  $\hat{\sigma}_{qf}$ , describing the state of a deuteron in the  $q$ -th cell on the  $f$ -th bond. Two eigenvalues of the operator  $\sigma_{qf} = \pm 1$  correspond to two possible positions of the deuteron on the bond;  $\mathbf{R}_{qf}$  is the position vector of the  $qf$ -th cell,  $\mathbf{r}_f$  is the relative position vector of the  $qf$ -th cell relative to  $q_1$ -th. The fourth term in (2.1) is the interaction of deuterons with external electric fields  $E_\gamma$ ;  $\mu_{f\gamma}$  are the effective dipole moments of the hydrogen bonds.

The short-range interaction constants  $V_{ff'}$  and  $\Phi$  are connected to the configurational deuteron energies  $\varepsilon_s, \varepsilon_a, \varepsilon_0, \varepsilon_1$  as follows [76]:

$$\begin{aligned} V &= V_{12} = V_{23} = V_{34} = V_{41} = \frac{1}{2}(\varepsilon_s - \varepsilon_0), \\ U_s &= V_{13} = V_{24} = -\varepsilon_a + \frac{1}{2}(\varepsilon_s + \varepsilon_0), \quad \Phi = 4\varepsilon_a - 8\varepsilon_1 + 2(\varepsilon_s + \varepsilon_0). \quad (2.2) \end{aligned}$$

The free energy of the deuteron subsystem described by the Hamiltonian (2.1) is the part of the total free energy of the crystals responsible for phase transitions. To calculate it we use the group expansion method [197], where the interactions within a selected group of particles are taken into

account exactly, whereas their interactions with other particles considered within a self-consistent field approximation. Since four-particle interactions (2.1) are peculiar to the orthophosphates, the smallest deuteron groups that should be taken into account to get an appropriate description of the system are the four-particle groups. It is not essential whether we take into account the larger groups.

Within the framework of the four-particle cluster approximation, the free energy of the deuteron subsystem described by the Hamiltonian (2.1) reads [76]

$$F = \frac{\bar{v}}{2} N \chi_{\gamma\gamma}^0 E_\gamma^2 - \frac{1}{\beta} \sum_q (\ln Z_4 - \frac{1}{2} \sum_f \ln Z_{1f}) + \frac{1}{2} \sum_{qq'} \sum_{ff'} J_{ff'}(qq') \left\langle \frac{\sigma_{qf}}{2} \right\rangle \left\langle \frac{\sigma_{q'f'}}{2} \right\rangle, \quad (2.3)$$

where  $Z_4 = \text{Spe}^{-\beta \hat{H}_{q\gamma}^{(4)s,a}}$ ,  $Z_{1f} = \text{Spe}^{-\beta \hat{H}_{qf\gamma}^{(1)s,a}}$  ( $\beta = \frac{1}{k_B T}$ ) are the four-particle and single-particle partition functions. The four-particle Hamiltonian  $\hat{H}_{q\gamma}^{(4)s,a}$  is given by the expressions

$$\begin{aligned} \hat{H}_{q\gamma}^{(4)s,a} = & V_s \left( \frac{\sigma_{q1} \sigma_{q2}}{2} + \frac{\sigma_{q2} \sigma_{q3}}{2} + \frac{\sigma_{q3} \sigma_{q4}}{2} + \frac{\sigma_{q4} \sigma_{q1}}{2} \right) \\ & + U_s \left( \frac{\sigma_{q1} \sigma_{q3}}{2} + \frac{\sigma_{q2} \sigma_{q4}}{2} \right) + \Phi \frac{\sigma_{q1} \sigma_{q2} \sigma_{q3} \sigma_{q4}}{2} - \sum_f \frac{z_{qf}^{\gamma sa}}{\beta} \frac{\sigma_{qf}}{2}. \end{aligned} \quad (2.4)$$

The effective fields  $z_{qf}^{\gamma sa}$  ( $\gamma = x, y, z$ ) read

$$\begin{aligned} z_q^{zs} &= \beta \left[ -\Delta_z^z + 2\nu_c^s(0)\eta_s^{(1)z} + \mu_3^s E_3 \right], \\ z_{q1}^{xs} &= \beta \left[ -\Delta_{11}^x + \frac{1}{2} J_{11}(0)\eta_{1s}^{(1)x} + \frac{1}{2} J_{13}(0)\eta_{3s}^{(1)x} + J_{12}(0)\eta_{24s}^{(1)x} + \mu_1^s E_1 \right], \\ z_{q3}^{xs} &= \beta \left[ -\Delta_{31}^x + \frac{1}{2} J_{13}(0)\eta_{1s}^{(1)x} + \frac{1}{2} J_{11}(0)\eta_{3s}^{(1)x} + J_{12}(0)\eta_{24s}^{(1)x} - \mu_1^s E_1 \right], \\ z_{q24}^{xs} &= z_{q2}^{xs} = z_{q4}^{xs} = \beta \left[ -\Delta_{24}^x + \frac{1}{2} J_{12}(0)(\eta_{1s}^{(1)x} + \eta_{3s}^{(1)x}) + \frac{1}{2} (J_{11}(0) + J_{13}(0))\eta_{24s}^{(1)x} \right], \\ z_{q13}^{ys} &= z_{q1}^{ys} = z_{q3}^{ys} = \beta \left[ -\Delta_{13}^y + \frac{1}{2} (J_{11}(0) + J_{13}(0))\eta_{13s}^{(1)y} + \frac{1}{2} J_{12}(0)(\eta_{2s}^{(1)y} + \eta_{4s}^{(1)y}) \right], \\ z_{q2}^{ys} &= \beta \left[ -\Delta_{22}^y + 2\frac{1}{2} J_{12}(0)\eta_{13s}^{(1)y} + \frac{1}{2} J_{11}(0)\eta_{2s}^{(1)y} + \frac{1}{2} J_{13}(0)\eta_{4s}^{(1)y} - \mu_2^s E_2 \right], \\ z_{q4}^{ys} &= \beta \left[ -\Delta_{42}^y + \frac{1}{2} J_{12}(0)\eta_{13s}^{(1)y} + \frac{1}{2} J_{13}(0)\eta_{2s}^{(1)y} + \frac{1}{2} J_{11}(0)\eta_{4s}^{(1)y} + \mu_2^s E_2 \right], \end{aligned} \quad (2.5)$$

$$\begin{aligned} z_{q14}^{za} &= z_{q1}^{za} = z_{q4}^{za} = \beta \left[ \Delta_{qa}^x - 2\nu_a(\mathbf{k}_z)\eta_{qa}^{(1)} - \Delta_{qa}^z + 2\nu_c^a(0)\eta_a^{(1)z} + \mu_3^a E_3 \right], \\ z_{q23}^{za} &= z_{q2}^{za} = z_{q3}^{za} = \beta \left[ -\Delta_{qa}^x + 2\nu_a(\mathbf{k}_z)\eta_{qa}^{(1)} - \Delta_{qa}^z + 2\nu_c^a(0)\eta_a^{(1)z} + \mu_3^a E_3 \right], \\ z_{q13}^{xa} &= -z_{q1}^{xa} = z_{q3}^{xa} = \beta \left[ -\Delta_{q13}^x + 2\nu_a(\mathbf{k}_z)\eta_{qa}^{(1)} + 2\nu_a^a(0)\eta_{13a}^{(1)x} + \mu_1^a E_1 \right], \\ z_{q24}^{xa} &= z_{q2}^{xa} = -z_{q4}^{xa} = \beta \left[ -\Delta_{q24}^x + 2\nu_a(\mathbf{k}_z)\eta_{qa}^{(1)} + 2\nu_a^a(0)\eta_{24a}^{(1)x} \right], \\ z_{q13}^{ya} &= -z_{q1}^{ya} = z_{q3}^{ya} = \beta \left[ -\Delta_{q13}^y + 2\nu_a(\mathbf{k}_z)\eta_{qa}^{(1)} + 2\nu_a^a(0)\eta_{13a}^{(1)y} \right], \\ z_{q24}^{ya} &= z_{q2}^{ya} = -z_{q4}^{ya} = \beta \left[ -\Delta_{q24}^y + 2\nu_a(\mathbf{k}_z)\eta_{qa}^{(1)} + 2\nu_a^a(0)\eta_{24a}^{(1)y} + \mu_2^a E_2 \right]. \end{aligned} \quad (2.6)$$

Single-particle deuteron Hamiltonians in the presence of the field  $E_i$  read

$$\hat{H}_{qfz}^{(1)s} = -\frac{\bar{z}_q^{zs}}{\beta} \frac{\sigma_{qf}}{2},$$

$$\begin{aligned}\hat{H}_{q1x}^{(1)s} &= -\frac{\bar{z}_{q1}^{xs}}{\beta} \frac{\sigma_{q1}}{2}, & \hat{H}_{q2x}^{(1)s} &= -\frac{\bar{z}_{q24}^{xs}}{\beta} \frac{\sigma_{q2}}{2}, & \hat{H}_{q3x}^{(1)s} &= -\frac{\bar{z}_{q3}^{xs}}{\beta} \frac{\sigma_{q3}}{2}, & \hat{H}_{q4x}^{(1)s} &= -\frac{\bar{z}_{q24}^{xs}}{\beta} \frac{\sigma_{q4}}{2}, \\ \hat{H}_{q1y}^{(1)s} &= -\frac{\bar{z}_{q13}^{ys}}{\beta} \frac{\sigma_{q1}}{2}, & \hat{H}_{q2y}^{(1)s} &= -\frac{\bar{z}_{q2}^{ys}}{\beta} \frac{\sigma_{q2}}{2}, & \hat{H}_{q3y}^{(1)s} &= -\frac{\bar{z}_{q13}^{ys}}{\beta} \frac{\sigma_{q3}}{2}, & \hat{H}_{q4y}^{(1)s} &= -\frac{\bar{z}_{q4}^{ys}}{\beta} \frac{\sigma_{q4}}{2},\end{aligned}\quad (2.7)$$

$$\begin{aligned}\hat{H}_{q1z}^{(1)a} &= -\frac{\bar{z}_{q14}^{za}}{\beta} \frac{\sigma_{q1}}{2}, & \hat{H}_{q2z}^{(1)a} &= -\frac{\bar{z}_{q23}^{za}}{\beta} \frac{\sigma_{q2}}{2}, & \hat{H}_{q3z}^{(1)a} &= -\frac{\bar{z}_{q23}^{za}}{\beta} \frac{\sigma_{q3}}{2}, & \hat{H}_{q4z}^{(1)a} &= -\frac{\bar{z}_{q14}^{za}}{\beta} \frac{\sigma_{q4}}{2}, \\ \hat{H}_{q1x}^{(1)a} &= -\frac{\bar{z}_{q13}^{xa}}{\beta} \frac{\sigma_{q1}}{2}, & \hat{H}_{q2x}^{(1)a} &= -\frac{\bar{z}_{q24}^{xa}}{\beta} \frac{\sigma_{q2}}{2}, & \hat{H}_{q3x}^{(1)a} &= -\frac{\bar{z}_{q13}^{xa}}{\beta} \frac{\sigma_{q3}}{2}, & \hat{H}_{q4x}^{(1)a} &= -\frac{\bar{z}_{q24}^{xa}}{\beta} \frac{\sigma_{q4}}{2}, \\ \hat{H}_{q1y}^{(1)a} &= -\frac{\bar{z}_{q13}^{ya}}{\beta} \frac{\sigma_{q1}}{2}, & \hat{H}_{q2y}^{(1)a} &= -\frac{\bar{z}_{q24}^{ya}}{\beta} \frac{\sigma_{q2}}{2}, & \hat{H}_{q3y}^{(1)a} &= -\frac{\bar{z}_{q13}^{ya}}{\beta} \frac{\sigma_{q3}}{2}, & \hat{H}_{q4y}^{(1)a} &= -\frac{\bar{z}_{q24}^{ya}}{\beta} \frac{\sigma_{q4}}{2}.\end{aligned}\quad (2.8)$$

The expressions for  $\bar{z}_q^{xs}, \dots, \bar{z}_{q24}^{ys}$  are obtained from (2.5) and (2.6) by replacing  $\Delta_3, \dots, \Delta_{q24}$  with  $2\Delta_3, \dots, 2\Delta_{q24}$ .

In obtaining the effective fields  $z_{qf}^{\gamma s, a}$  we take into account [76] the fact that in the system described by the Hamiltonian (2.1), both ferroelectric

$$\eta_s^{(1)z} = \langle \sigma_{q1} \rangle = \langle \sigma_{q2} \rangle = \langle \sigma_{q3} \rangle = \langle \sigma_{q4} \rangle, \quad (2.9)$$

and antiferroelectric

$$\eta_{qa}^{(1)} = \eta_a^{(1)} e^{i\mathbf{k}_z \cdot \mathbf{a}_q} = -\langle \sigma_{q1} \rangle = \langle \sigma_{q2} \rangle = \langle \sigma_{q3} \rangle = -\langle \sigma_{q4} \rangle \quad (2.10)$$

quasispin orderings are possible.

In the case of ferroelectric ordering, the proton correlation energies  $V_s, U_s$ , and  $\Phi_s$  are expressed via the ferroelectric energies  $\varepsilon = \varepsilon_a - \varepsilon_s, w = \varepsilon_1 - \varepsilon_s, w_1 = \varepsilon_0 - \varepsilon_s$ , that is [76]:

$$V_s = -\frac{1}{2}w_1, \quad U_s = -\varepsilon + \frac{1}{2}w_1, \quad \Phi_s = 4\varepsilon - 8w + 2w_1. \quad (2.11)$$

In the case of antiferroelectric ordering, the proton correlation energies  $V_a, U_a$ , and  $\Phi_a$  are expressed via the antiferroelectric energies  $\varepsilon' = \varepsilon_s - \varepsilon_a, w' = \varepsilon_1 - \varepsilon_a, w'_1 = \varepsilon_0 - \varepsilon_a$  [76]:

$$V_a = \frac{1}{2}\varepsilon' - \frac{1}{2}w'_1, \quad U_a = \frac{1}{2}\varepsilon' + \frac{1}{2}w'_1, \quad \Phi_a = 2\varepsilon' - 8w' + 2w'_1. \quad (2.12)$$

Now, the connection between the ferroelectric and antiferroelectric energies is as follows

$$\varepsilon' = -\varepsilon, \quad w' = w - \varepsilon, \quad w'_1 = w_1 - \varepsilon.$$

In the present paper we calculate the physical characteristics of  $\text{MD}_2\text{XO}_4$  and  $\text{ND}_4\text{D}_2\text{XO}_4$  using only (2.11) and taking into account different types of deuteron ordering in the two types of crystals (2.9), (2.10). Therefore, we shall call the proton ordering model used for the  $\text{KH}_2\text{PO}_4$  family compounds a unified model.

In (2.5) and (2.6)  $\nu_c(0)$  and  $\nu_a(\mathbf{k}_z)$  are the eigenvalues of the  $\sum_{R_q - R_{q'}} J_{ff'}(qq')$  matrices

$$\begin{aligned}4\nu_c(0) &= J_{11}(0) + 2J_{12}(0) + J_{13}(0), \\ 4\nu_a(\mathbf{k}_z) &= J_{11}(\mathbf{k}_z) - J_{13}(\mathbf{k}_z).\end{aligned}$$

The symmetry of the effective dipole moments of hydrogen bonds is as follows:

$$\begin{aligned}\mu_3^{sa} &= \mu_{13} = \mu_{23} = \mu_{33} = \mu_{43}, \\ \mu_1^s &= \mu_{11} = -\mu_{31}, \quad \mu_{21} = \mu_{41} = 0; \quad \mu_2^s = -\mu_{22} = \mu_{42}, \quad \mu_{12} = \mu_{32} = 0, \\ \mu_1^a &= -\mu_{11} = \mu_{31}, \quad \mu_{21} = \mu_{41} = 0; \quad \mu_2^a = \mu_{22} = -\mu_{42}, \quad \mu_{12} = \mu_{32} = 0.\end{aligned}$$

In (2.5), (2.6)  $\Delta_3, \dots, \Delta_{q24}$  are the effective fields exerted by the neighboring hydrogen bonds from outside the cluster. The cluster parameters  $\Delta_3, \dots, \Delta_{q24}$  are determined from the condition of the free energy minimum

$$\frac{\partial F}{\partial \Delta_3} = 0, \dots, \frac{\partial F}{\partial \Delta_{q24}} = 0.$$

This condition is also called a self-consistency condition: the mean values  $\langle \sigma_{qf} \rangle$  calculated within the four-particle and one-particle cluster approximations should coincide. Mathematically, the self-consistency condition is formulated as follows:

$$Sp \left( \hat{\rho}_{q\gamma}^{(4)} \frac{\sigma_{qf}}{2} \right) = Sp \left( \hat{\rho}_{qf\gamma}^{(1)} \frac{\sigma_{qf}}{2} \right), \quad (2.13)$$

where

$$\hat{\rho}_{q\gamma}^{(4)} = \frac{e^{-\beta \hat{H}_{q\gamma}^{(4)}}}{Sp e^{-\beta \hat{H}_{q\gamma}^{(4)}}}, \quad \hat{\rho}_{qf\gamma}^{(1)} = \frac{e^{-\beta \hat{H}_{qf\gamma}^{(4)}}}{Sp e^{-\beta \hat{H}_{qf\gamma}^{(4)}}}.$$

Polarization of  $\text{MD}_2\text{XO}_4$  is determined by the relations

$$\begin{aligned} P_1^s &= \chi_{11}^0 E_1 + \frac{\mu_1^s}{2v} (\eta_{1s}^{(1)x} - \eta_{3s}^{(1)x}), \\ P_2^s &= \chi_{22}^0 E_2 + \frac{\mu_2^s}{2v} (-\eta_{2s}^{(1)y} + \eta_{4s}^{(1)y}), \\ P_3^s &= \chi_{33}^0 E_3 + 2 \frac{\mu_3^s}{v} \eta_s^{(1)z}. \end{aligned} \quad (2.14)$$

Non-zero polarization of  $\text{ND}_4\text{D}_2\text{XO}_4$  arises only in the presence of external electric field

$$\begin{aligned} P_1^a &= \chi_{11}^0 E_1 + \frac{\mu_1^a}{v} \eta_{q13a}^{(1)x}, \\ P_2^a &= \chi_{22}^0 E_2 + \frac{\mu_2^a}{v} \eta_{q24a}^{(1)y}, \\ P_3^a &= \chi_{33}^0 E_3 + \frac{\mu_3^a}{v} (\eta_{q14a}^{(1)z} + \eta_{q23a}^{(1)z}). \end{aligned} \quad (2.15)$$

In (2.14) and (2.15)  $\eta_{fs}^{(1)\gamma}$ ,  $\eta_{q23a}^{(1)\gamma}$  and  $\eta_{q24a}^{(1)\gamma}$  are the single-particle deuteron distribution functions calculated with the four-particle Hamiltonian, with the fields  $\Delta_3^z, \dots, \Delta_{q24}^x$  excluded using (2.13).

Differentiating (2.14) and (2.15) with respect to  $E_\gamma$ , we obtain expressions for the corresponding static susceptibilities of  $\text{MD}_2\text{XO}_4$  and  $\text{ND}_4\text{D}_2\text{XO}_4$ :

$$\begin{aligned} \chi_{11}^s(0) &= \chi_{11}^0 + \bar{v} \frac{(\mu_1^s)^2}{v^2} \frac{1}{2T} \frac{2\chi_1^s}{D_s - 2\chi_1^s \varphi_{1s}^\eta(0)}, \\ \chi_{22}^s(0) &= \chi_{22}^0 + \bar{v} \frac{(\mu_2^s)^2}{v^2} \frac{1}{2T} \frac{2\chi_1^s}{D_s - 2\chi_1^s \varphi_{1s}^\eta(0)}, \\ \chi_{33}^s(0) &= \chi_{33}^0 + \bar{v} \frac{(\mu_3^s)^2}{v^2} \frac{1}{T} \frac{2\chi_3^s}{D_s - 2\chi_3^s \varphi_{3s}^\eta(0)}, \end{aligned} \quad (2.16)$$

$$\begin{aligned} \chi_{11}^a(0) &= \chi_{11}^0 + \bar{v} \frac{(\mu_1^a)^2}{v^2} \frac{1}{2T} \left[ \frac{\chi_1^a}{D_a - 2\chi_1^a \varphi_{1a}^\eta(0)} + \frac{\chi_2^a}{D_a - 2\chi_2^a \varphi_{1a}^\eta(0)} \right], \\ \chi_{22}^a(0) &= \chi_{22}^0 + \bar{v} \frac{(\mu_2^a)^2}{v^2} \frac{1}{2T} \left[ \frac{\chi_1^a}{D_a - 2\chi_1^a \varphi_{1a}^\eta(0)} + \frac{\chi_2^a}{D_a - 2\chi_2^a \varphi_{1a}^\eta(0)} \right], \\ \chi_{33}^a(0) &= \chi_{33}^0 + \bar{v} \frac{(\mu_3^a)^2}{v^2} \frac{1}{T} \frac{2\chi_3^a}{D_a - 2\chi_3^a \varphi_{3a}^\eta(0)}. \end{aligned} \quad (2.17)$$

Here we use the following notations

$$\begin{aligned}
\mathcal{z}_1^s &= a + b\text{ch}z^s, \\
\mathcal{z}_3^s &= (\text{ch}2z^s + b\text{ch}z^s) - \eta_s^{(1)}(\text{sh}2z^s + 2b\text{sh}z^s), \\
\mathcal{z}_1^a &= a + b\text{ch}z^a, \\
\mathcal{z}_2^a &= (a\text{ch}2z^a + b\text{ch}z^a) - \eta_a^{(1)}(a\text{sh}2z^a + 2b\text{sh}z^a), \\
\mathcal{z}_3^a &= 1 + b\text{ch}z^a, \\
\varphi_{3s}^\eta(0) &= \frac{1}{1 - (\eta_s^{(1)})^2} + \beta\nu_c^s(0), \quad \varphi_{1s}^\eta(0) = \frac{1}{1 - (\eta_s^{(1)})^2} + \beta\nu_a^s(0), \\
\varphi_{3a}^\eta(0) &= \frac{1}{1 - (\eta_a^{(1)})^2} + \beta\nu_c^a(0), \quad \varphi_{1a}^\eta(0) = \frac{1}{1 - (\eta_a^{(1)})^2} + \beta\nu_a^a(0).
\end{aligned}$$

If there is no external field, then

$$\begin{aligned}
\eta_s^{(1)} &= \frac{1}{D_s}(\text{sh}2z^s + 2b\text{sh}z^s), \\
\eta_a^{(1)} &= \frac{1}{D_a}(a\text{sh}2z^a + 2b\text{sh}z^a),
\end{aligned} \tag{2.18}$$

where

$$\begin{aligned}
D_s &= \text{ch}2z^s + 4b\text{ch}z^s + 2a + d, \\
D_a &= a\text{ch}2z^a + 4b\text{ch}z^a + a + d + 1, \\
a &= e^{-\beta\varepsilon}, \quad b = e^{-\beta w}, \quad d = e^{-\beta w_1},
\end{aligned}$$

and

$$z^s = \frac{1}{2} \ln \frac{1 + \eta_s^{(1)}}{1 - \eta_s^{(1)}} + \beta\nu_c^s(0)\eta_s^{(1)}, \quad z^a = \frac{1}{2} \ln \frac{1 + \eta_a^{(1)}}{1 - \eta_a^{(1)}} + \beta\nu_a(\mathbf{k}_z)\eta_a^{(1)}.$$

In the paraelectric phase, due to the unified choice of the short-range deuteron energies in MD<sub>2</sub>XO<sub>4</sub> and ND<sub>4</sub>D<sub>2</sub>XO<sub>4</sub>, the obtained expressions for the static susceptibilities are identical

$$\begin{aligned}
\chi_{11p}^{s,a}(0) &= \chi_{11}^0 + \bar{v} \frac{\mu_1^2}{v^2 T} \frac{1}{2b + d + 1 - 2(a + b)\beta\nu_a(0)} (a + b), \\
\chi_{33p}^{s,a}(0) &= \chi_{33}^0 + \bar{v} \frac{\mu_3^2}{v^2 T} \frac{1}{2a + 2b + d - 1 - 2(1 + b)\beta\nu_c(0)} (1 + b).
\end{aligned} \tag{2.19}$$

Now we shall calculate the thermal characteristics of deuteron subsystems of the MD<sub>2</sub>XO<sub>4</sub> and ND<sub>4</sub>D<sub>2</sub>XO<sub>4</sub> crystals. From (2.3) we find the free energy of the deuteron subsystem in the absence of external field  $E_\gamma$ :

$$f_{s,a} = \frac{F_{s,a}}{N} = 2\nu_i(\mathbf{k})\eta_{s,a}^{(1)2} + 2T \ln 2 - 2T \ln[1 - \eta_{s,a}^{(1)2}] - 2T \ln D_{s,a}, \tag{2.20}$$

where  $\nu_i(\mathbf{k}) = \nu_c^s(0)$  (MD<sub>2</sub>XO<sub>4</sub>) and  $\nu_i(\mathbf{k}) = \nu_a^a(\mathbf{k}_z)$  (ND<sub>4</sub>D<sub>2</sub>XO<sub>4</sub>).

The molar entropy reads

$$S_{s,a} = -R \frac{\partial f_{s,a}}{\partial T} = R \left\{ 2 \ln \frac{D_{s,a}}{2} (1 - \eta_{s,a}^{(1)2}) + 4T \varphi_{s,a}^T \eta_{s,a}^{(1)} + 2 \frac{M_{s,a}}{D_{s,a}} \right\}, \tag{2.21}$$

where R is the gas constant, and

$$\begin{aligned}
\varphi_s^T &= -\frac{1}{T^2} \tilde{\nu}_3(0)\eta_s^{(1)}, \quad \varphi_a^T = -\frac{1}{T^2} \tilde{\nu}_1(\mathbf{k}_z)\eta_a^{(1)}, \quad \tilde{\nu}_i(\mathbf{k}) = \frac{\nu_i(\mathbf{k})}{k_B}, \\
M_s &= 4b \frac{\tilde{w}}{T} \text{ch}z^s + 2a \frac{\tilde{\varepsilon}}{T} + d \frac{\tilde{w}_1}{T}, \quad \tilde{w} = \frac{w}{k_B}, \quad \tilde{\varepsilon} = \frac{\varepsilon}{k_B}, \quad \tilde{w}_1 = \frac{w_1}{k_B}, \\
M_a &= a \frac{\tilde{\varepsilon}}{T} \text{ch}2z^a + 4b \frac{\tilde{w}}{T} \text{ch}z^a + a \frac{\tilde{\varepsilon}}{T} + d \frac{\tilde{w}_1}{T}.
\end{aligned}$$

In the paraelectric phase the molar entropy is

$$S_{s,a} = R \left\{ 2 \ln \frac{1}{2} (2a + 4b + d + 1) + \frac{2}{T} \frac{2a\tilde{\varepsilon} + 4b\tilde{w} + d\tilde{w}_1}{2a + 4b + d + 1} \right\}.$$

Contributions of deuteron subsystems to the molar specific heat of the  $\text{MD}_2\text{XO}_4$  and  $\text{ND}_4\text{D}_2\text{XO}_4$  crystals are obtained from the entropy

$$\begin{aligned} \Delta C_{s,a} &= T \frac{\partial S_{s,a}}{\partial T} = \frac{2R}{D_{s,a}} \left\{ 2T \varphi_{s,a}^T (q_{s,a} - \eta_{s,a}^{(1)} M_{s,a}) + N_{s,a} - \frac{M_{s,a}^2}{D_{s,a}} \right\} \\ &+ \frac{4R}{D_{s,a}} \frac{1}{D_{s,a} - 2\chi_{3,2}^{s,a} \varphi_i^\eta(\mathbf{k})} \left[ D_{s,a} T \varphi_{s,a}^T + (q_{s,a} - \eta_{s,a}^{(1)} M_{s,a}) \varphi_i^\eta(\mathbf{k}) \right] \\ &\times [2\chi_{3,2}^{s,a} T \varphi_{s,a}^T + (q_{s,a} - \eta_{s,a}^{(1)} M_{s,a})]. \end{aligned} \quad (2.22)$$

Here we use the notations

$$\begin{aligned} N_s &= 4b \left( \frac{\tilde{w}}{T} \right)^2 \text{ch} z^s + 2a \left( \frac{\tilde{\varepsilon}}{T} \right)^2 + d \left( \frac{\tilde{w}_1}{T} \right)^2, \\ N_a &= a \left( \frac{\tilde{\varepsilon}}{T} \right)^2 \text{ch} 2z^a + 4b \left( \frac{\tilde{w}}{T} \right)^2 \text{ch} z^a + a \left( \frac{\tilde{\varepsilon}}{T} \right)^2 + d \left( \frac{\tilde{w}_1}{T} \right)^2, \\ \varphi_3^\eta(0) &= \varphi_{3s}^\eta(0), \quad \varphi_1^\eta(\mathbf{k}_z) = \frac{1}{1 - \eta_a^{(1)z}} + \frac{\nu_a(\mathbf{k}_z)}{T}, \\ q_s &= 2b \frac{\tilde{w}}{T} \text{sh} z^s, \quad q_a = a \frac{\tilde{\varepsilon}}{T} \text{sh} 2z^a + 2b \frac{\tilde{w}}{T} \text{sh} z^a. \end{aligned}$$

### 3. Longitudinal relaxation of $\text{MD}_2\text{XO}_4$ and $\text{ND}_4\text{D}_2\text{XO}_4$

The dynamic characteristics of the  $\text{MD}_2\text{XO}_4$  and  $\text{ND}_4\text{D}_2\text{XO}_4$  crystals will be explored using the dynamic model of deuterated orthophosphates based on a stochastic Glauber model [143]. Using the method developed in [144–154], the system of equations for the time-dependent deuteron distribution functions is obtained as follows:

$$-\alpha \frac{d}{dt} \left\langle \prod_f \sigma_{qf} \right\rangle = \sum_{f'} \left\langle \prod_f \sigma_{qf} \left[ 1 - \sigma_{qf'} \text{th} \frac{\beta}{2} \varepsilon_{qf'}^{\gamma s,a} \right] \right\rangle, \quad (3.1)$$

where  $\alpha$  is the time constant that effectively determines the time scale of the dynamic processes in the system;  $\varepsilon_{qf}^{\gamma s,a}$  is the local field in the presence of the external field  $E_\gamma(\gamma = \overset{1,2,3}{x,y,z})$ , acting on the deuteron of the  $f$ -th bond in the  $q$ -th cell. Using the Hamiltonian (2.4), we obtain the following expressions

$$\text{th} \frac{\beta}{2} \varepsilon_{qf}^{zs} = \text{th} \frac{\beta}{2} \left( \varepsilon_{qf}^{s,a} + \frac{z^{zs}}{\beta} \right), \quad \text{th} \frac{\beta}{2} \varepsilon_{q_1^a}^{za} = \text{th} \frac{\beta}{2} \left( \varepsilon_{qf}^{s,a} + \frac{z_{q_1^a}^{za}}{\beta} \right), \quad \text{th} \frac{\beta}{2} \varepsilon_{q_3^a}^{za} = \text{th} \frac{\beta}{2} \left( \varepsilon_{qf}^{s,a} + \frac{z_{q_2^a}^{za}}{\beta} \right). \quad (3.2)$$

Here we use the notations

$$\begin{aligned} \varepsilon_{q_1^a}^{s,a} &= -V \left( \frac{\sigma_{q_2}}{2} + \frac{\sigma_{q_4}}{2} \right) - U \frac{\sigma_{q_3}}{2} - \Phi \frac{\sigma_{q_2}}{2} \frac{\sigma_{q_3}}{2} \frac{\sigma_{q_4}}{2}, \\ \varepsilon_{q_2^a}^{s,a} &= -V \left( \frac{\sigma_{q_1}}{2} + \frac{\sigma_{q_3}}{2} \right) - U \frac{\sigma_{q_4}}{2} - \Phi \frac{\sigma_{q_1}}{2} \frac{\sigma_{q_3}}{2} \frac{\sigma_{q_4}}{2}, \\ \varepsilon_{q_3^a}^{s,a} &= -V \left( \frac{\sigma_{q_2}}{2} + \frac{\sigma_{q_4}}{2} \right) - U \frac{\sigma_{q_1}}{2} - \Phi \frac{\sigma_{q_1}}{2} \frac{\sigma_{q_2}}{2} \frac{\sigma_{q_4}}{2}, \\ \varepsilon_{q_4^a}^{s,a} &= -V \left( \frac{\sigma_{q_1}}{2} + \frac{\sigma_{q_3}}{2} \right) - U \frac{\sigma_{q_2}}{2} - \Phi \frac{\sigma_{q_1}}{2} \frac{\sigma_{q_2}}{2} \frac{\sigma_{q_3}}{2}. \end{aligned} \quad (3.3)$$

The right hand sides of (3.2) can be written as

$$\begin{aligned}
\text{th} \frac{\beta}{2} \varepsilon_{q_1}^{\gamma s, a} &= P_{q_1}^{\gamma s, a} \sigma_{q_3} + Q_{q_1}^{\gamma s, a} (\sigma_{q_2} + \sigma_{q_4}) + R_{q_1}^{\gamma s, a} \sigma_{q_2} \sigma_{q_3} \sigma_{q_4} \\
&\quad + N_{q_1}^{\gamma s, a} \sigma_{q_2} \sigma_{q_4} + M_{q_1}^{\gamma s, a} \sigma_{q_3} (\sigma_{q_2} + \sigma_{q_4}) + L_{q_1}^{\gamma s, a}, \\
\text{th} \frac{\beta}{2} \varepsilon_{q_2}^{\gamma s, a} &= P_{q_2}^{\gamma s, a} \sigma_{q_4} + Q_{q_2}^{\gamma s, a} (\sigma_{q_1} + \sigma_{q_3}) + R_{q_2}^{\gamma s, a} \sigma_{q_1} \sigma_{q_3} \sigma_{q_4} \\
&\quad + N_{q_2}^{\gamma s, a} \sigma_{q_1} \sigma_{q_3} + M_{q_2}^{\gamma s, a} \sigma_{q_4} (\sigma_{q_1} + \sigma_{q_3}) + L_{q_2}^{\gamma s, a}, \\
\text{th} \frac{\beta}{2} \varepsilon_{q_3}^{\gamma s, a} &= P_{q_3}^{\gamma s, a} \sigma_{q_1} + Q_{q_3}^{\gamma s, a} (\sigma_{q_2} + \sigma_{q_4}) + R_{q_3}^{\gamma s, a} \sigma_{q_1} \sigma_{q_2} \sigma_{q_4} \\
&\quad + N_{q_3}^{\gamma s, a} \sigma_{q_2} \sigma_{q_4} + M_{q_3}^{\gamma s, a} \sigma_{q_1} (\sigma_{q_2} + \sigma_{q_4}) + L_{q_3}^{\gamma s, a}, \\
\text{th} \frac{\beta}{2} \varepsilon_{q_4}^{\gamma s, a} &= P_{q_4}^{\gamma s, a} \sigma_{q_2} + Q_{q_4}^{\gamma s, a} (\sigma_{q_1} + \sigma_{q_3}) + R_{q_4}^{\gamma s, a} \sigma_{q_1} \sigma_{q_2} \sigma_{q_3} \\
&\quad + N_{q_4}^{\gamma s, a} \sigma_{q_1} \sigma_{q_3} + M_{q_4}^{\gamma s, a} \sigma_{q_2} (\sigma_{q_1} + \sigma_{q_3}) + L_{q_4}^{\gamma s, a}.
\end{aligned} \tag{3.4}$$

Equating the right hand sides of (3.2) and (3.4) and taking into account the fact that  $\sigma_{qf} = \pm 1$ , we obtain the following relations for the coefficients  $P_{q_1}^{\gamma s, a}, \dots, L_{q_4}^{\gamma s, a}$ :

$$\begin{aligned}
P_{qf}^{\gamma s, a} &= \frac{1}{8} (l_{qf1}^{\gamma s, a} - l_{qf2}^{\gamma s, a} + 2m_{qf1}^{\gamma s, a} - 2m_{qf2}^{\gamma s, a} + n_{qf1}^{\gamma s, a} - n_{qf1}^{\gamma s, a}), \\
Q_{qf}^{\gamma s, a} &= \frac{1}{8} (l_{qf1}^{\gamma s, a} - l_{qf2}^{\gamma s, a} - n_{qf1}^{\gamma s, a} + n_{qf1}^{\gamma s, a}), \\
R_{qf}^{\gamma s, a} &= \frac{1}{8} (l_{qf1}^{\gamma s, a} - l_{qf2}^{\gamma s, a} - 2m_{qf1}^{\gamma s, a} + 2m_{qf2}^{\gamma s, a} + n_{qf1}^{\gamma s, a} - n_{qf1}^{\gamma s, a}), \\
N_{qf}^{\gamma s, a} &= \frac{1}{8} (l_{qf1}^{\gamma s, a} + l_{qf2}^{\gamma s, a} - 2m_{qf1}^{\gamma s, a} - 2m_{qf2}^{\gamma s, a} + n_{qf1}^{\gamma s, a} + n_{qf1}^{\gamma s, a}), \\
M_{qf}^{\gamma s, a} &= \frac{1}{8} (l_{qf1}^{\gamma s, a} + l_{qf2}^{\gamma s, a} - n_{qf1}^{\gamma s, a} - n_{qf1}^{\gamma s, a}), \\
L_{qf}^{\gamma s, a} &= \frac{1}{8} (l_{qf1}^{\gamma s, a} + l_{qf2}^{\gamma s, a} + 2m_{qf1}^{\gamma s, a} + 2m_{qf2}^{\gamma s, a} + n_{qf1}^{\gamma s, a} + n_{qf1}^{\gamma s, a}).
\end{aligned} \tag{3.5}$$

Here we use the following notations

$$\begin{aligned}
l_{f_2}^{\gamma s} &= \text{th} [\pm \frac{\beta}{2} w + \frac{1}{2} z_f^{\gamma s}], \quad m_{f_2}^{\gamma s} = \text{th} [\pm \frac{\beta}{2} (\varepsilon - w) + \frac{1}{2} z_f^{\gamma s}], \quad n_{f_2}^{\gamma s} = \text{th} [\pm \frac{\beta}{2} (w - w_1) + \frac{1}{2} z_f^{\gamma s}], \\
l_{qf_2}^{za} &= \text{th} [\pm \frac{\beta}{2} w + \frac{1}{2} z_{qf}^{za}], \quad m_{qf_2}^{za} = \text{th} [\pm \frac{\beta}{2} (\varepsilon - w) + \frac{1}{2} z_{qf}^{za}], \quad n_{qf_2}^{za} = \text{th} [\pm \frac{\beta}{2} (w - w_1) + \frac{1}{2} z_{qf}^{za}].
\end{aligned} \tag{3.6}$$

To obtain the system of equations for the time-dependent deuteron distribution functions we have to take into account the symmetry of the static distribution functions:

$$\begin{aligned}
\eta_s^{(3)z} &= \langle \sigma_{q_1} \sigma_{q_2} \sigma_{q_3} \rangle = \langle \sigma_{q_1} \sigma_{q_2} \sigma_{q_4} \rangle = \langle \sigma_{q_1} \sigma_{q_3} \sigma_{q_4} \rangle = \langle \sigma_{q_2} \sigma_{q_3} \sigma_{q_4} \rangle, \\
\eta_{1s}^{(2)z} &= \langle \sigma_{q_1} \sigma_{q_2} \rangle = \langle \sigma_{q_2} \sigma_{q_3} \rangle = \langle \sigma_{q_3} \sigma_{q_4} \rangle = \langle \sigma_{q_4} \sigma_{q_1} \rangle, \\
\eta_{2s}^{(2)z} &= \langle \sigma_{q_1} \sigma_{q_3} \rangle = \langle \sigma_{q_2} \sigma_{q_4} \rangle,
\end{aligned} \tag{3.7}$$

$$\begin{aligned}
\eta_{q_{14a}}^{(3)z} &= \langle \sigma_{q_1} \sigma_{q_2} \sigma_{q_3} \rangle = \langle \sigma_{q_2} \sigma_{q_3} \sigma_{q_4} \rangle, \quad \eta_{q_{23a}}^{(3)z} = \langle \sigma_{q_1} \sigma_{q_2} \sigma_{q_4} \rangle = \langle \sigma_{q_1} \sigma_{q_3} \sigma_{q_4} \rangle, \\
\eta_{q_{14a}}^{(2)z} &= \langle \sigma_{q_1} \sigma_{q_4} \rangle, \quad \eta_{q_{12a}}^{(2)z} = \langle \sigma_{q_2} \sigma_{q_3} \rangle, \\
\eta_{q_{2a}}^{(2)z} &= -\langle \sigma_{q_1} \sigma_{q_2} \rangle = -\langle \sigma_{q_3} \sigma_{q_4} \rangle, \quad \eta_{q_{3a}}^{(2)z} = -\langle \sigma_{q_1} \sigma_{q_3} \rangle = -\langle \sigma_{q_2} \sigma_{q_4} \rangle.
\end{aligned} \tag{3.8}$$

Now, using (3.1) and (3.4) and taking into account the corresponding symmetry relations for the distribution functions (3.7) and (3.8), within the framework of the four-particle and single-particle approximations, we can obtain closed systems of five equations for MD<sub>2</sub>XO<sub>4</sub> and eight



equations for  $\text{ND}_4\text{D}_2\text{XO}_4$  for the time-dependent single-particle, four-particle, and pair deuteron distribution functions in the presence of the field  $E_3$  [198].

Let us consider now the case of small deviations of the considered system from equilibrium. We can separate in the obtained system of equations the static and dynamic parts. To do so, we present the distribution functions and the effective fields as sums of the equilibrium functions at  $E_3 = 0$  and their fluctuations

$$\begin{aligned} \eta_s^{(1)z} &= \eta_s^{(1)} + \eta_{st}^{(1)z}, \quad \eta_s^{(3)z} = \eta_s^{(3)} + \eta_{st}^{(3)z}, \quad \eta_{1s}^{(2)z} = \eta_{1s}^{(2)} + \eta_{1st}^{(2)z}, \quad \eta_{2s}^{(2)z} = \eta_{2s}^{(2)} + \eta_{2st}^{(2)z}, \\ z^{zs} &= z^s + z_t^{zs} = z^s + [-\beta\Delta_{3t}^z + 2\beta\nu_c^s(0)\eta_{st}^{(1)z} + \beta\mu_3^s E_{3t}], \end{aligned} \quad (3.9)$$

$$\begin{aligned} \eta_{q_{23}^{14}a}^{(1)z} &= \mp\eta_{qa}^{(1)} + \eta_{at}^{(1)z}, \quad \eta_{q_{23}^{14}a}^{(3)z} = \mp\eta_{qa}^{(3)} + \eta_{at}^{(3)z}, \quad \eta_{q_{12}^{11}a}^{(2)z} = \eta_{1a}^{(2)} \mp\eta_{qat}^{(2)z}, \quad \eta_{q_{2a}^{(2)z}} = \eta_{2a}^{(2)}, \quad \eta_{q_{3a}^{(2)z}} = \eta_{3a}^{(2)}, \\ z_{q_{23}^{14}a}^{za} &= \mp z^a + z_t^{za} = \mp z^a + [-\beta\Delta_{at}^z + 2\beta\nu_c^a(0)\eta_{at}^{(1)z} + \beta\mu_3^a E_{3t}]. \end{aligned} \quad (3.10)$$

The static distribution functions at  $E_3 = 0$  read

$$\begin{aligned} \eta_s^{(3)} &= \frac{1}{D_s}(\text{sh}2z^s - 2\text{bsh}z^s), \\ \eta_{1s}^{(2)} &= \frac{1}{D_s}(\text{ch}2z^s - d), \quad \eta_{2s}^{(2)} = \frac{1}{D_s}(\text{ch}2z^s - 2a + d), \\ \eta_a^{(3)} &= \frac{1}{D_a}(\text{ash}2z^a - 2\text{bsh}z^a), \\ \eta_{1a}^{(2)} &= \frac{1}{D_a}(\text{ach}2z^a - a - d + 1), \quad \eta_{2a}^{(2)} = \frac{1}{D_a}(\text{ach}2z^a - a + d - 1), \\ \eta_{3a}^{(2)} &= \frac{1}{D_a}(\text{ach}2z^a + a - d - 1). \end{aligned} \quad (3.11)$$

We expand the expressions for the coefficients  $P_{qf}^{\gamma s,a}, \dots, L_{qf}^{\gamma s,a}$  (3.5) in series in  $z_t^{zs,a}, z_{ft}^{xs,a}$ , respectively, up to the linear terms, neglecting the uniform field  $E_3$ . We get

$$\begin{aligned} P^{zs} &= P_0^s + \frac{z_t^{zs}}{2}P_1^s, \quad N^{zs} = N_0^s + \frac{z_t^{zs}}{2}N_1^s, \\ Q^{zs} &= Q_0^s + \frac{z_t^{zs}}{2}Q_1^s, \quad M^{zs} = M_0^s + \frac{z_t^{zs}}{2}M_1^s, \\ R^{zs} &= R_0^s + \frac{z_t^{zs}}{2}R_1^s, \quad L^{zs} = L_0^s + \frac{z_t^{zs}}{2}L_1^s, \\ P_{q_{23}^{14}a}^{za} &= P_0^a \mp \frac{z_t^{za}}{2}P_{q1}^a, \quad N_{q_{23}^{14}a}^{za} = \mp N_{q0}^a + \frac{z_t^{za}}{2}N_1^a, \\ Q_{q_{23}^{14}a}^{za} &= Q_0^a \mp \frac{z_t^{za}}{2}Q_{q1}^a, \quad M_{q_{23}^{14}a}^{za} = \mp M_{q0}^a + \frac{z_t^{za}}{2}M_1^a, \\ R_{q_{23}^{14}a}^{za} &= R_0^a \mp \frac{z_t^{za}}{2}R_{q1}^a, \quad L_{q_{23}^{14}a}^{za} = \mp L_{q0}^a + \frac{z_t^{za}}{2}L_1^a. \end{aligned} \quad (3.12)$$

In the case of  $\text{MD}_2\text{XO}_4$   $\mathbf{k} = 0$  and  $N_{q0}^{s,a} = N_0^s, \dots, R_{q1}^{s,a} = R_1^s$ , and in the case of  $\text{ND}_4\text{D}_2\text{XO}_4$   $\mathbf{k} = \mathbf{k}_z$  and  $N_{q0}^{s,a} = N_{q0}^a, \dots, R_{q1}^{s,a} = R_{q1}^a$ . The explicit expressions for these coefficients are given in [198].

Substituting the expansions (3.9), (3.10) and (3.12) into the corresponding system of equations and excluding  $\Delta_{st}^z$ , we obtain the following system of equations for the fluctuation parts of the deuteron distribution functions in the presence of the field  $E_3$ :

$$\frac{d}{dt} \begin{pmatrix} \eta_{st}^{(1)z} \\ \eta_{st}^{(3)z} \\ \eta_{1st}^{(2)z} \\ \eta_{2st}^{(2)z} \end{pmatrix} = \begin{pmatrix} c_{11}^s & c_{12}^s & c_{13}^s & c_{14}^s \\ c_{21}^s & c_{22}^s & c_{23}^s & c_{24}^s \\ c_{31}^s & c_{32}^s & c_{33}^s & c_{34}^s \\ c_{41}^s & c_{42}^s & c_{43}^s & c_{44}^s \end{pmatrix} \begin{pmatrix} \eta_{st}^{(1)z} \\ \eta_{st}^{(3)z} \\ \eta_{1st}^{(2)z} \\ \eta_{2st}^{(2)z} \end{pmatrix} - \begin{pmatrix} c_1^s \\ c_2^s \\ c_3^s \\ c_4^s \end{pmatrix} \frac{\mu_3^s E_{3t}}{2k_B T}, \quad (3.13)$$

$$\frac{d}{dt} \begin{pmatrix} \eta_{at}^{(1)z} \\ \eta_{at}^{(3)z} \\ \eta_{at}^{(2)z} \\ \eta_{qat} \end{pmatrix} = \begin{pmatrix} c_{11}^a & c_{12}^a & c_{q13}^a \\ c_{21}^a & c_{22}^a & c_{q23}^a \\ c_{q31}^a & c_{q32}^a & c_{33}^a \end{pmatrix} \begin{pmatrix} \eta_{at}^{(1)z} \\ \eta_{at}^{(3)z} \\ \eta_{at}^{(2)z} \\ \eta_{qat} \end{pmatrix} - \begin{pmatrix} c_1^a \\ c_2^a \\ c_{q3}^a \end{pmatrix} \frac{\mu_3^a E_{3t}}{2k_B T}. \quad (3.14)$$

Coefficients of the systems (3.13) and (3.14) are as follows:

$$\begin{aligned} c_{11}^{s,a} &= \frac{1}{\alpha} [(-1 + P_0^{s,a} + 2Q_0^{s,a}) - k_{s,a}(P_0^{s,a} + 2Q_0^{s,a}) - \beta\nu_c^{s,a}(0)k_{s,a}\varphi_{s,a}], \\ c_{12}^{s,a} &= \frac{1}{\alpha} (R_0^{s,a} - k_{s,a}R_0^{s,a}), \quad c_{13}^s = \frac{1}{\alpha} (2M_0^s - k_s 2M_0^s), \\ c_{14}^s &= \frac{1}{\alpha} (N_0^s - k_s N_0^s), \quad c_{q13}^a = \frac{1}{\alpha} (-M_{q0}^a + k_a M_{q0}^a), \\ c_{21}^{s,a} &= \frac{1}{\alpha} [(2P_0^{s,a} + 4Q_0^{s,a} + 3R_0^{s,a}) - l_{s,a}(P_0^{s,a} + 2Q_0^{s,a}) - \beta\nu_c^{s,a}(0)l_{s,a}\varphi_{s,a}], \\ c_{22}^{s,a} &= \frac{1}{\alpha} [-(3 - P_0^{s,a} - 2Q_0^{s,a}) - l_{s,a}R_0^{s,a}], \quad c_{23}^s = \frac{1}{\alpha} [2(N_0^s + M_0^s + L_0^s) - l_{s,a}2M_0^s], \\ c_{24}^s &= \frac{1}{\alpha} [(2M_0^s + L_0^s) - l_s N_0^s], \quad c_{q23}^a = \frac{1}{\alpha} [-(N_{q0}^a + M_{q0}^a + L_{q0}^a) + l_a M_{q0}^a], \\ c_{q31}^{s,a} &= \frac{1}{\alpha} [2(N_{q0}^{s,a} + M_{q0}^{s,a} + L_{q0}^{s,a}) - m_{qs,a}(P_0^{s,a} + 2Q_0^{s,a}) - \beta\nu_c^{s,a}(0)m_{qs,a}\varphi_{s,a}], \\ c_{q32}^{s,a} &= \frac{1}{\alpha} [2M_{q0}^{s,a} - m_{qs,a}R_0^{s,a}], \quad c_{33}^s = \frac{1}{\alpha} [-2(1 - P_0^s - R_0^s) - m_s 2M_0^s], \\ c_{34}^s &= \frac{1}{\alpha} [2Q_0^s - m_s N_0^s], \quad c_{33}^a = \frac{1}{\alpha} [-2(1 + R_0^a) + m_{qa} M_{q0}^a], \\ c_{41}^s &= \frac{1}{\alpha} [2(2M_0^s + L_0^s) - n_s(P_0^s + 2Q_0^s) - \beta\nu^s(0)n_s\varphi_s], \\ c_{42}^s &= \frac{1}{\alpha} [2N_0^s - n_s R_0^s], \quad c_{43}^s = \frac{1}{\alpha} [4Q_0^s - n_s 2M_0^s], \quad c_{44}^s = \frac{1}{\alpha} [-2(1 - R_0^s) - n_s N_0^s], \\ c_1^{s,a} &= \frac{1}{\alpha} k_{s,a}\varphi_{s,a}, \quad c_2^{s,a} = \frac{1}{\alpha} l_{s,a}\varphi_{s,a}, \quad c_{q3}^{s,a} = \frac{1}{\alpha} m_{qs,a}\varphi_{s,a}, \quad c_4^s = \frac{1}{\alpha} n_s\varphi_s, \end{aligned}$$

where

$$\begin{aligned} k_{s,a} &= X_{s,a}^{(1)}(X_{s,a}^{(1)} - 2\varphi_{s,a})^{-1}, \quad l_{s,a} = X_{s,a}^{(3)}(X_{s,a}^{(1)} - 2\varphi_{s,a})^{-1}, \\ m_{qs,a} &= X_{q1s,a}^{(2)}(X_{s,a}^{(1)} - 2\varphi_{s,a})^{-1}, \quad n_s = X_{2s}^{(2)}(X_s^{(1)} - 2\varphi_s)^{-1}, \\ \varphi_{s,a} &= 1 - (\eta_{s,a}^{(1)})^2, \\ X_s^{(1)} &= (P_1^s + 2Q_1^s)\eta_s^{(1)} + R_1^s\eta_s^{(3)} + 2M_1^s\eta_{1s}^{(2)} + N_1^s\eta_{2s}^{(2)} + L_1^s, \\ X_a^{(1)} &= -P_{q1}^a\eta_{qa}^{(1)} + R_{q1}^a\eta_{qa}^{(3)} + M_1^a\eta_{1a}^{(2)} - M_1^a\eta_{2a}^{(2)} - N_1^a\eta_{3a}^{(2)} + L_1^a, \\ X_s^{(3)} &= (2P_1^s + 4Q_1^s + 3R_1^s)\eta_s^{(1)} + (P_1^s + 2Q_1^s)\eta_s^{(3)} \\ &\quad + 2(N_1^s + M_1^s + L_1^s)\eta_{1s}^{(2)} + (2M_1^s + L_1^s)\eta_{2s}^{(2)} + 2M_1^s + N_1^s, \\ X_a^{(3)} &= -(2Q_{q1}^a + R_{q1}^a)\eta_{qa}^{(1)} + (P_{q1}^a + 2Q_{q1}^a)\eta_{qa}^{(3)} \\ &\quad + (N_1^a + M_1^a + L_1^a)(\eta_{1a}^{(2)} - \eta_{2a}^{(2)}) - (2M_1^a + L_1^a)\eta_{3a}^{(2)} + 2M_1^a + N_1^a, \\ X_{1s}^{(2)} &= 2(N_1^s + M_1^s + L_1^s)\eta_s^{(1)} + 2M_1^s\eta_s^{(3)} + 2(P_1^s + R_1^s)\eta_{1s}^{(2)} + 2Q_1^s\eta_{2s}^{(2)} + 2Q_1^s, \\ X_{q1a}^{(2)} &= 2(-(N_1^a + M_1^a - L_1^a)\eta_{qa}^{(1)} + M_1^a\eta_{qa}^{(3)} + R_{q1}^a\eta_{1a}^{(2)} - P_{q1}^a\eta_{2a}^{(2)} - Q_{q1}^a\eta_{3a}^{(2)} + Q_{q1}^a), \\ X_{2s}^{(2)} &= 2(2M_1^s + L_1^s)\eta_s^{(1)} + 2N_1^s\eta_s^{(3)} + 4Q_1^s\eta_{1s}^{(2)} + 2R_1^s\eta_{2s}^{(2)} + 2P_1^s. \end{aligned}$$

From (3.13) and (3.14) we find the following expressions for the single-particle distribution functions  $\eta_{st}^{(1)z}$ :

$$\eta_{st}^{(1)z} = \sum_{i=1}^4 c_{is}^z e^{-\frac{z}{\tau_{is}}} + \frac{\mu_3^a E_{3t}}{2k_B T} \frac{(i\omega)^3 n^{z(3)} + (i\omega)^2 n^{z(2)} + (i\omega) n^{z(1)} + n^{z(0)}}{(i\omega)^4 + (i\omega)^3 n_3^z + (i\omega)^2 n_2^z + (i\omega) n_1^z + n_0^z}, \quad (3.15)$$

$$\eta_{at}^{(1)z} = \sum_{i=1}^3 c_{ia}^z e^{-\frac{t}{\tau_{ia}^z}} + \frac{\mu_3^a E_{3t}}{2k_B T} \frac{(i\omega)^2 m^{z(2)} + (i\omega) m^{z(1)} + m^{z(0)}}{(i\omega)^3 + (i\omega)^2 m_2^z + (i\omega) m_1^z + m_0^z}, \quad (3.16)$$

where  $c_{is,a}^z$  are constant coefficients;  $\tau_{is,a}^z = -\frac{1}{q_{is,a}^z}$  are the relaxation times, and  $q_{is,a}^z$  are roots of the characteristic equations

$$(q_s^z)^4 + (q_s^z)^3 n_3^z + (q_s^z)^2 n_2^z + (q_s^z) n_1^z + n_0^z = 0,$$

$$(q_a^z)^3 + (q_a^z)^2 m_2^z + (q_a^z) m_1^z + m_0^z = 0.$$

Taking into account (3.15), we find the dynamic dielectric susceptibility of the  $\text{MD}_2\text{XO}_4$  crystals

$$\begin{aligned} \chi_{33}^s(\omega) &= \chi_{33}^{0s} + 2 \frac{\mu_3^s}{v} \lim_{E_{3t} \rightarrow 0} \frac{d\eta_{st}^{(1)z}}{dE_{3t}} \\ &= \chi_{33}^{0s} + \bar{v} \frac{(\mu_3^s)^2}{v^2} \frac{1}{T} \frac{\tau_{1s}^z \tau_{2s}^z \tau_{3s}^z \tau_{4s}^z [(i\omega)^3 n^{z(3)} + (i\omega)^2 n^{z(2)} + (i\omega) n^{z(1)} + n^{z(0)}]}{(1 + i\omega\tau_{1s}^z)(1 + i\omega\tau_{2s}^z)(1 + i\omega\tau_{3s}^z)(1 + i\omega\tau_{4s}^z)} \\ &= \chi_{33}^{0s} + \sum_{j=1}^4 \frac{\chi_{js}^z}{1 + i\omega\tau_{js}^z}. \end{aligned} \quad (3.17)$$

Respectively, the dynamic permittivity of  $\text{MD}_2\text{XO}_4$  reads

$$\varepsilon_{33}^{s'}(\omega) = \varepsilon_{33}^{0s} + \sum_{j=1}^4 \frac{4\pi\chi_{js}^z}{1 + (\omega\tau_{js}^z)^2}, \quad \varepsilon_{33}^{s''}(\omega) = \sum_{j=1}^4 \frac{4\pi\chi_{js}^z \omega\tau_{js}^z}{1 + (\omega\tau_{js}^z)^2}. \quad (3.18)$$

The dynamic susceptibility of  $\text{ND}_4\text{D}_2\text{XO}_4$  is obtained from (3.16) in the form

$$\begin{aligned} \chi_{33}^a(\omega) &= \chi_{33}^{0a} + 2 \frac{\mu_3^a}{v} \lim_{E_{3t} \rightarrow 0} \frac{d\eta_{at}^{(1)z}}{dE_{3t}} \\ &= \chi_{33}^{0a} + \bar{v} \frac{(\mu_3^a)^2}{v^2} \frac{1}{T} \frac{\tau_{1a}^z \tau_{2a}^z \tau_{3a}^z [(i\omega)^2 m^{z(2)} + (i\omega) m^{z(1)} + m^{z(0)}]}{(1 + i\omega\tau_{1s}^z)(1 + i\omega\tau_{2s}^z)(1 + i\omega\tau_{3s}^z)} \\ &= \chi_{33}^{0a} + \sum_{j=1}^3 \frac{\chi_{ja}^z}{1 + i\omega\tau_{ja}^z}. \end{aligned} \quad (3.19)$$

Respectively, the dynamic permittivity of  $\text{ND}_4\text{D}_2\text{XO}_4$  reads

$$\varepsilon_{33}^{a'}(\omega) = \varepsilon_{33}^{0a} + \sum_{j=1}^3 \frac{4\pi\chi_{ja}^z}{1 + (\omega\tau_{ja}^z)^2}, \quad \varepsilon_{33}^{a''}(\omega) = \sum_{j=1}^3 \frac{4\pi\chi_{ja}^z \omega\tau_{ja}^z}{1 + (\omega\tau_{ja}^z)^2}.$$

#### 4. Comparison of the calculated physical characteristics of the $\text{KH}_2\text{PO}_4$ family crystals with experimental data. Discussion

Based on the proposed unified model and within the developed theory let us numerically calculate the obtained thermal, dielectric, and longitudinal dynamic characteristics of the  $\text{M}(\text{H}_{1-x}\text{D}_x)_2\text{XO}_4$  type ferroelectrics and  $\text{N}(\text{H}_{1-x}\text{D}_x)_4(\text{H}_{1-x}\text{D}_x)_2\text{PO}_4$  type antiferroelectrics and compare the obtained results with the corresponding experimental data. It should be noted that the theory developed in the previous sections is valid, strictly speaking, for completely deuterated crystals only. However, we shall also consider pure and partially deuterated crystals ( $0 \leq x \leq 1$ ). The experimentally established relaxational character of the dielectric dispersion of  $\varepsilon_{33}^*(\nu, T)$  and  $\varepsilon_{11}^*(\nu, T)$  [199–203] in these crystals, according to [77–79,204], is associated with suppression of tunneling by short-range interactions. Therefore, the tunneling effects will be neglected in the considered crystals. We shall assume that the proposed theory with the averaged effective parameters

$\varepsilon(x)$ ,  $w(x)$ ,  $w_1(x)$ ,  $\nu_c(0, x)$ ,  $\nu_a(0, x)$ ,  $\mu_i(x)$ ,  $\alpha(x)$  is also valid for the crystals  $M(H_{1-x}D_x)_2XO_4$  and  $N(H_{1-x}D_x)_4(H_{1-x}D_x)_2PO_4$ . We shall also assume that to the partially deuterated crystals the following parameters correspond

$$\begin{aligned}\varepsilon(x) &= \varepsilon_H(1-x) + \varepsilon_D x, \\ w(x) &= w_H(1-x) + w_D x, \\ w_1(x) &= \infty, \\ \mu_i(x) &= \mu_{iH}(1-x) + \mu_{iD} x.\end{aligned}\quad (4.1)$$

Here  $\varepsilon_H$ ,  $w_H$ ,  $\mu_{iH}$  are the parameters for undeuterated  $MH_2XO_4$  and  $NH_4H_2PO_4$ , and  $\varepsilon_D$ ,  $w_D$ ,  $\mu_{iD}$  are the parameters for deuterated  $MD_2XO_4$  and  $ND_4D_2PO_4$ .

In the cases of ferroelectric and antiferroelectric phases, the most important problem is to solve the equations for the order parameters  $\eta_{s,a}^{(1)}$  (2.18). The temperature curves of spontaneous polarization in ferroelectrics and sublattice polarization in antiferroelectrics in the low-temperature phases are determined by those solutions of (2.18) that satisfy the condition of the free energy minimum (2.20). We shall also bear in mind the fact that the phase transition in these crystals is of the first order. Thus, at given values of  $\varepsilon(x)$  and  $w(x)$ , the long-range interaction parameters  $\nu_c(0, x)$  and  $\nu_a(\mathbf{k}_z, x)$  will be determined by minimization of the free energy (2.20) using the condition that the calculated values of the first order transition temperatures  $T_c(x)$  and  $T_N(x)$  coincide with the corresponding experimental values for these crystals. Also, the calculated values of spontaneous polarization jumps in ferroelectrics and sublattice polarization jumps in antiferroelectrics at the transition points  $T_c(x)$  and  $T_N(x)$  should agree with the experimentally observed ones. The Curie-Weiss temperatures  $T_0(x)$  for  $M(H_{1-x}D_x)_2XO_4$  will be determined from the equation

$$e^{-\frac{\varepsilon(x)}{T_0}} + e^{-\frac{\tilde{w}(x)}{T_0}} - \frac{1}{2} - \left(1 + e^{-\frac{\tilde{w}(x)}{T_0}}\right) \frac{\tilde{\nu}_c(0, x)}{T_0} = 0 \quad (4.2)$$

at given  $\varepsilon(x)$ ,  $w(x)$ ,  $\nu_c(0, x)$ .

Now our major task is using the above obtained expressions to study the variation of the calculated dielectric, thermal, and longitudinal dynamic characteristics of the  $M(H_{1-x}D_x)_2PO_4$  crystals in comparison with the theory parameters, to compare the obtained results with experimental data, and to determine the optimal theory parameters that provide a good quantitative agreement between the theory and experiment.

Let us first analyze the experimental data for  $T_c(x)$  for the  $K(H_{1-x}D_x)_2PO_4$  crystals presented in figure 2. A rather large dispersion of experimental points is seen.

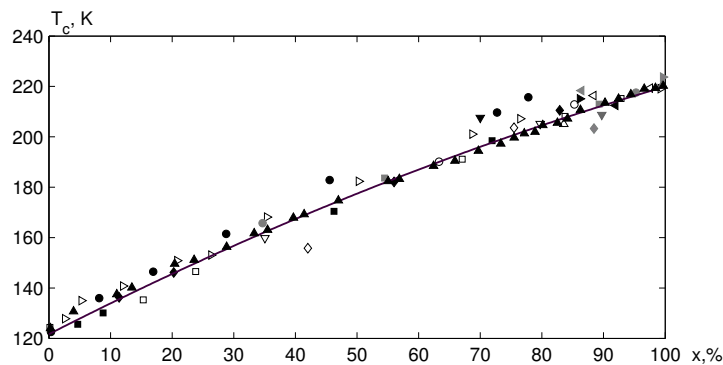


**Figure 2.** Dependence of the phase transition temperature in  $K(H_{1-x}D_x)_2PO_4$  on deuteron concentration  $x$ :  $\circ$  [205],  $\bullet$  [206],  $\bullet$  [207],  $\square$  [200],  $\blacksquare$  [208],  $\blacksquare$  [209],  $\diamond$  [199],  $\blacklozenge$  [210],  $\blacklozenge$  [211],  $\triangle$  [212],  $\blacktriangle$  [213],  $\blacktriangle$  [214,215],  $\nabla$  [216],  $\blacktriangledown$  [217],  $\blacktriangledown$  [218],  $\triangleright$  [219],  $\blacktriangleright$  [220],  $\blacktriangleright$  [201],  $\blacktriangleleft$  [222],  $\blacktriangleleft$  [223]. Line is the theoretical dependence  $T_c(x)$ .

In some papers [199,224,225] the dependence of the phase transition temperature in the  $\text{K}(\text{H}_{1-x}\text{D}_x)_2\text{PO}_4$  crystals on  $x$  is considered to be linear and is described by the empirical relation  $T_c = 123 + 106x \pm 2$  [199],  $T_c = 121.7 + 107x$  [225]. In these papers too few concentrations are usually taken into account, and  $T_c$  is measured with insufficient precision. The measurements [216,219,226] free from these drawbacks yield non-linear dependences  $T_c(x)$ , however, with different  $\frac{dT_c}{dx}$  and with the extrapolated values  $T_c(1,0)$ . A thorough investigation [214,215] of the deuteration dependence of the phase transition temperature for a large number of samples of  $\text{K}(\text{H}_{1-x}\text{D}_x)_2\text{PO}_4$  has confirmed the non-linear character of  $T_c(x)$ . Comparing the data of [214,215] with other measurements of  $T_c(x)$  we can note that the values of  $T_c(x)$  [214,215] agree with the data of [216,225] at  $0 \leq x \leq 0.4$  and of [226] at  $0 \leq x \leq 0.3$ . Some values of  $T_c$  given in [199] at  $x = 0.35; 0.68$  and in [225] at  $x=0.4$  coincide with the values of [214,215]. Overall, however, the values of  $T_c(x)$  obtained in [199,224–226] are by 5–10 K higher than those of [214,215]. A rather large spread of the data is caused, most likely, by imprecise determination of the deuterium concentration in the samples of  $\text{K}(\text{H}_{1-x}\text{D}_x)_2\text{PO}_4$ . Hereafter, we shall use the values of  $T_c(x)$  given in [214,215]. Using this dependence  $T_c(x)$  and those data for  $T_c(x)$  that deviate from the results of [214,215] we determined the correct values of deuteration in those samples of  $\text{K}(\text{H}_{1-x}\text{D}_x)_2\text{PO}_4$ . The obtained results are given in table 1.

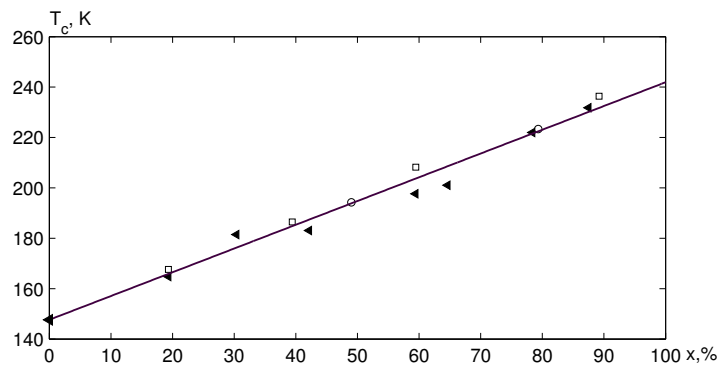
**Table 1.** Corrected values of deuteron concentration  $x$  for the  $\text{K}(\text{H}_{1-x}\text{D}_x)_2\text{PO}_4$  crystals.

$T_c$ (K)	135.3	145.6	146.0	155.0	159.0	161.0	182.0
	[226]	[226]	[200]	[199]	[216]	[226]	[226]
$x$ [ ]	0.08	0.17	0.23	0.35	0.35	0.29	0.46
$x[T_c(x)]$	0.11	0.20	0.21	0.29	0.33	0.34	0.54

$T_c$ (K)	190.2	191.0	204.8	205.6	209.5	213.2	218
	[205]	[200]	[216]	[212]	[226]	[205]	[222]
$x$ [ ]	0.64	0.67	0.80	0.84	0.73	0.86	0.87
$x[T_c(x)]$	0.63	0.64	0.79	0.81	0.86	0.91	0.98

In figure 3 we plot the experimental points for  $T_c(x)$  at different  $x$  for  $\text{Rb}(\text{H}_{1-x}\text{D}_x)_2\text{PO}_4$  crystals. In contrast to the case of  $\text{K}(\text{H}_{1-x}\text{D}_x)_2\text{PO}_4$ , the composition dependence of  $T_c(x)$  in  $\text{Rb}(\text{H}_{1-x}\text{D}_x)_2\text{PO}_4$  is almost linear.



**Figure 3.** Dependence of the phase transition temperature in  $\text{Rb}(\text{H}_{1-x}\text{D}_x)_2\text{PO}_4$  on deuteron concentration  $x$ :  $\circ$  [228],  $\square$  [228],  $\triangleleft$  [211],  $\blacktriangleleft$  [229]. Line is the theoretical dependence  $T_c(x)$ .

For the sake of comparison, in figure 4 we show the deuteration dependences of the transition temperatures in  $\text{Cs}(\text{H}_{1-x}\text{D}_x)_2\text{PO}_4$ ,  $\text{M}(\text{H}_{1-x}\text{D}_x)_2\text{XO}_4$ ,  $\text{N}(\text{H}_{1-x}\text{D}_x)_4(\text{H}_{1-x}\text{D}_x)_2\text{PO}_4$ . It turns out that the coefficient  $\frac{dT_c(x)}{dx}$  is practically the same for all these crystals, whereas the dependences

$T_c(x)$  for  $\text{Rb}(\text{H}_{1-x}\text{D}_x)_2\text{PO}_4$  and  $\text{N}(\text{H}_{1-x}\text{D}_x)_4(\text{H}_{1-x}\text{D}_x)_2\text{PO}_4$  coincide. In [227] the empirical dependences of the phase transition temperatures  $T_c$  on deuterium concentration  $x$  were obtained. In  $\text{Rb}(\text{H}_{1-x}\text{D}_x)_2\text{PO}_4$  up to  $x = 0.76$   $T_c(x) = (146.6 + 108.0x)\text{K}$ , and for  $\text{N}(\text{H}_{1-x}\text{D}_x)_4(\text{H}_{1-x}\text{D}_x)_2\text{PO}_4$   $T_N(x) = (148.8 + 94.1x)\text{K}$ .

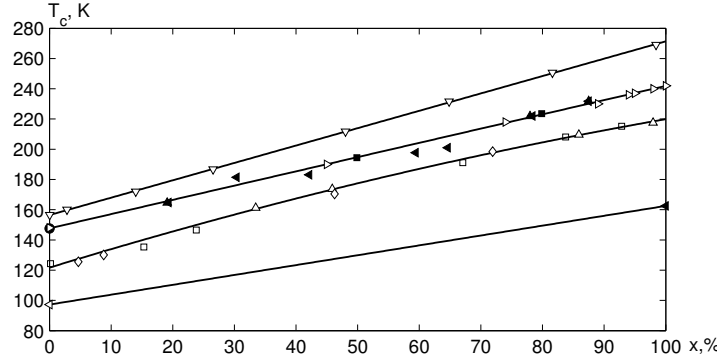


**Figure 4.** Dependence of the phase transition temperature on deuteron concentration  $x$  for the crystals  $\text{Cs}(\text{H}_{1-x}\text{D}_x)_2\text{PO}_4$  –  $\nabla$  [230],  $\text{Rb}(\text{H}_{1-x}\text{D}_x)_2\text{PO}_4$  –  $\blacktriangleleft$  [229],  $\blacksquare$  [228],  $\text{K}(\text{H}_{1-x}\text{D}_x)_2\text{PO}_4$  –  $\diamond$  [209],  $\square$  [200],  $\triangle$  [214,215],  $\text{K}(\text{H}_{1-x}\text{D}_x)_2\text{AsO}_4$  –  $\blacktriangleright$  [119],  $\blacktriangleleft$  [231],  $\text{N}(\text{H}_{1-x}\text{D}_x)_4(\text{H}_{1-x}\text{D}_x)_2\text{PO}_4$  –  $\blacktriangleright$  [232]. Lines are the theoretical dependences  $T_c(x)$ .

In order to evaluate the corresponding temperature and frequency dependences of the physical characteristics of the  $\text{M}(\text{H}_{1-x}\text{D}_x)_2\text{XO}_4$  crystals using the expressions obtained in the previous sections, we have to set the values of the following parameters:

- energies of proton and deuteron configurations  $\varepsilon_{\text{H}}$ ,  $w_{\text{H}}$ ,  $w_{1\text{H}}$  and  $\varepsilon_{\text{D}}$ ,  $w_{\text{D}}$ ,  $w_{1\text{D}}$ , respectively;
- parameters of the long-range interactions  $\nu_c(0)$ ,  $\nu_a(0)$  and  $\nu_a(\mathbf{k}^z)$  for the  $\text{N}(\text{H}_{1-x}\text{D}_x)_4(\text{H}_{1-x}\text{D}_x)_2\text{PO}_4$  crystals;
- effective dipole moments  $\mu_{3\text{H}}$ ,  $\mu_{3\text{D}}$ ,  $\mu_{1\text{H}}$ ,  $\mu_{1\text{D}}$ ;
- “seed” dielectric susceptibilities  $\chi_{33\text{H}}^0$ ,  $\chi_{33\text{D}}^0$ ,  $\chi_{11\text{H}}^0$ ,  $\chi_{11\text{D}}^0$ ;
- parameters  $\alpha_{\text{H}}$ ,  $\alpha_{\text{D}}$  setting the time scale of the relaxational processes.

In addition to the mentioned parameters, to calculate the obtained physical characteristics of the  $\text{M}(\text{H}_{1-x}\text{D}_x)_2\text{XO}_4$  crystals we have to set the volume of their primitive cells. Taking into account a rather weak temperature and deuteration dependences of the lattice constants of  $\text{M}(\text{H}_{1-x}\text{D}_x)_2\text{XO}_4$  crystals [233], we use the following values of the volumes:

$\text{K}(\text{H}_{1-x}\text{D}_x)_2\text{PO}_4$  –  $v = 0.1913 \cdot 10^{-21}\text{cm}^3$  [234],  $\text{Rb}(\text{H}_{1-x}\text{D}_x)_2\text{PO}_4$  –  $v = 0.2090 \cdot 10^{-21}\text{cm}^3$  [235],  $\text{K}(\text{H}_{1-x}\text{D}_x)_2\text{AsO}_4$  –  $v = 0.2052 \cdot 10^{-21}\text{cm}^3$  [233],  $\text{N}(\text{H}_{1-x}\text{D}_x)_4(\text{H}_{1-x}\text{D}_x)_2\text{PO}_4$  –  $v = 0.2110 \cdot 10^{-21}\text{cm}^3$  [236].

The energy  $w_{1\text{H}}$  of two proton configurations with four or zero protons near the given oxygen tetrahedron should be much higher than  $\varepsilon_{\text{H}}$  and  $w_{\text{H}}$ . Therefore we take  $w_{1\text{H}} = \infty$  and  $w_{1\text{D}} = \infty (d = 0)$ .

In order to determine the optimal values of the above mentioned parameters for the  $\text{M}(\text{H}_{1-x}\text{D}_x)_2\text{XO}_4$  crystals we shall use the experimental data for their physical characteristics. For  $\text{K}(\text{H}_{1-x}\text{D}_x)_2\text{PO}_4$ :  $T_c(x)$  [214,215],  $P_s(T)$  [12],  $\Delta C_p(T)$  [228,237,238],  $\varepsilon_{33}(0, T)$  [218,239,12],  $\varepsilon_{11}(0, T)$  [227],  $\varepsilon_{33}^*(\omega, T)$ ,  $\varepsilon_{11}^*(\omega, T)$  [200]; for  $\text{Rb}(\text{H}_{1-x}\text{D}_x)_2\text{PO}_4$ :  $T_c(x)$  [240],  $P_s(T)$  [218],  $\Delta C_p(T)$  [228],  $\varepsilon_{33}(0, T)$  [241],  $\varepsilon_{11}^*(\omega, T)$  [218],  $\varepsilon_{33}^*(\omega, T)$ ,  $\varepsilon_{11}^*(\omega, T)$  [203]; for  $\text{KH}_2\text{AsO}_4$ :  $T_c(x)$  [231],  $P_s(T)$  [231],  $\Delta C_p(T)$  [231],  $\varepsilon_{33}(0, T)$  [119],  $\varepsilon_{11}(0, T)$  [218],  $\varepsilon_{33}^*(\omega, T)$ ,  $\varepsilon_{11}^*(\omega, T)$  [203]; for  $\text{N}(\text{H}_{1-x}\text{D}_x)_4(\text{H}_{1-x}\text{D}_x)_2\text{PO}_4$ :  $T_N(x)$  [232],  $P_s(T)$  [242],  $\varepsilon_{11}(0, T)$ ,  $\varepsilon_{33}(0, T)$  [243],  $\varepsilon_{11}^*(\omega, T)$ ,  $\varepsilon_{33}^*(\omega, T)$  [232].

The fitting procedure will be explained based on the example of the  $\text{KH}_2\text{PO}_4$  crystal. With different chosen sets of the parameters  $\varepsilon_{\text{H}}$  and  $w_{\text{H}}$ , determining  $\nu_c(0)$  from the condition of the free energy minimum, we find those values of  $\varepsilon_{\text{H}}$ ,  $w_{\text{H}}$ , and  $\nu_c(0)$  that properly reproduce the observed temperature curves of  $P_{\text{s}}(T)$  and  $\Delta C_{\text{p}}$ . The value of the effective dipole moment  $\mu_{3\text{H}}^-$  in the ferroelectric phase is determined by fitting to experiment the theoretical temperature curves of spontaneous polarization and  $\varepsilon_{33}''(\omega, T)$  as well as the value of saturation polarization. The value of  $\mu_{3\text{H}}^+$  in the paraelectric phase is determined by fitting to experiment the theoretical temperature curve of longitudinal static dielectric permittivity, as well as the temperature and frequency dependences of  $\varepsilon_{33}''(\omega, T)$ .

Numerical analysis shows that to determine the optimal value of the dipole moment  $\mu_{1\text{H}}$  one has to take into account the experimental data not only for the static dielectric permittivity  $\varepsilon_{11}(0, T)$  but also for  $\varepsilon_{11}^*(\omega, T)$ . In order to obtain an adequate description of the temperature dependences of  $\varepsilon_{11}(0, T)$  and  $\varepsilon_{11}^*(\omega, T)$  we shall assume that the value of  $\mu_{1\text{H}}$  slightly increases with temperature as

$$\mu_{1\text{H}} = \mu_{1\text{H}}^0 + K_{\mu}(T - T_{\text{c}}).$$

The ‘‘seed’’ dielectric susceptibilities are determined from the condition of the best agreement between theory and experiment for static dielectric permittivities at temperatures far from the transition point.

The parameter  $\alpha_{\text{H}}$  is set using the condition that the theoretical frequency curves of  $\varepsilon_{33}^*(\omega, T)$  agree with the experimental ones. It is also assumed that the parameter  $\alpha_{\text{H}}$  is slightly temperature dependent

$$\alpha_{\text{H}} = [P_{\text{H}} + R_{\text{H}}|\Delta T|] \cdot 10^{-14}, \quad \Delta T = T - T_{\text{c}}.$$

In the same way we find the optimal values of the model parameters for  $\text{K}(\text{H}_{1-x}\text{D}_x)_2\text{PO}_4$ ,  $\text{Rb}(\text{H}_{1-x}\text{D}_x)_2\text{PO}_4$ ,  $\text{K}(\text{H}_{1-x}\text{D}_x)_2\text{AsO}_4$ , and  $\text{N}(\text{H}_{1-x}\text{D}_x)_4(\text{H}_{1-x}\text{D}_x)_2\text{PO}_4$ . The obtained values of the theory parameters for these crystals are presented in tables 2–5.

**Table 2.** Optimal sets of the model parameters for the  $\text{K}(\text{H}_{1-x}\text{D}_x)_2\text{PO}_4$  crystals.

$x$	$T_{\text{c}}$ (K)	$T_0$ (K)	$\frac{\varepsilon}{k_{\text{B}}}$ (K)	$\frac{w}{k_{\text{B}}}$ (K)	$\frac{\nu_{\text{c}}(0)}{k_{\text{B}}}$ (K)	$\frac{\nu_{\text{a}}(0)}{k_{\text{B}}}$ (K)	$\chi_{33}^0$ (esu-cm)	$\chi_{11}^0$ (esu-cm)	$C_{\text{CW}}$ (K)
0.00	122.5	122.5	56.00	400.0	20.21	7.00	0.85	0.80	2343
0.21	146.0	145.9	63.69	493.2	25.42	9.36	0.71	0.76	2644
0.64	191.0	190.3	79.44	684.0	34.49	14.19	0.49	0.69	3333
0.79	204.0	203.1	84.94	750.6	36.28		0.43		3614
0.84	208.0	207.0	86.77	772.8	36.71	16.44	0.41	0.66	3713
0.93	215.0	213.9	90.07	812.8	37.40	17.45	0.38	0.64	3895
1.00	220.1	218.9	92.63	843.8	37.78		0.36		4043

$x$	$\mu_{3-}, 10^{-18}$ (esu-cm)	$\mu_{3+}, 10^{-18}$ (esu-cm)	$\mu_1^0$ (esu-cm)	$\frac{k_{\mu}}{k_{\text{B}}}$ (esu-cm/K)	$P_-$ (s)	$R_-$ (s/K)	$P_+$ (s)	$R_+$ (s/K)	$P$ (s)	$R$ (s/K)
0.00	1.48	1.65	4.27	0.0056	0.41	0.0150	0.53	0.0160	0.55	0.0140
0.21	1.56	1.74	4.56	0.0053	0.95	0.0138	1.38	0.0220	1.29	0.0123
0.64	1.71	1.94	5.17	0.0046	1.87	0.0414	2.73	0.0174	2.82	0.0090
0.79	1.76	2.01			2.02	0.0106	2.94	0.0152		
0.84	1.78	2.03	5.45	0.0043	2.12	0.0103	3.17	0.0166	3.52	0.0074
0.93	1.81	2.07	5.57	0.0042	2.38	0.0098	3.37	0.0154	3.84	0.0067
1.00	1.84	2.10			2.91	0.0094	4.93	0.0338		

Let us present the results of numerical calculations for the physical characteristics of the considered crystals, bearing in mind the problem of validity of the proposed theory for these crystals.

It should be noted that using these values of the model parameters the calculated difference between the phase transition temperature and Curie-Weiss temperature for  $\text{KH}_2\text{PO}_4$  is  $(T_{\text{c}} - T_0)_{\text{H}} = 0.003$  K, which is lower than the experimental values 0.012 K [244], 0.06 [245,246], 0.074 K [19],

**Table 3.** Optimal sets of the model parameters for the  $\text{Rb}(\text{H}_{1-x}\text{D}_x)_2\text{PO}_4$  crystals.

$x$	$T_c$ (K)	$T_0$ (K)	$\frac{\varepsilon}{k_B}$ (K)	$\frac{w}{k_B}$ (K)	$\frac{\nu_c(0)}{k_B}$ (K)	$\frac{\nu_a(0)}{k_B}$ (K)	$\chi_{33}^0$ (esu·cm)	$\chi_{11}^0$ (esu·cm)	$C_{CW}$ (K)
0.00	147.6	147.6	60.00	431.0	30.78	28.00	0.55	1.25	2781
0.48	193.0	192.5	78.00	642.2	37.62		0.45		3185
0.80	223.0	222.1	90.00	783.0	42.32		0.39		3427

$x$	$\mu_{3-}, 10^{-18}$ (esu·cm)	$\mu_{3+}, 10^{-18}$ (esu·cm)	$\mu_1^0$ (esu·cm)	$k_\mu$ ( $\frac{\text{esu}\cdot\text{cm}}{\text{K}}$ )	$P_-$ (s)	$R_-$ ( $\frac{\text{s}}{\text{K}}$ )	$P_+$ (s)	$R_+$ ( $\frac{\text{s}}{\text{K}}$ )	$P$ (s)	$R$ ( $\frac{\text{s}}{\text{K}}$ )
0.00	1.50	1.93	3.68	0.0057	0.60	0.0150	1.00	0.0150	0.60	0.0110
0.48	1.68	2.00								
0.80	1.80	2.05								

**Table 4.** Optimal sets of the model parameters for the  $\text{K}(\text{H}_{1-x}\text{D}_x)_2\text{AsO}_4$  crystals.

$x$	$T_c$ (K)	$T_0$ (K)	$\frac{\varepsilon}{k_B}$ (K)	$\frac{w}{k_B}$ (K)	$\frac{\nu_c(0)}{k_B}$ (K)	$\frac{\nu_a(0)}{k_B}$ (K)	$\chi_{33}^0$ (esu·cm)	$\chi_{11}^0$ (esu·cm)	$C_{CW}$ (K)
0.00	97.0	95.7	35.50	375.0	19.71	20.00	0.70	0.70	2372
1.00	162.0	158.5	56.00	682.0	33.78		0.50		3542

$x$	$\mu_{3-}, 10^{-18}$ (esu·cm)	$\mu_{3+}, 10^{-18}$ (esu·cm)	$\mu_1^0$ (esu·cm)	$k_\mu$ ( $\frac{\text{esu}\cdot\text{cm}}{\text{K}}$ )	$P_-$ (s)	$R_-$ ( $\frac{\text{s}}{\text{K}}$ )	$P_+$ (s)	$R_+$ ( $\frac{\text{s}}{\text{K}}$ )	$P$ (s)	$R$ ( $\frac{\text{s}}{\text{K}}$ )
0.00	1.61	1.66	4.85	0.0064	0.50	0.0150	0.74	0.0180	0.65	0.0130
1.00	2.21	2.00								

**Table 5.** Optimal sets of the model parameters for the  $\text{N}(\text{H}_{1-x}\text{D}_x)_4(\text{H}_{1-x}\text{D}_x)_2\text{PO}_4$  crystals.

$x$	$T_c$ (K)	$\varepsilon$ (K)	$w$ (K)	$\nu_a(\mathbf{k}_z)$ (K)	$\nu_c^a(0)$ (K)	$\mu_{33}^a$ (esu·cm)	$\chi_{33}^0$	$P$ (s)	$R$ ( $\frac{\text{s}}{\text{K}}$ )
0.00	148.0	-20.0	470.0	59.88	-10.00	2.10	0.23	0.38	0.0090
0.45	190.0	-47.0	546.5	72.13	-13.38	2.40	0.28	3.29	0.0090
0.74	218.0	-64.4	595.8	80.81	-15.55	2.59	0.31	5.17	0.0090
0.89	230.0	-73.4	621.3	83.89	-16.68	2.69	0.33	6.14	0.0090
0.94	236.0	-76.4	629.8	86.09	-17.05	2.72	0.33	6.46	0.0090
0.95	237.0	-77.0	631.5	86.42	-17.13	2.73	0.33	6.53	0.0090
0.98	240.0	-78.8	636.6	87.39	-17.35	2.75	0.34	6.72	0.0090
1.00	242.0	-80.0	640.0	88.04	-17.50	2.76	0.34	6.85	0.0090

$x$	$\nu_a^a(0)$ (K)	$\mu_{1-}^a$ (esu·cm)	$\mu_{1+}^a$ (esu·cm)	$\chi_{11}^0$	$P$ (s)	$R$ ( $\frac{\text{s}}{\text{K}}$ )
0.00	-40.00	1.70	6.45	0.70	0.95	0.0110
0.45	-46.75	1.52	6.84	0.65	3.22	0.0074
0.74	-51.10	1.40	7.09	0.61	4.69	0.0051
0.89	-53.35	1.34	7.22	0.59	5.44	0.0039
0.94	-54.10	1.32	7.26	0.59	5.70	0.0035
0.95	-54.25	1.32	7.27	0.59	5.75	0.0034
0.98	-54.70	1.31	7.29	0.58	5.90	0.0032
1.00	-55.00	1.30	7.31	0.58	6.00	0.0030



0.053 [119]. Unfortunately, it is impossible to find the values of the model parameters that would yield a larger value of  $T_c - T_0$  and still provide a quantitative agreement with experiment for other characteristics of the crystal. Tunneling being taken into account increases the difference  $T_c - T_0$  up to 0.060 [121]. In  $\text{KD}_2\text{PO}_4$  the calculated difference is  $(T_c - T_0)_D = 1.159$  K, which is rather close to the experimental value 1, 5 K [216]. In  $\text{RbH}_2\text{PO}_4$  the theory yields  $(T_c - T_0)_H = 0.032$  K, which agrees with the value obtained with tunneling taken into account [121]. Using the value of  $T_0 = 147.57$  K from [247] for  $\text{RbH}_2\text{PO}_4$  we can find that here  $T_c - T_0 \sim 0.04$  K. In  $\text{KH}_2\text{AsO}_4$  the calculated difference is  $(T_c - T_0)_H = 1.281$  K; taken tunneling being taken into account increases it up to  $(T_c - T_0)_H = 1.611$  K [121], whereas the experiment gives 2.63 [248], 1.9 [231], 2.3 [249], 0.716 [118], 1.82 [119].

The calculated temperature curves of spontaneous polarization  $P_s(T)$  for  $\text{K}(\text{H}_{1-x}\text{D}_x)_2\text{PO}_4$  at different deuteration  $x$  along with experimental points are given in figure 5. In  $\text{KH}_2\text{PO}_4$  a first order phase transition is observed, though, close to the second order. At deuteration the ‘‘first-orderness’’ of the phase transition increases.

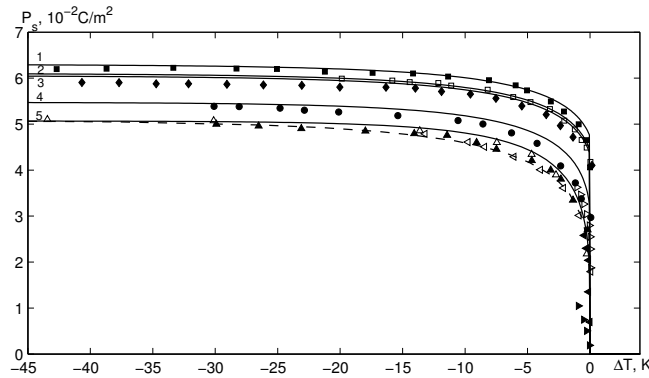


**Figure 5.** Temperature dependence of spontaneous polarization of  $\text{K}(\text{H}_{1-x}\text{D}_x)_2\text{PO}_4$  at different  $x$ : 1.0 – 1.  $\blacksquare$  [216]; 0.84 – 2.  $\square$  [119]; 0.8 – 3,  $\blacklozenge$  [216]; 0.33 – 4,  $\bullet$  [216]; 0.0 – 5,  $\triangle$  [250],  $\blacktriangle$  [216],  $\blacktriangleleft$  [251],  $\blacktriangleleft$  [245],  $\blacktriangleright$  [244],  $\blacktriangleright$  [224], [226]; 1.0 – 7,  $\bullet$  [238]. Symbols are experimental data; solid lines are theoretical values obtained in the present work; dashed lines are theoretical results of [121].

The theoretical dependences  $P_s(T)$  well describe the experimental temperature curve [216] for  $x = 1.0$  and  $0.80$ . At  $x = 0.33$  and  $x = 0.0$  starting from  $\Delta T \sim 15$  K the calculated values of  $P_s(T)$  are by  $\sim 10\%$  higher than the values of [216]. However, the proposed theory well describes the experimental [250,244]  $P_s(T)$  of  $\text{KH}_2\text{PO}_4$ . The values of  $P_s(T)$  for  $\text{KH}_2\text{PO}_4$  calculated in [121] with tunneling taken into account well agree with the results of [216]. The theory yields  $\frac{P_{\text{CH}}}{P_{\text{SH}}} = 0.23$ , whereas the values of this ratio obtained from experimental data are 0.36 [119] and 0.14 [245]. For a deuterated crystal  $\frac{P_{\text{CD}}}{P_{\text{SD}}} = 0.76$ , which is somewhat larger than the experimental 0.65 [216].

In figure 6 we plot the calculated  $P_s(T)$  for  $\text{M}(\text{H}_{1-x}\text{D}_x)_2\text{XO}_4$  crystals along with the experimental data for  $\text{KH}_2\text{PO}_4$ ,  $\text{KD}_2\text{PO}_4$ ,  $\text{RbH}_2\text{PO}_4$ ,  $\text{KH}_2\text{AsO}_4$ ,  $\text{KD}_2\text{AsO}_4$ . By the dashed lines we show the temperature curves of  $P_s$  calculated in [121] with tunneling taken into account.

The proposed theory provides a good quantitative description of the temperature dependence of polarization and the  $\frac{P_{\text{C}}}{P_{\text{S}}}$  ratio for these crystals. For  $\text{RbH}_2\text{PO}_4$  and  $\text{KH}_2\text{AsO}_4$  we get  $\frac{P_{\text{CH}}}{P_{\text{SH}}} = 0.34$  and  $\frac{P_{\text{CH}}}{P_{\text{SH}}} = 0.86$ , respectively, whereas the experiment yields 0.35 and 0.86 [119]. At the replacement of  $\text{K} \rightarrow \text{Rb}$ , the spontaneous polarization decreases at all temperatures by about 10%, and the phase transition is still of the first order. At the replacement of  $\text{P} \rightarrow \text{As}$ , the saturation polarization increases from  $5.0 \cdot 10^{-2}$  C/m<sup>2</sup> to  $5.2 \cdot 10^{-2}$  C/m<sup>2</sup>, with a very weak temperature dependence of  $P_s(T)$  and a clear first order phase transition at  $T = T_c$ . The calculated ratio for  $\text{KD}_2\text{AsO}_4$  obtained in [231] is  $\frac{P_{\text{CD}}}{P_{\text{SD}}} = 0.92$ .

The calculated temperature dependence of sublattice spontaneous polarization for the  $\text{NH}_4\text{H}_2\text{PO}_4$  crystal agrees with the results of [242] (figure 7). The ratio  $\frac{P_{\text{C}}}{P_{\text{S}}} = 0.93$  indicates the first order phase transition in  $\text{NH}_4\text{H}_2\text{PO}_4$ .

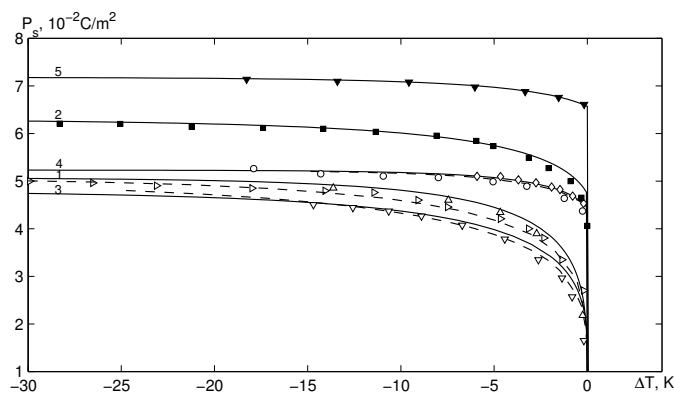


**Figure 6.** Temperature dependence of spontaneous polarization of  $\text{KH}_2\text{PO}_4$  – 1,  $\Delta$  [250],  $\triangleright$  [216];  $\text{KD}_2\text{PO}_4$  – 2,  $\blacksquare$  [216];  $\text{RbH}_2\text{PO}_4$  – 3,  $\nabla$  [218];  $\text{KH}_2\text{AsO}_4$  – 4,  $\circ$  [231],  $\diamond$  [119];  $\text{KD}_2\text{AsO}_4$  – 5,  $\blacktriangledown$  [231]. [121].

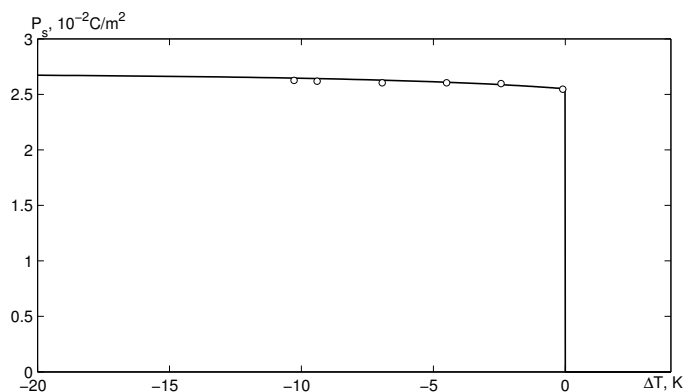


**Figure 7.** Temperature dependence of sublattice spontaneous polarization of  $\text{NH}_4\text{H}_2\text{PO}_4$ . Points  $\circ$  are experimental data [242]; the solid line is the theoretical values.

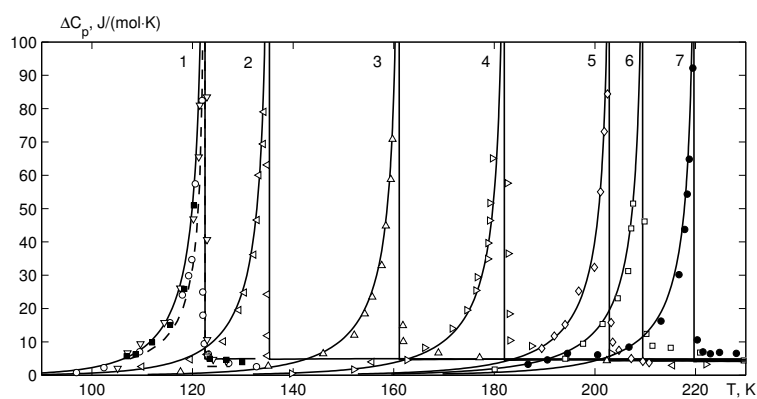


**Figure 8.** Temperature dependences of specific heat of  $\text{K}(\text{H}_{1-x}\text{D}_x)_2\text{PO}_4$  at different  $x$ : 0.0 – 1,  $\circ$  [226],  $\nabla$  [237],  $\blacksquare$  [252]; 0.11 – 2,  $\triangleleft$  [226]; 0.34 – 3,  $\Delta$  [226]; 0.54 – 4,  $\triangleright$  [226]; 0.78 – 5,  $\diamond$  [237]; 0.86 – 6,  $\square$  [226]; 1.0 – 7,  $\bullet$  [238]. Symbols are experimental data; solid lines are theoretical values obtained in the present work; dashed lines are theoretical results of [121].

As seen in figures 8–10, the proposed theory quantitatively well describes the temperature dependences of molar specific heat at constant pressure  $\Delta C_p$  of the  $\text{K}(\text{H}_{1-x}\text{D}_x)_2\text{PO}_4$ ,  $\text{Rb}(\text{H}_{1-x}\text{D}_x)_2\text{PO}_4$ ,  $\text{KH}_2\text{AsO}_4$ , and  $\text{KD}_2\text{AsO}_4$  crystals. The experimental values of  $\Delta C_p$  are determined by subtracting a lattice contribution to the specific heat, approximated by linear dependence in the phase transition region, from the total measured specific heat of the crystal.

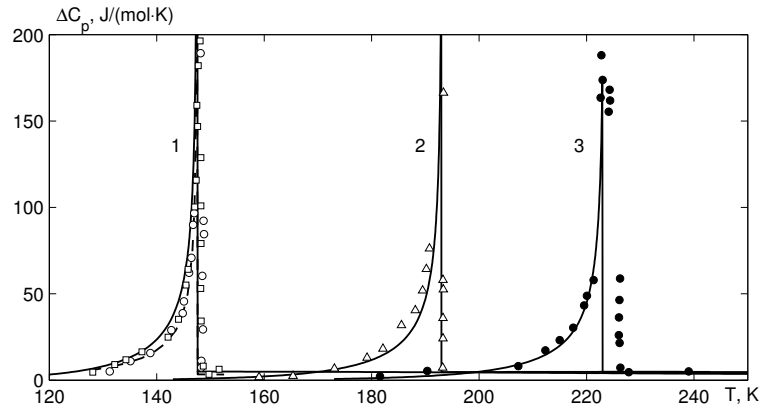


**Figure 9.** Temperature dependences of specific heat of  $\text{Rb}(\text{H}_{1-x}\text{D}_x)_2\text{PO}_4$  at different  $x$ : 0.0 – 1,  $\circ$  [228],  $\square$  [255]; 0.5 – 2,  $\triangle$  [228]; 0.8 – 3,  $\bullet$  [228]. Symbols are experimental data; solid lines are theoretical values obtained in the present work; dashed lines are theoretical results of [121].

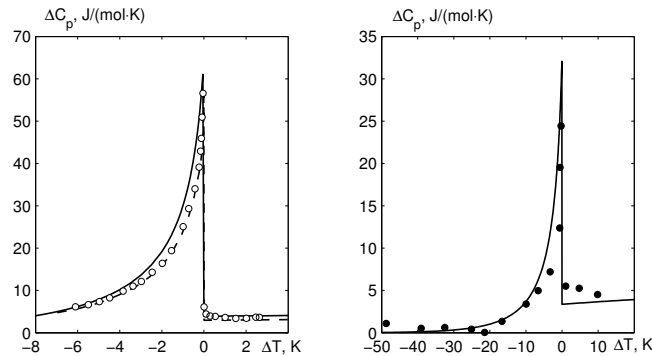


**Figure 10.** Temperature dependences of specific heat of  $\text{KH}_2\text{AsO}_4$  –  $\circ$  and  $\text{KD}_2\text{AsO}_4$  –  $\bullet$ . Symbols are experimental data [231], solid lines are theoretical values obtained in the present work; dashed lines are theoretical results of [121].

Analysis of the temperature dependences of polarization and proton molar specific heat on the theory parameters  $\varepsilon$  and  $w$  shows that the changes in  $\varepsilon$  at constant  $w$  hardly affects the values of  $P_s$  or  $\Delta C_p$ , whereas at constant  $\varepsilon$  an increase in  $w$  moves the theoretical curve  $\Delta C_p$  closer to the experimental points and increases convexity of the  $P_s(T)$  curve. Therefore, we choose the values of the parameters  $\varepsilon$  and  $w$  such that they satisfactorily describe both characteristics.

The temperature curves of proton molar specific heat of  $\text{KH}_2\text{PO}_4$ ,  $\text{KD}_2\text{PO}_4$ ,  $\text{RbH}_2\text{PO}_4$ ,  $\text{KH}_2\text{AsO}_4$ , and  $\text{KD}_2\text{AsO}_4$  crystals are compared in figure 11. The lowest values of  $\Delta C_p$  are in the arsenates. A decrease of  $x$  in  $\text{K}(\text{H}_{1-x}\text{D}_x)_2\text{PO}_4$  increases  $\Delta C_p$ . At the replacement of  $\text{K} \rightarrow \text{Rb}$  the value of proton specific heat increases.

Experimental data for the temperature dependence of proton specific heat of  $\text{N}(\text{H}_{1-x}\text{D}_x)_4(\text{H}_{1-x}\text{D}_x)_2\text{PO}_4$  at  $x = 0.0$  [253,254] and  $x = 0.95$  [254] are well described by the proposed theory (figure 12), except for a narrow region near  $|\Delta T| \sim 1$  K in the low-temperature

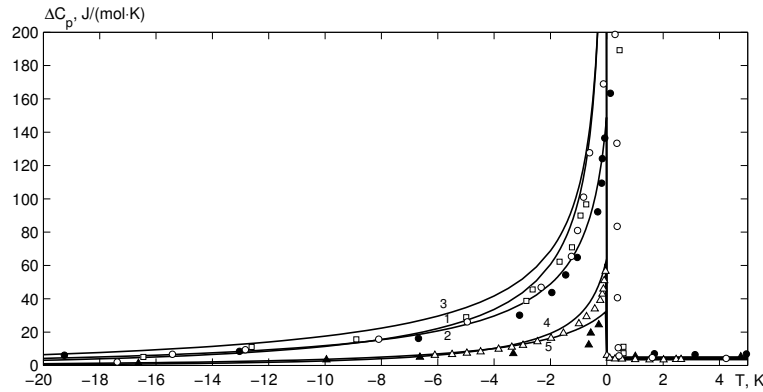


**Figure 11.** Temperature dependence of specific heat for  $\text{KH}_2\text{PO}_4$  – 1,  $\circ$  [237];  $\text{KD}_2\text{PO}_4$  – 2,  $\bullet$  [238];  $\text{RbH}_2\text{PO}_4$  – 3,  $\square$  [255];  $\text{KH}_2\text{AsO}_4$  – 4,  $\triangle$  [231];  $\text{KD}_2\text{AsO}_4$  – 5,  $\blacktriangle$  [231]. Symbols are experimental points; solid lines are theoretical values obtained in the present work; dashed lines are theoretical results of [121].

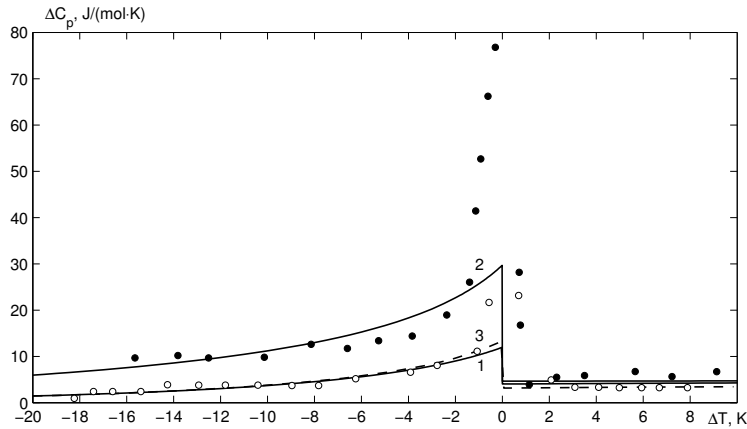


**Figure 12.** Temperature dependence of molar specific heat of  $\text{N}(\text{H}_{1-x}\text{D}_x)_4(\text{H}_{1-x}\text{D}_x)_2\text{PO}_4$  at different  $x$ : 0.0 – 1,  $\circ$  [254], 3[253]; 0.95 – 2,  $\bullet$  [254]. Symbols are experimental points; solid lines are theoretical values obtained in the present work; dashed lines are theoretical results of [121].

phase, where the measurements of  $\Delta C_p$  show a clear endothermic anomaly at the transition point. The calculated herein transition entropy of the  $\text{NH}_4\text{H}_2\text{PO}_4$  crystal is  $S_C = 5.09\text{J/K}\cdot\text{mole}$  (cf. the values  $4.39\text{ J/K}\cdot\text{mole}$  obtained in [253] and  $4.47\text{J/K}\cdot\text{mole}$  obtained in [254]). For  $x = 0,95$  we obtain  $S_C = 5.52\text{J/K}\cdot\text{mole}$ .

The calculated temperature dependences of inverse static dielectric permittivities  $\varepsilon_{33}^{-1}(0, T)$  of the  $\text{K}(\text{H}_{1-x}\text{D}_x)_2\text{PO}_4$  crystals at different values of  $x$  along with experimental points are presented in figure 13. A perceptible dispersion of experimental data is seen for  $\text{KH}_2\text{PO}_4$ . We can well describe the temperature curves of  $\varepsilon_{33}^{-1}(0, T)$ , obtained in some papers, whereas the description of other experiments is worse, especially at  $\Delta T > 50\text{ K}$ . At large  $x$  the Curie-Weiss law for  $\varepsilon_{33}^{-1}(0, T)$  is obeyed in a rather wide temperature range  $\Delta T$ . With a decreasing  $x$  this range narrows, and a notable non-linearity in the temperature dependence of  $\varepsilon_{33}^{-1}(0, T)$  appears. The calculated Curie-Weiss constants  $C_{\text{CW}}(x)$  for  $\text{K}(\text{H}_{1-x}\text{D}_x)_2\text{PO}_4$  at different deuteration are:  $C_{\text{CW}}(0.0) = 2360\text{ K}$ ,  $C_{\text{CW}}(0.2) = 2644\text{ K}$ ,  $C_{\text{CW}}(0.33) = 2826\text{ K}$ ,  $C_{\text{CW}}(0.55) = 3177\text{ K}$ ,  $C_{\text{CW}}(0.84) = 3713\text{ K}$ ,  $C_{\text{CW}}(0.93) = 3895\text{ K}$ ,  $C_{\text{CW}}(1.0) = 4047\text{ K}$ . Deuteration of  $\text{KH}_2\text{PO}_4$  increases  $\varepsilon_{33}^{-1}(0, T)$  in the paraelectric phase and decreases in the ferroelectric phase.

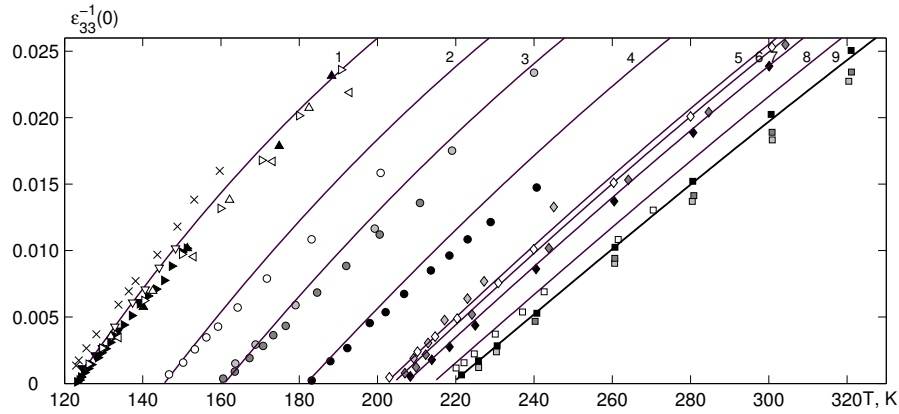


**Figure 13.** Temperature dependence of inverse longitudinal permittivity of  $\text{K}(\text{H}_{1-x}\text{D}_x)_2\text{PO}_4$  at different  $x$ : 0.0 – 1.  $\Delta$  [216],  $\blacktriangle$  [241],  $\nabla$  [239],  $\blacktriangledown$  [259],  $\triangleright$  [119],  $\triangleleft$  [7]; 0.2 – 2,  $\circ$  [226]; 0.33 –  $\bullet$  [216]; 0.34 – 3,  $\bullet$  [226]; 0.55 – 4,  $\bullet$  [226]; 0.78 –  $\diamond$  [210]; 0.79 – 5,  $\diamond$  [239]; 0.8 – 6,  $\blacklozenge$  [216]; 0.84 – 7,  $\blacklozenge$  [218]; 0.93 – 8,  $\square$  [226]; 1.0 – 9,  $\square$  [219],  $\blacksquare$  [213],  $\blacksquare$  [216]. Symbols are experimental points; solid lines are theoretical results.

In figure 14 we plot the calculated  $\varepsilon_{33}^{-1}(0, T)$  as well as experimental points for  $\text{KH}_2\text{PO}_4$ ,  $\text{KD}_2\text{PO}_4$ ,  $\text{RbH}_2\text{PO}_4$ ,  $\text{KH}_2\text{AsO}_4$ , and  $\text{KD}_2\text{AsO}_4$ . The Curie-Weiss constants calculated for these crystals are 2781 K for  $\text{RbH}_2\text{PO}_4$ , 2371 K for  $\text{KH}_2\text{AsO}_4$ , and 3542 K for  $\text{KD}_2\text{AsO}_4$ . The value of the longitudinal static permittivity increases at all temperatures at isomorphous replacement of  $\text{K} \rightarrow \text{Rb}$  and decreases at  $\text{P} \rightarrow \text{As}$ .

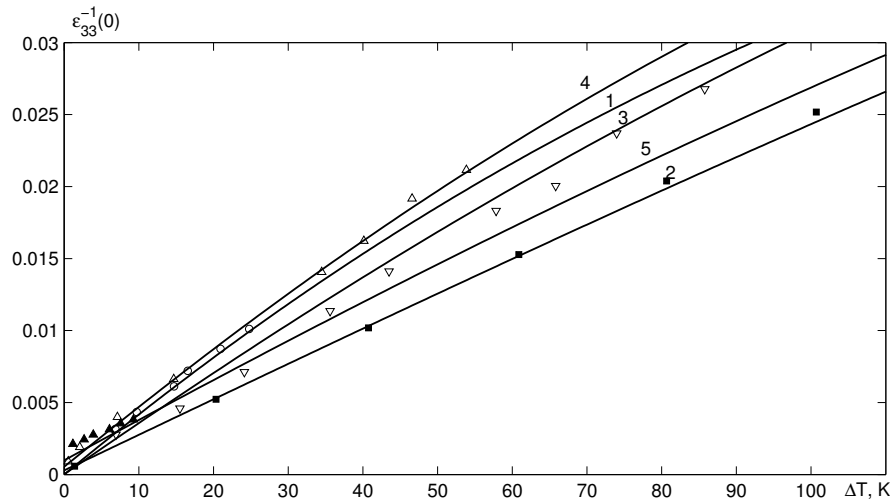


**Figure 14.** Temperature dependence of inverse longitudinal permittivity of  $\text{KH}_2\text{PO}_4$  – 1,  $\bullet$  [239];  $\text{KD}_2\text{PO}_4$  – 2,  $\blacksquare$  [216],  $\text{RbH}_2\text{PO}_4$  – 3,  $\nabla$  [241];  $\text{KH}_2\text{AsO}_4$  – 4,  $\Delta$  [119];  $\text{KD}_2\text{AsO}_4$  – 4,  $\blacktriangle$  [231]. Symbols are experimental points; solid lines are theoretical results.

The temperature dependences of static dielectric permittivities  $\varepsilon_{33}(0, T)$  of  $\text{N}(\text{H}_{1-x}\text{D}_x)_4(\text{H}_{1-x}\text{D}_x)_2\text{PO}_4$  crystals at different values of  $x$  along with the corresponding experimental points are given in figure 15.

With temperature increasing in the antiferroelectric phase, the permittivity  $\varepsilon_{33}(0, T)$  is almost constant; it has a jump-like increase at  $T = T_N$  from 5 to  $\sim 20$ –30. At a further increase of temperature, the permittivity decreases. With increasing  $x$  the values of  $\varepsilon_{33}(0, T)$  practically do not change.

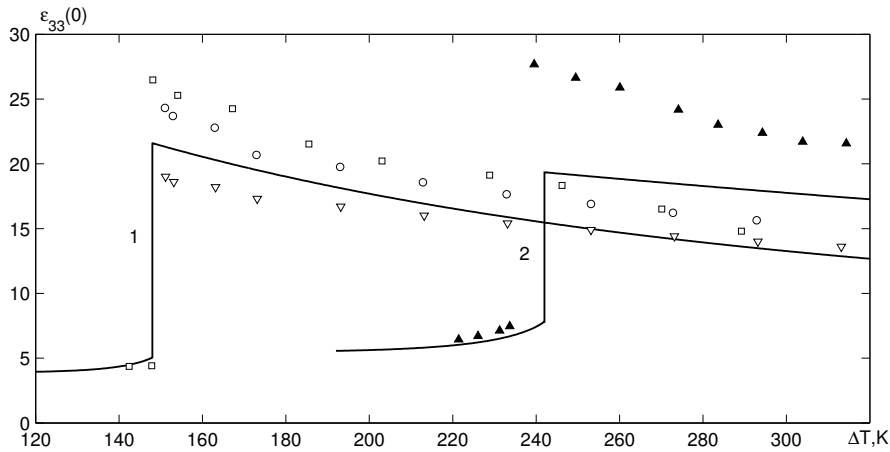


**Figure 15.** Temperature dependence of longitudinal dielectric permittivity of  $N(H_{1-x}D_x)_4(H_{1-x}D_x)_2PO_4$  at different  $x$ : 0.0 – 1,  $\circ$  [260],  $\nabla$  [7],  $\square$  [261]; 1.0 – 2,  $\blacktriangle$  [243]. Symbols are experimental points; solid lines are theoretical results.

The values of parameters  $\mu_3$  used in order to evaluate the static permittivities  $\varepsilon_{33}(0, T)$  were chosen by fitting to experiment the calculated temperature dependence of frequency-dependent permittivities  $\varepsilon_{33}^*(\omega, T)$ . The calculated temperature curves of  $\varepsilon_{33}(0, T)$  well agree with experiment in the low-temperature phase at all compositions and in the high-temperature phase at low concentrations of deuterium.

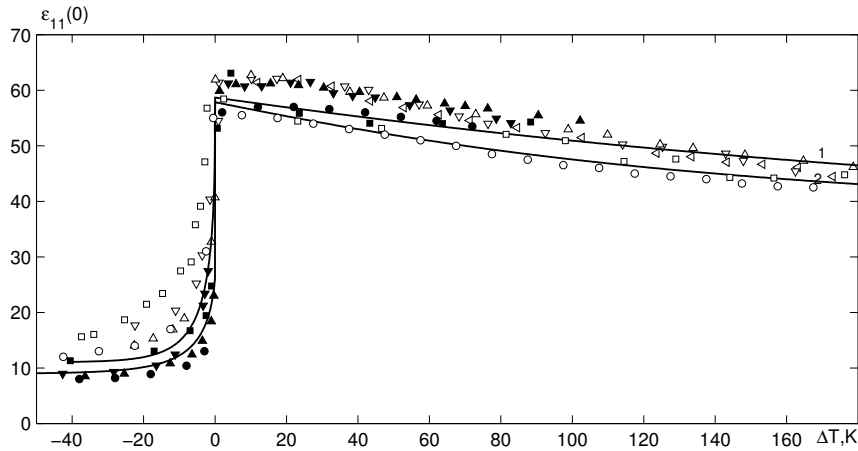


**Figure 16.** Temperature dependence of transverse permittivity of  $K(H_{1-x}D_x)_2PO_4$  at different  $x$ : 0.0 – 2,  $\square$  [8],  $\triangleleft$  [7],  $\nabla$  [257],  $\triangle$  [256],  $\circ$  [227]; 0.84 –  $\blacktriangledown$  [218]; 0.88 –  $\blacksquare$  [258]; 0.98 – 1,  $\bullet$  [227]; 1.00 –  $\blacktriangle$  [257]. Symbols are experimental points; solid lines are theoretical results.

Experimental data for the temperature dependence of transverse static dielectric permittivity  $\varepsilon_{11}(0, T)$  of the  $K(H_{1-x}D_x)_2PO_4$  crystals can be divided into two groups (figure 16): obtained in [7,218,256,257] for  $x=0.0, 0.84, 0.98$  and obtained in [258,8,227], where the values of  $\varepsilon_{11}(0, T)$  are by 6–10% lower. Also, a  $\lambda$ -like behavior of  $\varepsilon_{11}(0, T)$  was observed near  $T_c$  in [8,7,258], in contrast to the dome-like shape of the  $\varepsilon_{11}(0, T)$  found in [218,256,257,227]. In [227] it was shown that the appearance of the  $\lambda$ -like peak in  $\varepsilon_{11}(0, T)$  is caused by an imprecise orientation of  $x$ -cuts of the samples used. Detailed measurements of the temperature dependences of  $\varepsilon_{11}(0, T)$  for the  $K(H_{1-x}D_x)_2PO_4$  crystals with different deuterations were performed. A weak composition

dependence of  $\varepsilon_{11}(0, T)$  was revealed (figure 16). The magnitude of  $\varepsilon_{11}^{\max}(0)$  increases with increasing  $x$  from 56.4 at  $x=0$  up to 57.4 at  $x=0.98$ . At the transition point, the jumps of  $\varepsilon_{11}(0, T)$  are observed, whose values increase with increasing  $x$ .

The calculated temperature dependences of dielectric permittivity  $\varepsilon_{11}(0, T)$  for  $\text{N}(\text{H}_{1-x}\text{D}_x)_4(\text{H}_{1-x}\text{D}_x)_2\text{PO}_4$  at different deuteration along with the experimental data are presented in figure 17.

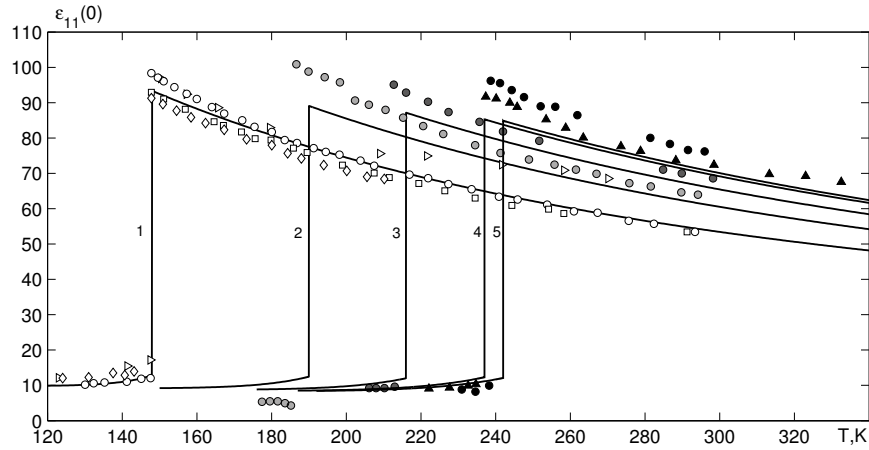


**Figure 17.** The temperature dependence of transverse permittivity  $\text{N}(\text{H}_{1-x}\text{D}_x)_4(\text{H}_{1-x}\text{D}_x)_2\text{PO}_4$  at different  $x$ : 0.0 – 1,  $\diamond$  [262],  $\square$  [263],  $\triangleright$  [264],  $\circ$  [265]; 0.45 – 2,  $\bullet$  [265]; 0.74 – 3,  $\bullet$  [265]; 0.95 – 4,  $\bullet$  [265]; 1.0 – 5,  $\blacktriangle$  [243]. Symbols are experimental points; solid lines are theoretical results.

With increasing temperature the permittivity  $\varepsilon_{11}(0, T)$  is practically constant in the low-temperature phase and has a jump-like increase at  $T = T_N$ . With further increase of temperature, the values of  $\varepsilon_{11}(0, T)$  decrease and are practically independent of deuteration. It should be noted that the values of the parameters  $\mu_1^a$  used in calculations of the static dielectric permittivities  $\varepsilon_{11}(0, T)$  of these crystals were determined with taking into account the temperature curves of the dynamic permittivities  $\varepsilon_{11}^*(\omega, T)$ . A good quantitative description of the available experimental data for the temperature curves of  $\varepsilon_{11}(0, T)$  of these crystals is obtained in the low-temperature phase and at low deuterium concentration in the paraelectric phase.

Let us now consider the longitudinal dynamic characteristic of ferroelectric crystals  $\text{M}(\text{H}_{1-x}\text{D}_x)_2\text{XO}_4$ . The major features of dynamical characteristics of these compounds are as follows. As calculations show, the major contribution to the dispersion of  $\varepsilon_{33}^s(\omega, T)$  in these crystals is made by the first relaxation mode  $\chi_{1s,a}^z \gg \chi_{js,a}^z$ , that is, the dispersion is nearly of the Debye type. An essential contribution to  $\varepsilon_{33}^s(\omega, T)$  is made by the charged configurations ( $\omega \neq 0$ ) and by the long-range interactions. Only  $\tau_{1s,a}^z$ , calculated within the four-particle cluster approximation, are strongly temperature dependent. The relaxation times  $\tau_{2,3,4s}^z$  and  $\tau_{2,3a}^z$ , in contrast to  $\tau_{1s,a}^z$ , are hardly temperature dependent and much smaller than  $\tau_{1s,a}^z$ .

In figure 18–21 we show the calculated temperature dependences of dielectric permittivities  $\varepsilon'_{33}(\omega, T)$  and  $\varepsilon''_{33}(\omega, T)$  for the  $\text{KH}_2\text{PO}_4$ ,  $\text{KD}_2\text{PO}_4$ ,  $\text{RbH}_2\text{PO}_4$ , and  $\text{KH}_2\text{AsO}_4$  crystals along with the experimental points at different frequencies.

Starting from a certain frequency  $\nu_k$ , the low-frequency maximum in the temperature curve of  $\varepsilon'_{33}(\omega, T)$  changes to a sharp dip (minimum) at  $\Delta T = 0$  K, which widens and deepens with increasing frequency, reaching the value of  $\varepsilon_{33}^0$  at  $\nu \sim 10^{11}$  Hz. The maximum of the temperature curve of  $\varepsilon'_{33}(\omega, T)$  taking place at the temperature  $\Delta T_n = |T_n - T_c|$  increases with the frequency increase and smears out, whereas the value of  $\Delta T_n$  increases. An increase in frequency reduces the values of  $\varepsilon'_{33}(\omega, T)$  at all  $\Delta T = |T - T_c|$ . The maximal values of  $\varepsilon'_{33}(\omega)$  and the values of  $\Delta T_n$  in the paraelectric phase are much larger than in the ferroelectric phase. The dispersion of

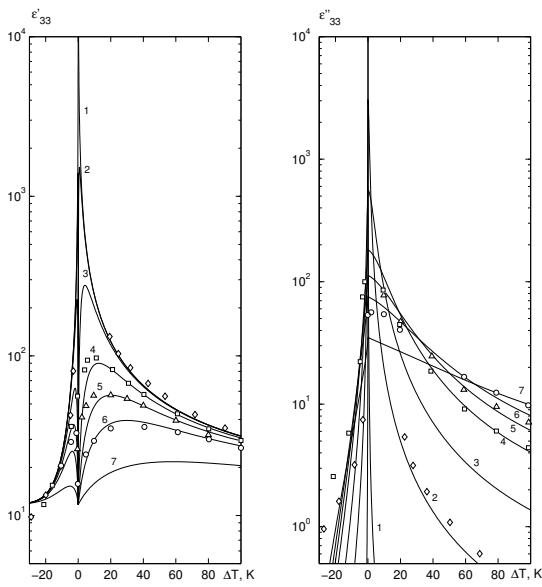


**Figure 18.** The temperature dependences of  $\varepsilon'_{33}$  and  $\varepsilon''_{33}$  of  $\text{KH}_2\text{PO}_4$  at different frequencies  $\nu$  (GHz): 0.038 – 1; 9.2 – 2,  $\diamond$  [199]; 50 – 3; 154.2 – 4,  $\square$  [200]; 249 – 5,  $\triangle$  [200]; 372 – 6,  $\circ$  [200]; 800 – 7. Symbols are experimental points; solid lines are theoretical results.

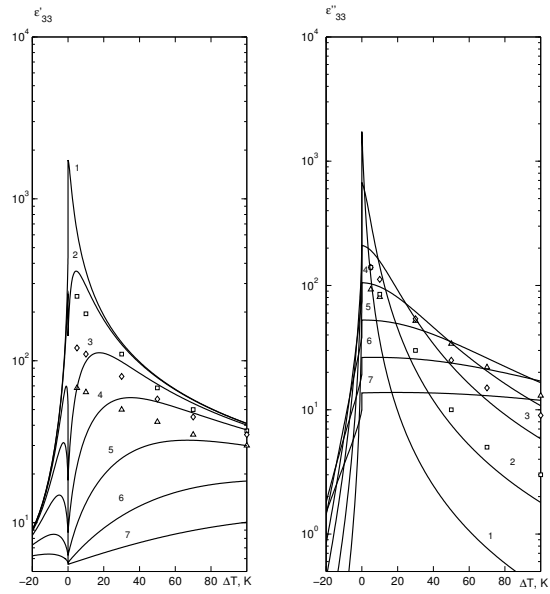


**Figure 19.** The temperature dependences of  $\varepsilon'_{33}$  and  $\varepsilon''_{33}$  of  $\text{KD}_2\text{PO}_4$  at different frequencies  $\nu$  (GHz): 0.609 – 1; 3.0 – 2,  $\square$  [201]; 10.0 – 3,  $\diamond$  [201]; 20.0 – 4,  $\triangle$  [201]; 40.0 – 5; 80.0 – 6; 154.2 – 7. Symbols are experimental points; solid lines are theoretical results.

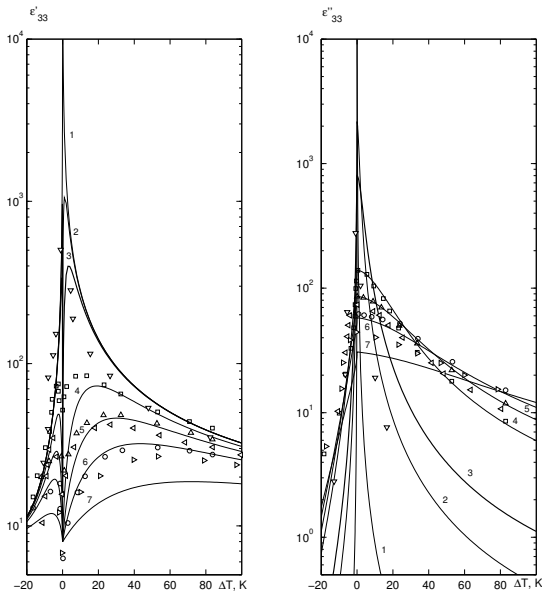


**Figure 20.** The temperature dependences of  $\varepsilon'_{33}$  and  $\varepsilon''_{33}$  of  $\text{RbH}_2\text{PO}_4$  at different frequencies  $\nu$  (GHz): 0.25 – 1; 10.0 – 2; 27.0 – 3,  $\nabla$  [267]; 154.2 – 4,  $\square$  [203]; 198.0 –  $\triangleleft$  [222]; 250.2 – 5,  $\triangle$  [203]; 366.0 –  $\triangleright$  [222]; 372.0 – 6,  $\circ$  [203]; 700.0 – 7. Symbols are experimental points; lines are theoretical results.

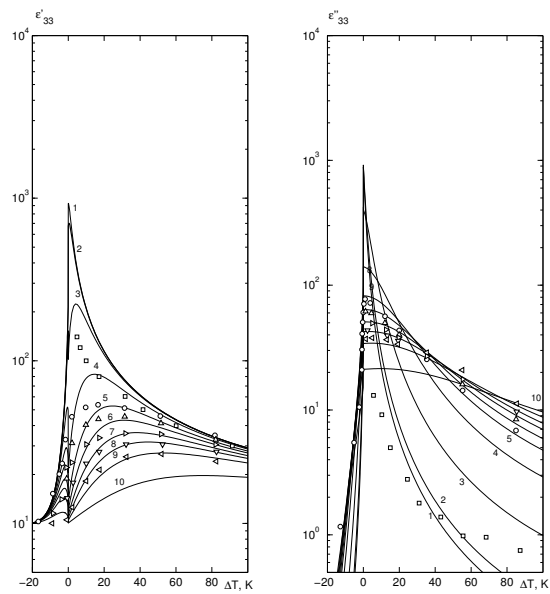


**Figure 21.** The temperature dependences of  $\varepsilon'_{33}$  and  $\varepsilon''_{33}$  of  $\text{KH}_2\text{AsO}_4$  at different frequencies  $\nu$  (GHz): 6.9 – 1; 9.2 – 2,  $\square$  [199]; 30.0 – 3; 90.0 – 4; 154.2 – 5,  $\circ$  [203]; 198.9 – 6,  $\triangle$  [203]; 250.2 – 7,  $\triangleright$  [203]; 299.1 – 8,  $\nabla$  [203]; 372.0 – 9,  $\triangleleft$  [203]; 600.0 – 10. Symbols are experimental points; lines are theoretical results.



$\varepsilon'_{33}(\omega, T)$  in the ferroelectric phase is observed in a narrow temperature range  $\Delta T \sim 20$  K, whereas in the paraelectric phase this range is much wider (about 200 K). The minimum of  $\varepsilon'_{33}(\omega, T)$  at  $\Delta T = 0$  arises at the frequency  $\nu_k = (2\pi\tau_1^z)^{-1}$ , that is at the center of the dispersion region. For  $\text{KH}_2\text{PO}_4$   $\nu_k = 0.038$  GHz; for  $\text{KD}_2\text{PO}_4$   $\nu_k = 0.43$  GHz; for  $\text{RbH}_2\text{PO}_4$   $\nu_k = 0.25$  GHz; for  $\text{KH}_2\text{AsO}_4$   $\nu_k = 6.9$  GHz.

With the increase of the deuteration level  $x$  in the  $\text{K}(\text{H}_{1-x}\text{D}_x)_2\text{PO}_4$  system, the value of  $\varepsilon'_{33}(\omega, T)$  decreases, whereas the range  $\Delta T_n$  widens. With isomorphic replacement  $\text{K} \rightarrow \text{Rb}$ ,  $\text{P} \rightarrow \text{As}$  the maximal values of  $\varepsilon'_{33}(\omega, T)$  remain almost the same, whereas the range  $\Delta T_n$  slightly increases. With a decreasing  $\Delta T$ , the magnitude of  $\varepsilon''_{33}(\omega, T)$  in these crystals increases in the ferroelectric phase, reaching maximum at  $\Delta T = 0$ , and decreases in the paraelectric phase. With an increase of frequency, the maximal values of permittivity  $\varepsilon''_{33}(\omega, T)$  as well as the rate of their change with an increase of  $\Delta T$  decrease. At  $\nu_k$  we have  $\varepsilon'_{33}(\omega, T) = \varepsilon''_{33}(\omega, T)$ , namely,  $3740 \cdot 10^2$  in  $\text{KD}_2\text{PO}_4$ ,  $17.4 \cdot 10^2$  in  $\text{KD}_2\text{PO}_4$ ,  $430 \cdot 10^2$  in  $\text{RbH}_2\text{PO}_4$ , and  $9.2 \cdot 10^2$  in  $\text{KH}_2\text{AsO}_4$ .

It should be noted that the experimental data [199,200,203,266] for undeuterated  $\text{MH}_2\text{XO}_4$  crystals correspond to the region of the dielectric permittivity dispersion, whereas for  $\text{KD}_2\text{PO}_4$  the submillimetric spectroscopy frequencies [200] correspond to the high-frequency “tail” of the dispersion, and the data of [201] are for the low-frequency tail. Additional experimental measurements of  $\varepsilon'_{33}(\omega, T)$  above 10 GHz are required to verify the validity of the developed theory for the longitudinal dynamic characteristics of the highly deuterated  $\text{M}(\text{H}_{1-x}\text{D}_x)_2\text{XO}_4$  crystals.

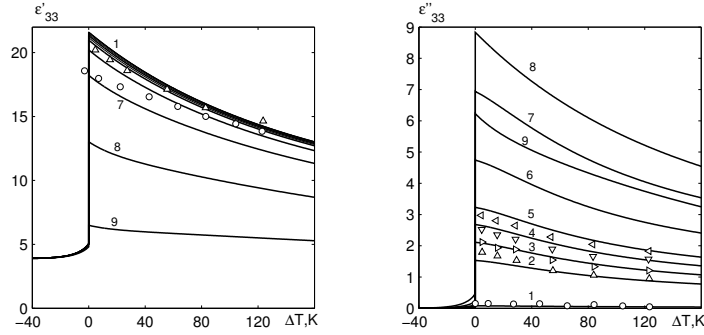


**Figure 22.** The temperature dependences of  $\varepsilon'_{33}$  and  $\varepsilon''_{33}$  of  $\text{NH}_4\text{H}_2\text{PO}_4$  at different frequencies  $\nu$  (GHz): 9.2 – 1,  $\circ$  [199]; 180.0 – 2,  $\Delta$  [232]; 249.9 – 3,  $\triangleright$  [232]; 320.1 – 4,  $\nabla$  [232]; 390.0 – 5,  $\triangleleft$  [232]; 600.0 – 6; 1000.0 – 7; 2000.0 – 8; 5000.0 – 9. Symbols are experimental points; lines are theoretical results.

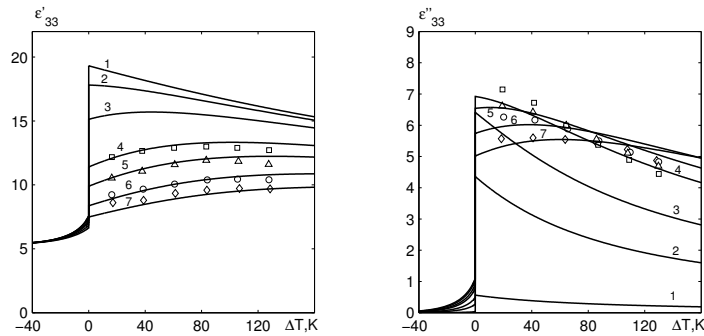


**Figure 23.** The temperature dependences of  $\varepsilon'_{33}$  and  $\varepsilon''_{33}$  of  $\text{N}(\text{H}_{0.02}\text{D}_{0.98})_4(\text{H}_{0.02}\text{D}_{0.98})_2\text{PO}_4$  at different frequencies  $\nu$  (GHz): 9.2 – 1; 80.0 – 2; 150.0 – 3; 262.0 – 4,  $\square$  [158,232]; 330.0 – 5  $\triangle$  [158,232]; 437.0 – 6  $\circ$  [158,232]; 540.0 – 7  $\diamond$  [158,232]. Symbols are experimental points; lines are theoretical results.

In figures 22–23 we show the calculated temperature dependences of dielectric permittivities  $\varepsilon'_{33}(\omega, T)$  and  $\varepsilon''_{33}(\omega, T)$  of  $N(\text{H}_{1-x}\text{D}_x)_4(\text{H}_{1-x}\text{D}_x)_2\text{PO}_4$  at  $x = 0.0$  and  $x = 0.98$  along with the experimental points at different frequencies. A good quantitative description of the experimental data of [158,232] is obtained.

It should be noted that the temperature curve of  $\varepsilon'_{33}(\omega)$  at  $T = T_N$  and  $x = 0.98$  has a maximum at frequencies below the dispersion frequency and a shallow minimum at higher frequencies. With an increase of frequency, the maximal values of the permittivities decrease and shift to larger  $\Delta T$ . At  $T = T_N$  the value of  $\varepsilon'_{33}(\omega)$  in  $\text{NH}_4\text{H}_2\text{PO}_4$  is maximal at all frequencies. At the transition point the imaginary part of the permittivity  $\varepsilon''_{33}(\omega)$  at  $x = 0.0$  also has maxima at all frequencies. At  $x = 0.98$   $\varepsilon''_{33}(\omega)$  has maxima at  $T = T_N$ , which, however, transform to minima at high frequencies.

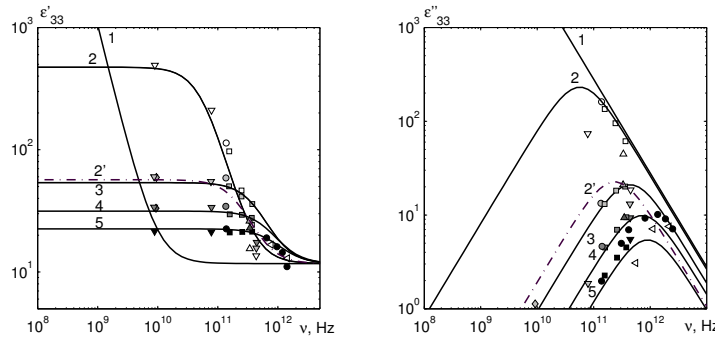


**Figure 24.** The frequency dependences of  $\varepsilon'_{33}$  and  $\varepsilon''_{33}$  of  $\text{KH}_2\text{PO}_4$  at different temperatures  $\Delta T(\text{K})$ : 0 – 1; 5 – 2,  $\circ$  [266],  $\square$  [200],  $\diamond$  [199],  $\triangle$  [222],  $\nabla$  [268]; 50 – 3,  $\bullet$  [266],  $\blacksquare$  [200],  $\blacklozenge$  [199],  $\blacktriangle$  [222],  $\blacktriangledown$  [268]; 100 – 4,  $\bullet$  [266],  $\blacksquare$  [200],  $\blacklozenge$  [199],  $\blacktriangle$  [222],  $\blacktriangledown$  [268]; 173 – 5,  $\bullet$  [266],  $\blacksquare$  [200],  $\blacklozenge$  [199],  $\blacktriangle$  [222],  $\blacktriangledown$  [268]; 167 –  $\blacktriangleleft$  [270]; -5 – 2'. Symbols are experimental points; lines are theoretical results.

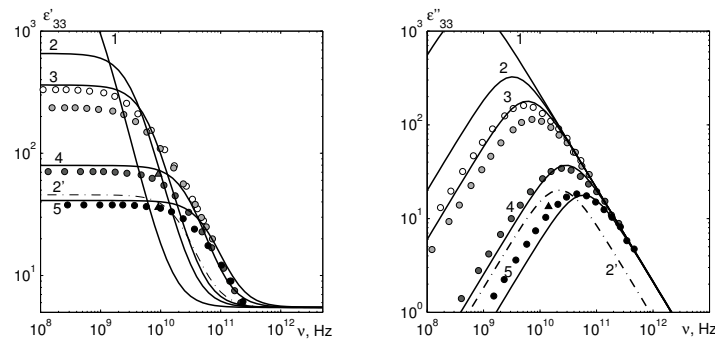


**Figure 25.** The frequency dependences of  $\varepsilon'_{33}$  and  $\varepsilon''_{33}$  of  $\text{KD}_2\text{PO}_4$  at different temperatures  $\Delta T(\text{K})$ : 0 – 1; 5 – 2,  $\triangle$  [213]; 10K – 3,  $\circ$  [213]; 50 – 4,  $\bullet$  [213],  $\blacktriangle$  [199]; 100 – 5,  $\bullet$  [213],  $\blacktriangle$  [199]; -5 – 2'. Symbols are experimental points; lines are theoretical results.

Investigations of the frequency dependences of the real and imaginary parts of the dielectric permittivity are very important for ferroelectric materials. In figures 24–27 we show the calculated frequency dependences of  $\varepsilon'_{33}(\omega, T)$  and  $\varepsilon''_{33}(\omega, T)$  for  $\text{KH}_2\text{PO}_4$ ,  $\text{KD}_2\text{PO}_4$ ,  $\text{RbH}_2\text{PO}_4$ , and  $\text{KH}_2\text{AsO}_4$  crystals at different temperatures  $\Delta T$  along with the corresponding experimental data. It should be mentioned that at low frequencies ( $\nu < 10^7$  Hz) for these crystals  $\varepsilon'_{33}(\omega, T) = \varepsilon_{33}(0, T)$ , whereas at high frequencies ( $\nu > 10^{13}$  Hz)  $\varepsilon'_{33}(\omega, T) = \varepsilon_{33}^0$ . At  $\nu_{T3} = (2\pi\tau^z(T))^{-1}$  the dielectric contribution  $\varepsilon_T = \varepsilon_{33}(0, T) - \varepsilon_{33}^0$  is twice decreased. With increasing  $\Delta T$ , the magnitude of  $\varepsilon'_{33}(\omega, T)$  and the rate of the changes in  $\varepsilon'_{33}(\omega, T)$  with frequency decrease.  $\varepsilon''_{33}(\omega, T) \rightarrow 0$  both at low ( $\omega \rightarrow 0$ ) and

high ( $\omega \rightarrow \infty$ ) frequencies. At  $\nu_{T3}$  the value of  $\varepsilon''_{33}(\omega, T)$  is maximal; with increasing  $\Delta T$  it lowers down and shifts to higher frequencies. At the same distance from the transition point  $|\Delta T| = 5$  K,

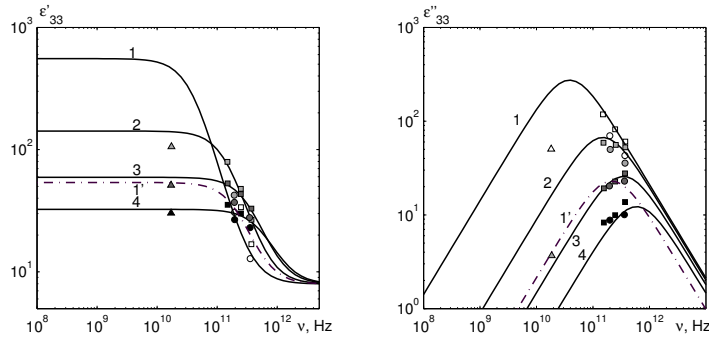


**Figure 26.** The frequency dependences of  $\varepsilon'_{33}$  and  $\varepsilon''_{33}$  of  $\text{RbH}_2\text{PO}_4$  at different temperatures  $\Delta T$ (K): 5 – 1,  $\circ$  [222],  $\square$  [203],  $\triangle$  [267]; 20 – 2,  $\circ$  [222],  $\square$  [203],  $\triangle$  [267]; 50K – 3,  $\bullet$  [222],  $\blacksquare$  [203],  $\blacktriangle$  [267]; 100 – 4,  $\bullet$  [222],  $\blacksquare$  [203],  $\blacktriangle$  [267]; -5 – 1'. Symbols are experimental points; lines are theoretical results.

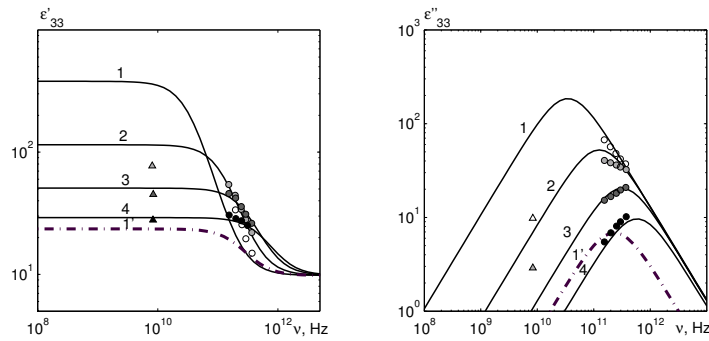


**Figure 27.** The frequency dependences of  $\varepsilon'_{33}$  and  $\varepsilon''_{33}$  of  $\text{KH}_2\text{AsO}_4$  at different temperatures  $\Delta T$ (K): 5 – 1,  $\circ$  [203]; 20 – 2,  $\circ$  [203],  $\triangle$  [199]; 50 – 3,  $\bullet$  [203],  $\blacktriangle$  [199]; 100 – 4,  $\bullet$  [203],  $\blacktriangle$  [199]; -5 – 1'. Symbols are experimental points; lines are theoretical results.

in the ferroelectric phase the values of  $\varepsilon'_{33}(\omega, T)$  and  $\varepsilon''_{33}(\omega, T)$  are smaller than in the paraelectric phase, whereas the permittivity dispersion is shifted to higher frequencies.

In figure 24 it is seen that in  $\text{KH}_2\text{PO}_4$  the calculated values of  $\varepsilon'_{33}(\omega, T)$  and  $\varepsilon''_{33}(\omega, T)$  well agree with the data of [200,199,266]. The calculated frequency dependence of  $\varepsilon'_{33}(\omega, T)$  also agrees with the data of [268] at some frequencies, and the calculated  $\varepsilon''_{33}(\omega, T)$  agrees with this experiment at high frequencies. The theoretical frequency curve of  $\varepsilon''_{33}(\omega, T)$  at  $\Delta T = 173$  K shifts to low frequencies and goes below the experimental points of [269]. The calculated frequency dependences of  $\varepsilon'_{33}(\omega, T)$  and  $\varepsilon''_{33}(\omega, T)$  for  $\text{KD}_2\text{PO}_4$  at different temperatures on the whole well agree with the experimental points of [213] (see figure 25). However, at the dispersion frequencies at  $\Delta T \rightarrow 0$  the measured in [213]  $\varepsilon'_{33}(\omega, T)$  has a maximum, not a minimum. Description of experimental data for  $\varepsilon'_{33}(\omega, T)$  and  $\varepsilon''_{33}(\omega, T)$  in  $\text{RbH}_2\text{PO}_4$  [203,222,267] (figure 26) and  $\text{KH}_2\text{AsO}_4$  [203,199] (figure 27) is also satisfactory.

The calculated frequency dependences of  $\varepsilon^*_{33}(\omega)$  of  $\text{N}(\text{H}_{1-x}\text{D}_x)_4(\text{H}_{1-x}\text{D}_x)_2\text{PO}_4$  at  $x = 0.0$  and  $x = 0.98$ , as well as experimental points are presented in figures 28–29. As one can see, the theoretical curves of  $\varepsilon^*_{33}(\omega)$  at different temperatures  $\Delta T$  well agree with the experiment. It should be noted that the experimental data for  $\varepsilon^*_{33}(\omega)$  at  $x = 0.98$  [232] correspond to the dispersion region, whereas at  $x = 0.0$  they are below the dispersion. At  $\Delta T = 0$  K the dispersion frequency

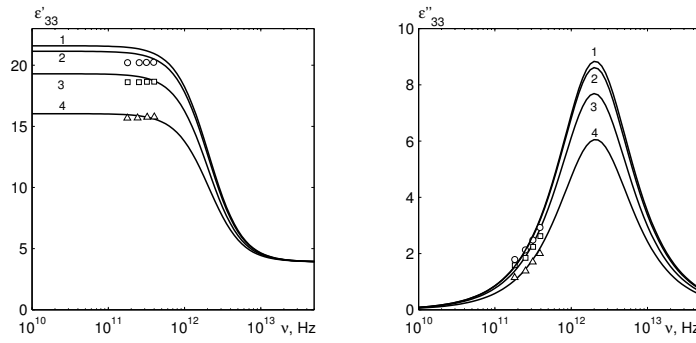


**Figure 28.** The frequency dependence of  $\varepsilon'_{33}$  and  $\varepsilon''_{33}$  of  $\text{NH}_4\text{H}_2\text{PO}_4$  at different temperatures  $\Delta T(\text{K})$  [232]: 0.0 – 1; 5.0 – 2,  $\circ$  ; 28.0 – 3,  $\square$  ; 82.0 – 4,  $\triangle$  . Symbols are experimental points; lines are theoretical results.

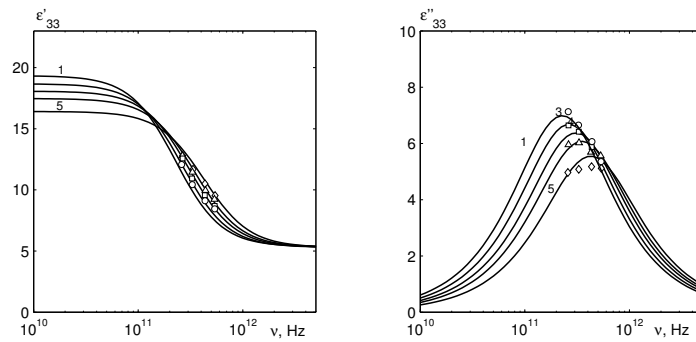


**Figure 29.** The frequency dependence of  $\varepsilon'_{33}$  and  $\varepsilon''_{33}$  of  $\text{N}(\text{H}_{0.02}\text{D}_{0.98})_4(\text{H}_{0.02}\text{D}_{0.98})_2\text{PO}_4$  at different temperatures  $\Delta T(\text{K})$  [158,232]: 0.0 – 1; 19.0 – 2,  $\circ$  ; 41.0 – 3,  $\square$  ; 64.0 – 4,  $\triangle$  ; 108.0 – 5,  $\diamond$  . Symbols are experimental points; lines are theoretical results.

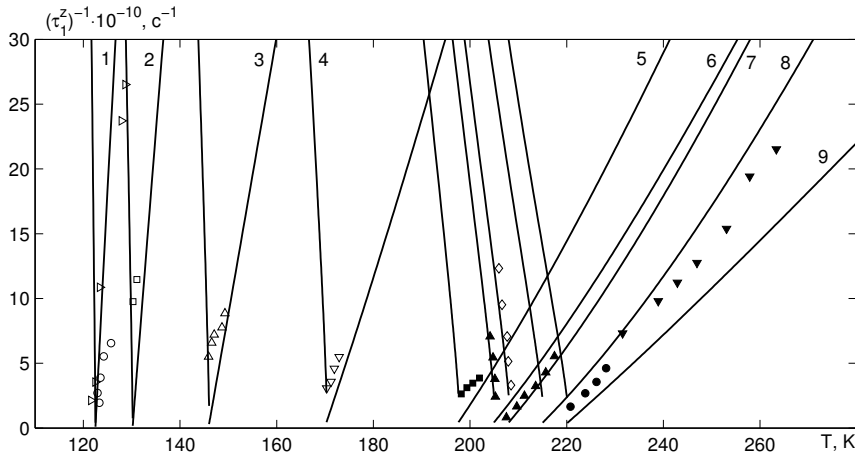


**Figure 30.** Temperature dependence of the inverse polarization relaxation time at different  $x$ : 0.0 – 1.  $\triangleright$  [271],  $\triangleleft$  [272],  $\circ$  [273]; 0.07 – 2.  $\square$  [209]; 0.21 – 3.  $\triangle$  [209]; 0.43 – 4.  $\nabla$  [209]; 0.72 – 5.  $\blacksquare$  [209]; 0.805 – 6.  $\blacktriangle$  [212]; 0.84 – 7.  $\diamond$  [274]; 0.93 – 8.  $\blacktriangledown$  [272]; 1.0 – 9.  $\bullet$  [275]. Symbols are experimental points; lines are theoretical results.

for the longitudinal permittivity at  $x = 0.0$  is 2062 GHz. With deuteration the dispersion frequency decreases down to 228.5 GHz. With increasing temperature  $\Delta T$ , the dispersion frequency slightly increases for  $\varepsilon_{33}^*(\omega, T)$  at  $x = 0.98$ . At  $x = 0.0$  the dispersion frequency of  $\varepsilon_{33}^*(\omega, T)$  remains practically unchanged with an increasing  $\Delta T$ .

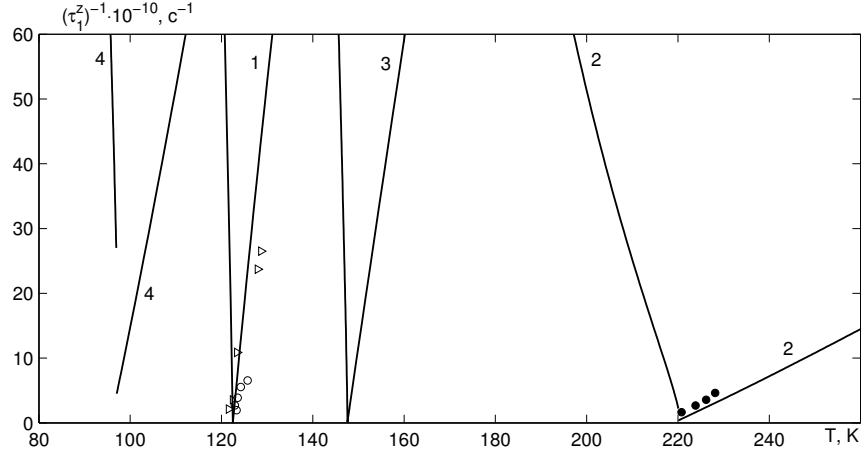


**Figure 31.** Temperature dependence of inverse polarization relaxation time  $(\tau_1^z)^{-1}$  of: 1 –  $\text{KH}_2\text{PO}_4$ ; 2 –  $\text{KD}_2\text{PO}_4$ ; 3 –  $\text{RbH}_2\text{PO}_4$ ; 4 –  $\text{KH}_2\text{AsO}_4$ ; Symbols are experimental points; lines are theoretical results.

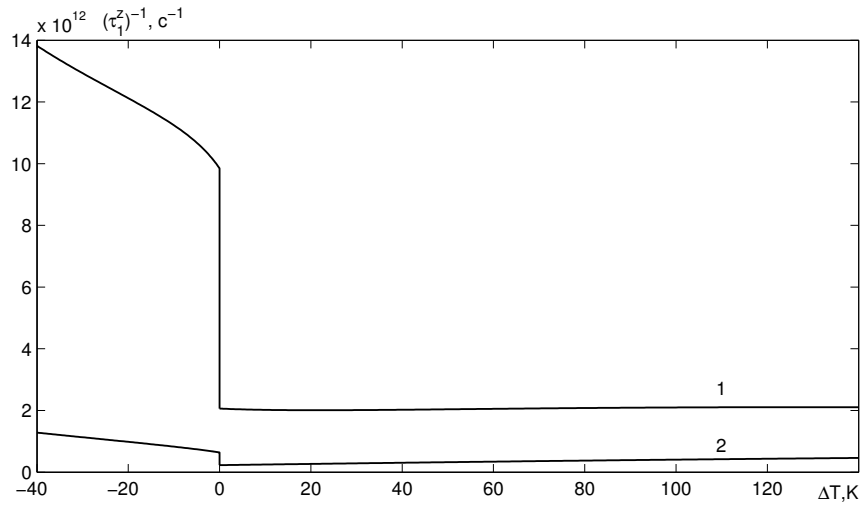


**Figure 32.** Temperature dependence of inverse polarization relaxation time  $(\tau_1^z)^{-1}$  of  $\text{N}(\text{H}_{1-x}\text{D}_x)_4(\text{H}_{1-x}\text{D}_x)_2\text{PO}_4$  at different  $x$ : 0.0 – 1; 0.98 – 2.

In figure 30 we depicted the calculated temperature dependence of the inverse relaxation time  $(\tau_{1s}^z)^{-1}$  for  $\text{K}(\text{H}_{1-x}\text{D}_x)_2\text{PO}_4$  at different  $x$  along with the experimental points. Overall, a satisfactory agreement between the proposed theory and the experiment is obtained. The difference between the calculated  $(\tau_{1s}^z)^{-1}$  and those obtained from experimental dielectric spectral and ultrasound measurements [212] is related to the fact that, in addition to the ferroelectric relaxation, other dissipation mechanisms (e. g. scattering by impurities) also contribute to the observed relaxation times. The temperature curve of  $(\tau_{1s}^z)^{-1}$  is nonlinear, especially at high  $x$ . Deuteration increases the relaxation time  $(\tau_{1s}^z)$  and reduces the dispersion frequency in  $\text{K}(\text{H}_{1-x}\text{D}_x)_2\text{PO}_4$ . In the

paraelectric phase the relaxation time ( $\tau_{1s}^z$ ) is larger than in the ferroelectric phase. The changes in the temperature dependences of the inverse relaxation time  $(\tau_{1s}^z)^{-1}$  at isomorphic replacements  $K \rightarrow Rb$ ,  $P \rightarrow As$  are illustrated in figure 31. In figure 32 we show the temperature dependences of inverse relaxation times  $(\tau_{1a}^z)^{-1}$  for  $N(H_{1-x}D_x)_4(H_{1-x}D_x)_2PO_4$  at  $x = 0.0$  and  $x = 1.0$ . It is seen that in the paraelectric phase the value of  $(\tau_{1a}^z)^{-1}$  is slightly temperature dependent. At the first order phase transition  $(\tau_{1s,a}^z)^{-1}$  has a jump.

## 5. Concluding remarks

In this paper using the proposed unified proton ordering model we develop a theory of relaxational phenomena and thermodynamic properties of ferroelectric compounds of the  $KH_2PO_4$  family. Within the four-particle cluster approximation for short-range interactions and mean field approximation for the long-range interactions and without tunneling taken into account we calculate their thermodynamic and longitudinal dynamic characteristics. Calculations of the physical characteristics of partially deuterated crystals are performed within the mean crystal approximation.

General dependences of thermodynamic and longitudinal dynamic characteristics of ferroelectric crystals of the  $KH_2PO_4$  family on the values of the model parameters are established. Using these dependences we propose an approach to determination of optimal values of the model parameters for the  $K(H_{1-x}D_x)_2PO_4$  type ferroelectrics and  $N(H_{1-x}D_x)_4(H_{1-x}D_x)_2PO_4$  type antiferroelectrics. We have shown that at the proper choice of the theory parameters the proposed theory provides a satisfactory quantitative description of the available experimental data for these compounds even without tunneling taken into account. Tunneling being taken into account [120–122], however, provides a much better quantitative description of the available experimental data for thermodynamic characteristics of undeuterated ferroelectrics of the  $KH_2PO_4$  family. Without tunneling the shape of the calculated temperature curves of spontaneous polarization and proton contribution to the specific heat is somewhat deformed, especially for  $KH_2PO_4$  and  $RbH_2PO_4$  crystals, where the phase transitions are close to the second order (see figures 5,6,8,9). In the case of  $KH_2AsO_4$  (see figure 6), where a strong first order phase transition takes place, the temperature curves of spontaneous polarization calculated with and without tunneling taken into account practically coincide. Also, tunneling taken into account somewhat improves an agreement between the theory and experiment for  $T_c - T_0$ . Thus, in order to describe thermodynamic characteristics of undeuterated and slightly deuterated [123–126] ferroelectrics  $KH_2PO_4$  and  $RbH_2PO_4$  it is worthwhile to take tunneling into account.

It should be noted that in [196] based on the unified proton ordering model proposed in this paper and in the cluster approximation, we calculated the physical characteristics of the  $Rb_{1-y}(NH_4)_yH_2PO_4$  type systems. A satisfactory quantitative description of experimental data was obtained. Of course, the results obtained in [196] at  $y = 0$  and  $y = 1$  agree with the results of the present paper.

This work as well as [120–123,126], and [166–180], where the observed field and pressure dependences of the physical characteristics of  $KH_2PO_4$  family crystals were properly described, have significantly strengthened the positions of the proton ordering model for these compounds. The results of [164], [181–184] also indicate the validity of the model.

## References

1. Uehling E.A. Theories of Ferroelectricity in  $KH_2PO_4$  – In: Lecture in Theoretical Physics. New-York-London, 1963, **5**, 138–217.
2. Sielsbee H.B., Uehling E.A., Schmidt V.H., Phys. Rev., 1964, **133**, No. 1A, A165.
3. Blinc R. Ferroelectricity. - In: Theory of Condensed Matter. - Vienna, I.E.A.E., 1968, 395–442.
4. Vaks V.G., Introduction into microscopic theory of ferroelectrics, Moscow, 1973 (in Russian).
5. Blinc R., Zeks B. Ferroelectrics and antiferroelectrics. Lattice dynamics. Moscow, 1975 (in Russian).
6. Vaks V.G., Zinenko V.I., Shneider V.E., Usp. Fiz. Nauk, 1983, **141**, No. 4(10), 629 (in Russian).
7. Mason W. Piezoelectric crystals and their application in ultraacoustics. Moscow, 1952 (in Russian).
8. Kentsig V. Ferroelectrics and antiferroelectrics. Moscow, 1960 (in Russian).

9. Iona F., Shirane D. Ferroelectric crystals. Moscow, 1965 (in Russian).
10. Zheludev I.S. Physics of crystal dielectrics. Moscow, 1968 (in Russian).
11. Zheludev I.S. Basis of ferroelectricity. Moscow, 1973 (in Russian).
12. Lines M., Glass A. Ferroelectrics and related to them materials. Moscow, 1981 (in Russian).
13. Strukov B.A., Levanyuk A.P. Physical basis of ferroelectric phenomena in crystals. Moscow, 1983 (in Russian).
14. Aksenov V.L., Plakida N.M., Stamenkovich S. Neutron scattering by ferroelectrics. Moscow, 1984 (in Russian).
15. Smolenskiy G.A., Bokov V.A., Isupov V.A., Krayniy N.N., Pasyukov R.E., Sokolov A.I., Yushin N.K. Physics of ferroelectric phenomena. Leningrad, 1985 (in Russian).
16. Matsubara T. Jap. J. Appl. Phys., 1985, **24**, Suppl. 24–2, 1.
17. Schmidt V.H., Ferroelectrics, 1987, **72**, 157.
18. Blinc R., Zeks B., Ferroelectrics, 1987, **72**, 193.
19. Halvin S., Ferroelectrics, 1987, **71**, 183.
20. Takagi Y., Ferroelectrics, 1987, **72**, 67.
21. Samara G.A., Ferroelectrics, 1987, **71**, 161.
22. Muller K.A., Ferroelectrics, 1987, **72**, 273.
23. Litov E., Garland C.W, Ferroelectrics, 1987, **72**, 19.
24. Gervais F., Simon P., Ferroelectrics, 1987, **72**, 77.
25. Stasyuk I.V. Doctoral dissertation, Kiev, 1985.
26. Levitskii R.R., Doctoral dissertation, Kiev, 1990.
27. Matsushita E., Matsubara T., J. Phys. Soc. Jpn., 1987, **56**, No. 1, 200.
28. Frazer B.C., Pepinsky R., Acta Cryst., 1953, **6**, 273.
29. Bacon G.E., Pease R.S., Proc. Roy. Soc., 1955, **A230**, No. 1182, 359.
30. Keeling R.O. Jr., Pepinsky R., Z. Kristallographie, 1955, **106**, No. 3, 236.
31. Tenzer L., Frazer B.C., Pepinsky R., Acta Crystallogr., 1958, **11**, 505.
32. Hewat A.W., Nature, 1973, **246**, 90.
33. Wood E.A., Merz W.J., Matthias B.T., Phys. Rev., 1952, **87**, No. 3, 544.
34. Uesu Y., Kobayashi J., Phys. Stat. Sol. (a), 1976, **34**, 475.
35. Nelmes R.J. Choudhary R.N.P., Sol. State Commun., 1978, **26**, No. 11, 823.
36. Iwata Y., Koyano N., Shibuya I., J. Phys. Soc. Japan, 1980, **49**, No. 1, 304.
37. Frazer B.C., Semmingsen D., Ellenson W.D., Shirane D., Phys. Rev. B, 1979, **20**, No. 7, 2745.
38. Blinc R., Zeks B., Levstik A., Filipic C, Slak S., Burgar M., Zupancic I., Shuvalov L.A., Baranov A.I., Phys. Rev. Lett., 1979, **43**, No. 3, 231.
39. Grigas J., Levitsky R.R., Mits Ye.V., Paprotny W., Zachek I.R., Ferroelectrics, 1985, **64**, No. 1–3, 349.
40. Levitsky R.R., Zachek I.R., Mits Ye.V., Grigas J., Paprotny W., Ferroelectrics, 1986, **67**, No. 1–3, 109.
41. Negran T.J., Glass A.M., Brickenkamp C.S., Rosenstein R.D., Osterheld R.K., Susott R., Ferroelectrics, 1974, **6**, 179.
42. Helmes R.J., Choudhary R.N.P., Ferroelectrics, 1978, **21**, 467.
43. Scalapino D.J., Imry Y., Pincus P., Phys. Rev. B, 1975, **11**, No. 5, 2042.
44. De Carvalho A.V., Salinas S.R., J.Phys.Soc.Japan, 1978, **44**, No. 1, 238.
45. Levitsky R.R., Zachek I.R., Kutny I.V., Schur J.I., Grigas J., Mizeris R., Ferroelectrics, 1990, **110**, 85.
46. Levitsky R.R., Zachek I.R., Mits Ye.V., Preprint of the Bogolyubov Institute for Theoretical Physics, ITP-87–114R, Kyiv, 1987 (in Russian).
47. Levitsky R.R., Zachek I.R., Mits Ye.V., Preprint of the Bogolyubov Institute for Theoretical Physics, ITP-87–115R, Kyiv, 1987 (in Russian).
48. Zachek I.R., Mits Ye.V., Levitsky R.R., Preprint of the Bogolyubov Institute for Theoretical Physics, ITP-89–7R, Kyiv, 1987 (in Russian).
49. Slater J.C, J. Chem. Phys., 1941, **9**, No. 1, 16.
50. Takagi Y., J. Phys. Soc. Jpn., 1948, **3**, 273.
51. Senko H.E., Phys. Rev. B, 1961, **121**, No. 6, 1599.
52. Yomosa Sh., Nagamiya T., Progr. Theor. Phys., 1949, **4**, No. 3, 263.
53. Nagamiya T., Prog. Theor. Phys., 1952, **7**, No. 3, 275.
54. Ishibashi Y., Ohya S., Takagi Y., J. Phys. Soc. Jpn., 1972, **33**, No. 6, 1545.
55. Lamotte B., Gaillard J., Constantinescu O., J. Chem. Phys., 1972, **57**, No. 8, 3319.

56. Ishibashi Y., Ohya S., Takagi Y., *J. Phys. Soc. Jpn.*, 1974, **37**, No. 4, 1035.
57. Blinc R., *J. Phys. Chem. Solids*, 1960, **13**, No. 3, 204.
58. De Gennes P.G., *Solid State Commun.*, 1963, **1**, No. 6, 132.
59. Tokunaga M., Matsubara T., *Progr.Theor.Phys.*, 1966, **35**, No. 4, 581.
60. Stasyuk I.V., Levitskii R.R., *Ukr. J. Phys.*, 1969, **14**, No. 7, 1097 (in Russian).
61. Blinc R., Svetina S. *Phys. Rev.*, 1966, **147**, No. 2, 430.
62. Levitskii R.R., Stasyuk I.V., To theory of ferroelectrics with hydrogen bonds  $\text{KH}_2\text{PO}_4$ . – In: *Materials of 3th work meeting on statistical physics*. P.3, Kyiv, 1972 (in Russian).
63. Blinc R., Ribaric M., *Phys. Rev.*, 1963, **130**, No. 5, 1816.
64. Villain J., Stamenkovic S., *Phys. Stat. Sol.*, 1966, **5**, No. 2, 585.
65. Kobayashi K., *J. Phys. Soc. Japan*, 1968, **24**, No. 3, 497.
66. Cochran W., *Adv. Phys.*, 1969, **18**, No. 72, 157.
67. Stasyuk I.V., Levitskii R.R., *Phys. Stat. Sol. (b)*, 1970, **39**, No. 1, K35.
68. Stasyuk I.V., Levitskii R.R., *Ukr. J. Phys.*, 1970, **15**, No. 3, 458.
69. Stasyuk I.V., Kaminskaya N.M., *Ukr. J. Phys.*, 1974, **19**, No. 2, 237; Stasyuk I.V., Kaminskaya N.M., *Ukr. J. Phys.*, 1974, **19**, No. 2, 244.
70. Konsin N.I., *Fiz. Tverd. Tela*, 1974, **16**, No. 8, 2337 (in Russian).
71. Ganguli S., Hath D., Chaudhuri B.K., *Phys. Rev. B*, 1980, **21**, No. 7, 2937.
72. Chaudhuri B.K., Ganguli S., Nath D., *Phys. Rev. B*, 1981, **23**, No. 5, 2308.
73. Levitskii R.R., Sorokov S.I., Preprint of the Bogolyubov Institute for Theoretical Physics, ITP-81-144R, Kyiv, 1982 (in Russian).
74. Stasyuk I.V., Levitskii R.R., To theory of antiferroelectrics with hydrogen bond. – In: *Physical electronics*, Lviv, 1970 (in Russian).
75. Stasyuk I.V., Levitskii R.R., *Izv. AN SSSR, ser. fiz.*, 1971, **35**, No. 9, 1775 (in Russian).
76. Levitskii R.R., Korinevskii N.A., Stasyuk I.V., *Ukr. J. Phys.*, 1974, **19**, No. 8, 1289 (in Russian).
77. Stasyuk I.V., Levitskii R.R., Korinevskii N.A., *Phys. Stat. Sol. (b)*, 1979, **91**, No. 2, 541.
78. Levitskii R.R., Stasyuk I.V., Korinevsky H.A., *Ferroelectrics*, 1978, **21**, 481.
79. Korinevskii N.A., Levitskii R.R., *Teor. Mat. Fiz.*, 1980, **42**, No. 3, 416 (in Russian).
80. Kozitskii Y.V., Levitskii R.R., *Ukr. J. Phys.*, 1978, **23**, No. 4, 661.
81. Stasyuk I.V., *Teor. Mat. Fiz.*, 1971, **3**, No. 3, 431 (in Russian).
82. Benerjee S., Nath D., Chaudhuri B.K., *Phys. Rev. B*, 1981, **24**, No. 11, 6469.
83. Aksenov V.L., Konvent H., Schreiber J., *Teor. Mat. Fiz.*, 1979, **38**, No. 3, 388 (in Russian).
84. Aksenov V.L., Konvent H., Schreiber J., *Phys. Stat. Sol. (b)*, 1978, **88**, No. 1, K43.
85. Aksenov V.L., Schreiber J., *Phys. Lett.*, 1978, **69A**, No. 1, 56.
86. Aksenov V.L., Bobet M., Plakida N.M., *Teor. Mat. Fiz.*, 1988, **76**, No. 1, 47 (in Russian).
87. Kawasaki E., Sawada K., *Progr. Theor. Phys.*, 1970, **60**, No. 5, 1260.
88. Stasyuk I.V., Levitskii R.R., Preprint of the Bogolyubov Institute for Theoretical Physics, ITP-70-14R, Kyiv, 1970 (in Russian).
89. Stinchcombe R.B., *J. Phys. C*. 1973, **6**, No. 15, I 2459. II 2484. III 2507.
90. Levitskii R.R., Stasyuk I.V., *Ukr. J. Phys.*, 1974, **19**, No. 8, 1331 (in Russian).
91. Levitskii R.R., Kozitskii Y.V., Preprint of the Bogolyubov Institute for Theoretical Physics, ITP-74-108R, Kyiv, 1974 (in Russian).
92. Levitskii R.R., Sorokov S.I., *Ukr. J. Phys.*, 1979, **24**, No. 12, 1814.
93. Levitskii R.R., Sorokov S.I., *Ukr. J. Phys.*, 1980, **25**, No. 1, 10.
94. Levitskii R.R., Sorokov S.I., Pyndzyn I.N., Preprint of the Bogolyubov Institute for Theoretical Physics, ITP-85-40R, Kyiv, 1985 (in Russian).
95. Vakarchuk I.O., Rudavskii Y.K., *Teor. Mat. Fiz.*, 1981, **49**, No. 2, 234 (in Russian).
96. Meister H., Skalyo J., Frazer B.C., Shirane G., *Phys. Rev.*, 1969, **184**, No. 2, 550.
97. Kaminov I.P., Damen T.C., *Phys. Rev. Lett.*, 1968, **20**, No. 20, 1105.
98. Peercy P.S., *Sol. State Commun.*, 1975, **16**, No. 4, 439.
99. Peercy P.S., *Phys. Rev. B*, 1975, **12**, No. 7, 2725.
100. Courtens E., Common R., *Ferroelectrics*, 1980, **24**, 19.
101. Peercy P.S., *Phys. Rev. B*, 1976, **13**, No. 9, 3945.
102. Shigenari T., Takagi Y., *J. Phys. Soc. Japan*, 1977, **42**, No. 5, 1650.
103. Popova E.A., Bastrov D.S., *Fiz. Tverd. Tela*, 1978, **20**, No. 9, 2712 (in Russian).
104. Blinc R., Pirc R., Zeks B., *Phys. Rev. B*, 1976, **13**, No. 7, 2943.
105. Pirc H., Prelovcek P., *Phys. Rev. B*, 1977, **15**, No. 9, 4303.
106. Schreiber J., Aksenov V. L., *Ferroelectrics*, 1980, **29**, No. 1/2, 43.



107. Levitskii R.R., Sorokov S.I., Preprint of the Bogolyubov Institute for Theoretical Physics, ITP-79-80R, Kyiv, 1979 (in Russian).
108. Levitskii R.R., Sorokov S.I., Preprint of the Bogolyubov Institute for Theoretical Physics, ITP-80-14R, Kyiv, 1980 (in Russian).
109. Levitskii R.R., Sorokov S.I., Kutniy I.V., Preprint of the Bogolyubov Institute for Theoretical Physics, ITP-82-49R, Kyiv, 1982 (in Russian).
110. Scott J.F., *Rev. Mod. Phys.*, 1974, **46**, No. 1, 83.
111. Stamenovic S., *Condens. Matter Phys.*, 2002, **5**, No. 4 (32), 641.
112. Stasyuk I.V., Levitskii R.R., Zachek I.R., Moina A.P., *Phys. Rev. B*, 2000, **62**, No. 10, 6198.
113. Levitskii R.R., Zachek I.R., Vdovych A.S., Preprint of the Institute for Condensed Matter Physics, ICMP-06-08U, Lviv, 2006 (in Ukrainian).
114. Levitskii R.R., Zachek I.R., Vdovych A.S., Preprint of the Institute for Condensed Matter Physics, ICMP-07-24U, Lviv, 2007 (in Ukrainian).
115. Levitsky R.R., Korinevsky N.A., Stasjuk I.V., *Phys. Stat. Sol. (b)*, 1978, **88**, No. 1, 51.
116. Levitskii R.R., Sorokov S.I., *Condens. Matter Phys.*, 1994, No. 3, 79.
117. Vaks V.G., Zinenko V.I., *J. Exp. Theor. Phys.*, 1973, **64**, No. 2, 650 (in Russian).
118. Vaks V.G., Zein N.E., Strukov B.A., *Phys. Stat. Sol. (a)*, 1975, **30**, 801.
119. Chabin M., Gilletta F., *Ferroelectrics*, 1977, **15**, 149.
120. Levitskii R.R., Lisnii B.M., Baran O.R., *Condens. Matter Phys.*, 2001, **4**, No. 3, 523.
121. Levitskii R.R., Lisnii B.M., *J. Phys. Study*, 2002, **6**, No. 1, 91 (in Ukrainian).
122. Levitskii R.R., Lisnii B.M., Baran O.R., *Condens. Matter Phys.*, 2002, **5**, No. 3, 553.
123. Levitskii R.R., Andrusyk A.Ya., Lisnii B.M., *Ferroelectrics*, 2004, **298**, 1.
124. Andrusyk A.Ya., Levitskii R.R., Lisnii B.M., Preprint of the Institute for Condensed Matter Physics, ICMP-06-22U, Lviv, 2006 (in Ukrainian).
125. Levitskii R.R., Lisnii B.M., Andrusyk A.Ya., Preprint of the Institute for Condensed Matter Physics, ICMP-06-21U, Lviv, 2006 (in Ukrainian).
126. Levitskii R.R., Lisnii B.M., Andrusyk A.Ya., *Condens. Matter Phys.*, 2007, **10**, No. 2(50), 269.
127. Levitsky R.R., Zachek I.R., Volkov A.A., Kozlov G.V., Lebedev S.P., Preprint of the Bogolyubov Institute for Theoretical Physics, ITP-80-13R, Kyiv, 1980 (in Russian).
128. Yoshimitsu K., Matsubara T., *Suppl. Progr. Theor. Phys.*, 1968, 109.
129. Levitsky R.R., Zachek I.R., Preprint of the Bogolyubov Institute for Theoretical Physics, ITP-77-29R, Kiev, 1977.
130. Poplavko Y.M. *Physics of Dielectrics*. Kyiv, 1980 (in Russian).
131. Havlin S., Litov E., Sompolinsky H., *Phys. Lett. A*, 1975, **51**, No. 1, 33.
132. Havlin S., Litov E., Sompolinsky H., *Phys. Lett. A*, 1975, **53**, No. 1, 41.
133. Takagi V., Shigenari T., *J. Phys. Soc. Japan.*, 1975, **39**, No. 2, 440.
134. Havlin S., Sompolinsky H., *Phys. Lett. A*, 1976, **51**, No. 2, 171.
135. Levitsky R.R., Zachek I.R., Preprint of the Bogolyubov Institute for Theoretical Physics, ITP-80-106R, Kiev, 1980 (in Russian).
136. Levitsky R.R., Zachek I.R., Preprint of the Bogolyubov Institute for Theoretical Physics, ITP-82-8R, Kiev, 1982 (in Russian).
137. Tyablikov S.V. *Methods of quantum theory of magnetism*, Moscow, 1975 (in Russian).
138. Yukhnovskii I.R., Levitskii R.R., Sorokov S.I., Derzhko O.V., *Izv. AN SSSR, ser. fiz.*, 1991, **55**, No. 3, 481 (in Russian).
139. Yukhnovskii I.R., Levitskii R.R., Sorokov S.I., *Condens. Matter Phys.*, 1993, **1**, 43 (in Ukrainian).
140. Levitskii R.R., Sorokov S.I., Baran O.R., *Condens. Matter Phys.*, 2000, **3**, No. 3(23), 515.
141. Levitskii R.R., Sorokov S.I., Preprint of the Bogolyubov Institute for Theoretical Physics, ITP-88-34R, Kyiv, 1988 (in Russian).
142. Levitskii R.R., Sorokov S.I., Moina A.P. Preprint of the Institute for Condensed Matter Physics, ICMP-97-24U, Lviv, 1997 (in Ukrainian).
143. Glauber J., *J. Math. Phys.*, 1963, **4**, No. 2, 294.
144. Levitsky R.R., Zachek I.R., Preprint of the Bogolyubov Institute for Theoretical Physics, ITP-77-30R, Kiev, 1977 (in Russian).
145. Levitsky R.R., Zachek I.R., Varanitsky V.I., Preprint of the Bogolyubov Institute for Theoretical Physics, ITP-79-11E, Kiev, 1979.
146. Zachek I.R., Levitsky R.R., *Teor. Mat. Fiz.*, 1980, **43**, No. 1, 128 (in Russian).
147. Levitsky R.R., Zachek I.R., Varanitsky V.I., *Ukr. J. Phys.*, 1980, **25**, No. 12, 1961 (in Russian).
148. Levitsky R.R., Zachek I.R., Preprint of the Bogolyubov Institute for Theoretical Physics, ITP-80-

- 105R, Kiev, 1980 (in Russian).
149. Levitsky R.R., Zachek I.R., Mits Ye.V., Preprint of the Bogolyubov Institute for Theoretical Physics, ITP-82-131R, Kyiv, 1982 (in Russian).
150. Levitsky R.R., Zachek I.R., Mits Ye.V., Preprint of the Bogolyubov Institute for Theoretical Physics, ITP-83-138R, Kyiv, 1983 (in Russian).
151. Levitsky R.R., Zachek I.R., Mits Ye.V., Moina A.P. Physical collection. Lviv: NTS, 1998, **3**, 417 (in Ukrainian).
152. Levitsky R.R., Zachek I.R., Mits Ye.V., Preprint of the Bogolyubov Institute for Theoretical Physics, ITP-80-109R, Kyiv, 1980 (in Russian).
153. Levitsky R.R., Zachek I.R., Mits Ye.V., Volkov. A.A., Kozlov G.V., Lebedev S.P., Preprint of the Bogolyubov Institute for Theoretical Physics, ITP-81-94R, Kyiv, 1981 (in Russian).
154. Levitsky R.R., Zachek I.R., Mits Ye.V., Preprint of the Bogolyubov Institute for Theoretical Physics, ITP-81-93R, Kyiv, 1981 (in Russian).
155. Stasyuk I.V., Levitskii R.R., Saban A.Ya. Theory of induced by external fields effects and relaxational phenomena in the crystals with structural and ferroelectric phase transitions. – In: Problems of Modern Statistical Physics, Kyiv, 1985, (in Russian).
156. Levitsky R.R., Zachek I.R., Mits Ye.V., Relaxational phenomena in ferroelectrics with hydrogen bonds. – In: Problems of Modern Statistical Physics, Kyiv, 1989, (in Russian).
157. Levitsky R.R., Mits Ye.V., Zachek I.R., Preprint of the Bogolyubov Institute for Theoretical Physics, ITP-81-137R, Kyiv, 1981 (in Russian).
158. Levitsky R.R., Zachek I.R., Mits Ye.V., Volkov. A.A., Kozlov G.V., Lebedev S.P., Preprint of the Bogolyubov Institute for Theoretical Physics, ITP-82-2R, Kyiv, 1982 (in Russian).
159. Levitsky R.R., Zachek I.R., Mits Ye.V., Volkov. A.A., Kozlov G.V., Lebedev S.P., Relaxational phenomena in ferroelectrics with hydrogen bonds of orthophosphate type. – In: Physics of many-particle systems, Kyiv, 1983, (in Russian).
160. Tanaka H., Tokunaga H., Tatsuzaki I., Sol. State Commun., 1984, **49**, No. 2, 153.
161. Tokunaga M., Tominaga Y., Tatsuzaki I., Ferroelectrics, 1985, **63**, 171.
162. Tominaga Y., Tokunaga M., Tatsuzaki I., Jap. J. Appl. Phys., 1935, **24**, Suppl.24-2, 917.
163. Tokunaga M., Progr. Theor. Phys. Suppl., 1984, No. 80, 156.
164. Stasyuk I.V., Ivankiv Ya.D., Preprint of the Bogolyubov Institute for Theoretical Physics, ITP-87-57R, Kyiv, 1987 (in Russian).
165. Blinc R., Z. Naturforsch, 1986, **41a**, 249.
166. Stasyuk I.V., Levitskii R.R., Zachek I.R., Moina A.P., Duda A.S., Condens. Matter Phys., 1996, No. 8, 129.
167. Levitskii R.R., Zachek I.R., Moina A.P., J. Phys. Study, 1997, **1**, No. 4, 577 (in Ukrainian).
168. Levitskii R.R., Moina A.P., Condens. Matter Phys., 1998, **1**, No. 2(14), 365.
169. Stasyuk I.V., Levitskii R.R., Moina A.P., Phys. Rev. B, 1999, **59**, No. 13, 8530.
170. Stasyuk I.V., Levitskii R.R., Moina A.P., Condens. Matter Phys., 1999, **2**, No. 4(20), 731.
171. Levitskii R.R., Moina A.P., Zachek I.R., Condens. Matter Phys., 1999, **2**, No. 4(20), 515.
172. Stasyuk I.V., Levitskii R.R., Moina A.P., Zachek I.R., Duda A.S., Romanyuk M.O., Stadnyk V.J., Shcherbina Ye.V., J. Phys. Study, 1999, **3**, No. 4, 502.
173. Stasyuk I.V., Levitskii R.R., Zachek I.R., Moina A.P., Duda A.S., J. Phys. Study, 2000, **4**, No. 2, 190 (in Ukrainian).
174. Levitskii R.R., Slivka A.G., Moina A.P., Lukach P.M., Guivan A.M. Preprint arXiv:cond-mat/0012053, 2000.
175. Stasyuk I.V., Levitskii R.R., Zachek I.R., Duda A.S., Condens. Matter Phys., 2001, **4**, No. 3(27), 553.
176. Stasyuk I.V., Levitskii R.R., Moina A.P., Lisnii B.M., Ferroelectrics, 2001, **254**, 213.
177. Levitskii R.R., Slivka A.G., Moina A.P., Lukach P.M., Guivan A.M., J. Phys. Stud., 2002, **6**, No. 2, 197.
178. Stasyuk I.V., Levitskii R.R., Moina A.P., Lisnii B.M., Ukr. J. Phys., 2003, **13**, No. 8, 837 (in Ukrainian).
179. Levitskii R.R., Zachek I.R., Vdovych A.S., Preprint of the Institute for Condensed Matter Physics, ICMP-03-02U, Lviv, 2003 (in Ukrainian).
180. Levitskii R.R., Zachek I.R., Vdovych A.S. Preprint of the Institute for Condensed Matter Physics, ICMP-03-03U, Lviv, 2003 (in Ukrainian).
181. Koval S., Kohanoff J., Migoni R.L., Tosatti E., Phys. Rev. Lett., 2002, **89**, No. 18, 187602.
182. Koval S., Kohanoff J., Lasave, Colizzi G., Migoni R.L., Phys.Rev B, 2005, **71**, 184102.
183. Busmann-Holder A., Michel K.H., Phys. Rev. Lett., 1998, **80**, No. 10, 2173.

184. Reiter G.F., Mayers J., Platzman P., Phys. Rev. Lett., 2002, **89**, 135505.
185. Courtens E., J. Phys. (Paris) Lett., 1982, **43**, L199.
186. Courtens E., Vogt H., Z. Phys. B, 1986, **62**, 143.
187. Courtens E., Jap. J. Appl. Phys., 1985, **24**, 70.
188. Trybula Z., Schmidt V.H., Drumheller E.J., Phys. Rev., 1991, **43**, No 1, 1287.
189. Trybula Z., Kaszynski J., Ferroelectrics, 2004, **298**, 347.
190. Trybula Z., Kaszynski J., Maluszynska H., Ferroelectrics, 2005, **316**, 125.
191. Trybula Z., Kaszynski J., Los Sz., Mielcarek S., Trybula M., Phys. Stat. Sol. (b), 2004, **241**, No. 2, 447.
192. Dolinsek J., Arcon D., Zalar B., Pirc R., Blinc R., Phys. Rev. B, 1996, **54**, No. 10, R6811.
193. Prelovcek P., Blinc R.J., Phys. C.: Solid State Phys., 1982, **15**, L985.
194. Matsushita E., Matsubara T., Prog. Theor. Phys., 1984, **71**, No. 2, 235.
195. Matsushita E., Matsubara T., J. Phys. Soc. Jap., 1985, **54**, No. 3, 1161.
196. Levitskii R.R., Sorokov S.I., Stankowski J., Trybula Z., Vdovych A.S., Condens. Matter Phys., 2008, **11**, No. 3(55), 523.
197. Kubo R., J. Phys. Soc. Jpn., 1962, **17**, 1100.
198. Levitsky R.R., Zachek I.R., Vdovych A.S., Preprint of the Institute for Condensed Matter Physics, ICMP-08-04U, Lviv, 2008 (in Ukrainian).
199. Kaminov I.P., Phys. Rev., 1965, **138**, No. 5A, 1539.
200. Volkov A.A., Kozlov G.V., Lebedev S.P., Velichko I.A., Fiz. Tverd. Tela, 1979, **21**, No. 11, 3304 (in Russian).
201. Hill R.M., Ichiki S.K., Phys. Rev., 1963, **132**, No. 4, 1603.
202. Pereverzeva L.P., Poplavko Yu.M., Rez I.S., Kuznetsova L.I., Kristallografiya, 1976, **21**, No. 5, 981 (in Russian).
203. Volkov A.A., Kozlov G.V., Lebedev S.P., Prokhorov A.M., Ferroelectrics, 1980, **25**, No. 1-4, 531.
204. Blinc R., Schmidt V.H., Ferroelectrics Letters, 1984, **1**, 119.
205. Gauss K.E., Happ H., Phys. Stat. Sol. (b), 1976, **78**, No. 1, 133.
206. Zhukov S.G., Kulbachinskii V.A., Smirnov P.S., Strukov B.A., Chudinov S.M., Izv. AN SSSR, ser. fiz., 1985, **49**, No. 2, 255 (in Russian).
207. Baddur A., Strukov B.A., Velichko I.A., Setkina V.N., Kristallografiya, 1972, **17**, No. 5, 1065 (in Russian).
208. Skalyo J., Frazer B.C., Jr., Shirane G., Daniels W.B., J. Phys. Chem. Solids, 1969, **30**, No. 8, 2045.
209. Kasahara M., Tatsuzaki I., J. Phys. Soc. Japan, 1981, **50**, No. 2, 551.
210. Strukov B.A., Amin M., Sonin A.S. Fiz. Tverd. Tela, 1967, No. 8, 2421 (in Russian).
211. Volkova E.N., Podshivalov Yu.S., Rashkovich L.N., Strukov B.A., Izv. AN SSSR, ser. fiz., 1975, **39**, No. 4, 787 (in Russian).
212. Litov E., Uehling E.A., Phys. Rev. B, 1970, **1**, No. 9, 3713.
213. Hill R.M., Ichiki S.K., Phys. Rev., 1963, **130**, No. 1, 150.
214. Kramarenko V.A., Volkova E.N., Tsibizova M.D. Temperatures of phase transitions in the  $\text{K}(\text{D}_x\text{H}_{1-x})_2\text{PO}_4$  and  $\text{Rb}(\text{D}_x\text{H}_{1-x})_2\text{PO}_4$  crystals in connection with their real structure. – In: XI all-Union conf. on physics of ferroelectrics. Vol.2, Kiev, IF AN USSR, 1986, p. 28 (in Russian).
215. Volkova E.N., Kramarenko V.A., Tsibizova M.D., Pis'ma v Zhurn. tehn. fiz., 1988, **14**, No. 5, 408 (in Russian).
216. Samara G.A., Ferroelectrics, 1973, **5**, 25.
217. Samara G.A., Phys. Lett. A., 1967, **25**, No. 9, 664.
218. Gilletta P., Chabin M., Phys. Stat. Sol. (b), 1980, **100**, K77.
219. Breziria B., Fouskova A., Smutny P., Phys. Stat. Sol. (a), 1972, **11**, No. 2, K149.
220. Sliker T.R., Burlage S.R., J. Appl. Phys., 1963, **34**, No. 7, 1837.
221. Luther G., Ferroelectrics, 1976, **12**, No. 1-4, 243.
222. Meriakri V.V., Ushatkin E.F. Investigation of inorganic materials by submillimeter spectroscopy methods. – In: Physical methods of investigation of inorganic materials. Moscow, 1981, 195-205 (in Russian).
223. Sherman A.B., Vayda D., Velichko I.A., Gutner O.S., Lemanov V.V., Fiz. Tverd. Tela, 1971, **13**, No. 12, 3716 (in Russian).
224. Hazario I., Gonzalo J.A., Sol. St. Commun., 1969, **7**, No. 18, 1305.
225. Yoiacono G.M., Balashio J.F., Osborne W., Appl. Phys. Lett., 1974, **24**, No. 10, 455.
226. Strukov B.A., Baddur A., Koptsik V.A., Velichko I.A., Fiz. Tverd. Tela, 1972, **14**, No. 4, 1034 (in Russian).

227. Volkova E.N., Candidate Dissertation, Moscow, 1991 (in Russian).
228. Strukov B.A., Baddur A., Zinenko V.N., Mishchenko A.V., Kopsik V.A., *Fiz. Tverd. Tela*, 1973, **15**, No. 6, 1388 (in Russian).
229. Volkova E.N., Berezhnoy B.M., Izrailenko A.N., Mishchenko A.V., Rashkovich L.N., *Izv. AN SSSR, ser. fiz.*, 1971, **35**, No. 9, 1858 (in Russian).
230. Deguchi K., Nakamura E., Okaue E., Aramaki N., *J. Phys. Soc. Japan*, 1982, **51**, No. 11, 3575.
231. Fairall C.W., Reese W., *Phys. Rev. B*, 1972, **6**, No. 1, 193.
232. Kozlov G.V., Lebedev S.P., Prokhorov A.M., Volkov A.A., *J. Phys. Soc. Japan*, 1980, **49**, 188.
233. William R., Cook, Jr., *J. Appl. Phys.*, 1967, **38**, No. 4, 1637.
234. Nelmes R.J., Meyer G.M., Tibballs J.E., *J. Phys. C*, 1982, **15**, No. 1, 59.
235. Kennedy N.S.J., Nelmes R.J., *J. Phys. C*, 1980, **13**, No. 26, 4841.
236. Fukami T., *J. Phys. Soc. Jpn.*, 1988, **57**, No. 4, 1287.
237. Strukov B.A., Amin M., Kopsik V.A., *J. Phys. Soc. Japan.*, 1970, **28**, Suppl, 207.
238. Reese W., May L.P., *Phys. Rev.*, 1968, **167**, No. 2, 504.
239. Mayer R.J., Bjorkstam J.L., *J. Phys. Chem. Solids.*, 1962, **23**, 619.
240. Kryzhanovskaya N.D., Tovchenko G.V., Tuznik E.F., Mishchenko A.V., *Izv. AN SSSR, ser. fiz.*, 1975, **39**, No. 5, 1031 (in Russian).
241. Vasilevskaya A.S., Sonin A.S., *Fiz. Tverd. Tela*, 1971, **13**, No. 6, 1550 (in Russian).
242. Lomova L.G., Sonin A.S., *Fiz. Tverd. Tela*, 1968, **10**, No. 5, 1565 (in Russian).
243. Mason W.P., Mattias B.T., *Phys. Rev.*, 1952, **88**, No. 3, 477.
244. Benepe J.W., Reese W., *Phys. Rev. B*, 1971, **3**, No. 9, 3032.
245. Strukov B.A., Korzhuev M.A., Baddur A., Kopsik V.A., *Fiz. Tverd. Tela*, 1971, **13**, No. 7, 1872 (in Russian).
246. Sidnenko E.V., Gladkii V.V., *Kristallografiya*, 1973, **18**, No. 1, 138 (in Russian).
247. Gladkii V.V., Sidnenko E.V., *Fiz. Tverd. Tela*, 1971, **13**, No. 6, 1642 (in Russian).
248. Blinc R., Burgar M., Levstik A., *Sol. Stat. Commun.*, 1973, **12**, No. 6, 573.
249. Gladkii V.V., Magataev V.K., Sidnenko E.V., *Ferroelectrics*, 1973, **5**, 107.
250. Wiseman G.G., *Iee Transactions on Electron Devices*, 1969, **16**, No. 6, 588.
251. Samara G.A., *Ferroelectrics*, 1979, **22**, No. 3–4, 925.
252. Reese W., May L.F., *Phys. Rev.*, 1967, **162**, No. 2, 510.
253. Stephenson C.C. Zetteemayer A.C., *J. Amer. Chem. Soc.*, 1944, **66**, No. 8, 1405.
254. Amin M., Strukov B.A., *Fiz. Tverd. Tela*, 1970, **12**, No. 7, 2035 (in Russian).
255. Amin M., Strukov B.A., *Fiz. Tverd. Tela*, 1968, **10**, No. 10, 3158 (in Russian).
256. Deguchi K., Nakamura E., *J. Phys. Soc. Japan.*, 1980, **49**, No. 5, 1887.
257. Havlin S., Litov E., Sompolinsky H., *Phys. Rev. B*, 1976, **14**, No. 3, 1297.
258. Shuvalov L.A., Zheludev I.S., Mnatsakanyan A.V., Ludupov Ts.Zh., Fiala I., *Izv. AN SSSR, ser. fiz.*, 1967, **31**, No. 11, 1919 (in Russian).
259. Bornarel J., *Ferroelectrics*, 1984, **54**, 245.
260. Mason W.P., *Phys. Rev.*, 1946, **69**, No. 5–6, 173.
261. Matthias B., Merz W., Scherrer P., *Helv. Phys. Acta*, 1947, **20**, 273.
262. Ono Y., Hikita T., Ikeda T., *J. Phys. Soc. Jpn.*, 1987, **56**, No. 2, 577.
263. Lee K.S., Kim K.T., Kim J.J., *Jpn. J. Appl. Phys.*, 1985, **24**, Suppl. 24–2, 969.
264. Chaudhuri B.K., Ganguli S., Hath D., *J. Indian and Appl. Phys.*, 1980, **18**, 573.
265. Volkova E.N., Izrailenko A.N., *Kristallografiya*, 1983, **28**, No. 6, 1217 (in Russian).
266. Gauss K.E., Happ H., Rother G., *Phys. Stat. Sol. B*, 1975, **72**, No. 2, 623.
267. Pereverzeva L.P., *Izv. AN SSSR, ser. fiz.*, 1971, **35**, No. 12, 2613 (in Russian).
268. Meriakri V.V., Poplavko Yu.M., Ushatkin E.F., *J. Tehn. Fiz.*, 1974, **44**, No. 5, 1111 (in Russian).
269. Happ H., Rother G., *Phys. Stat. Sol. (b)*, 1977, **79**, No. 2, 473.
270. Onjango P., Smith W., Angress J.F.I.R., *J. Phys. Chem. Solids*, 1975, **36**, No. 4, 309.
271. Garland C.W., Novotny D.B., *Phys. Rev.*, 1969, **177**, No. 2, 971.
272. Vajda D., *Acta Phys. Slov.*, 1980, **30**, No. 1, 99.
273. Litov E., Garland C.M., *Phys. Rev. B*, 1970, **2**, No. 11, 4597.
274. Shimshoni M., Harnik E., *Phys. Letters. A*, 1970, **32**, No. 5, 321.
275. Reese R.L., Fritz J.J., Cummins H.Z., *Phys. Rev. B*, 1973, **7**, No. 9, 4165.

## Термодинаміка та динамічні властивості сегнетоактивних сполук сім'ї $\text{KN}_2\text{PO}_4$ . Уніфікована модель

Р.Р.Левицький<sup>1</sup>, І.Р.Зачек<sup>2</sup>, А.С.Вдович<sup>1</sup>, С.І.Сороков<sup>1</sup>

<sup>1</sup> Інститут фізики конденсованих систем НАН України вул. Свенціцького, 1, Львів, 79011, Україна

<sup>2</sup> Національний університет "Львівська політехніка" вул. С. Бандери 12, 79013, Львів, Україна

Отримано 21 листопада 2008 р., в остаточному вигляді – 15 січня 2009 р.

В рамках запропонованої уніфікованої протонної моделі сегнетоактивних сполук сім'ї  $\text{KN}_2\text{PO}_4$  в наближенні чотиричастинкового кластера за короткосяжними і середнього поля за далекосяжними взаємодіями розраховано термодинамічні та поздовжні динамічні характеристики сегнетоелектриків типу  $\text{KD}_2\text{PO}_4$  та антисегнетоелектриків типу  $\text{ND}_4\text{D}_2\text{PO}_4$ . Розрахунок частково дейтерованих сегнетоелектриків типу  $\text{K}(\text{H}_{1-x}\text{D}_x)_2\text{PO}_4$  та антисегнетоелектриків типу  $\text{N}(\text{H}_{1-x}\text{D}_x)_4(\text{H}_{1-x}\text{D}_x)_2\text{PO}_4$ , проведено в наближенні середнього кристалу. Показано, що при належному виборі мікропараметрів запропонована теорія дає добрий кількісний опис експериментальних даних для сегнетоактивних сполук сім'ї  $\text{KN}_2\text{PO}_4$ .

**Ключові слова:** сегнетоелектрики, кластерне наближення

**PACS:** 77.22.Ch, 77.22.Gm, 77.84.Fa

